Model of the Injection of CO_2 at Hellisheiði

Possible Effects of the Proposed CO_2 Injection and Mineral Storage Operations

Thomas Ratouis and Matt Villante

Carbfix

Útgefandi: Carbfix hf.
Umsjón og ábyrgð: Thomas Ratouis, Matt Villante

Content

Figures

Tables

1 Introduction

Reservoir models for the Environmental Impact Assessment of future mineral storage operations at the Hellisheiði geothermal power station have been developed. These models consist of three-dimensional field-scale models that represent the injection of dissolved gas within the deep geothermal system and the intermediate system. The models simulate the flow of injected CO_2 underground using physical reservoir processes according to the best modelling practices used in the geothermal industry (Nugraha et al., 2022). The model inputs include the topography, rainfall/infiltration, temperature model, production/injection data, and geology based on the 3D geological model developed for Hellisheiði and updated for the purpose of the EIA (Gunnarsdóttir & Poux, 2016). A reservoir model simulates and predicts the behaviour of CO_2 injected into the subsurface as it interacts with geologic structures and rocks. Provided favorable physical and geochemical properties, this results in rapid in-situ carbon mineralization. The model is built to assess the impact of injection on the intermediate system and groundwater system as well as to:

- Define the boundary of the system by simulating the maximum migration of the dissolved CO_2. The migration of dissolved CO_2 within the storage reservoir will be numerically modelled as a function of time,
- Ensure effective trapping of CO_2 in the storage reservoir by calculating the bubble point pressure of CO_2 against the reservoir pressure,
- Demonstrate that favorable conditions for in situ carbon mineralization prevail within the storage reservoir, and
- Provide a preliminary estimate of the maximum storage capacity.

In addition, the impact on the production of geothermal fluid and reinjection of geothermal brine from ON Power - the operator of the geothermal power station - will be assessed. Prior to starting injection of CO_2, information gathered from site characterization and monitoring activities will be used to maintain and continuously update reservoir models to confirm that monitoring data and long-term forecasts are in agreement.

2 Mineral storage operation at the Hellisheidi Geothermal power plant

The Carbfix method imitates natural processes - namely the silicate weathering cycle - that regulate the Earth's climate on geologic timescales and accelerates them through application of the Carbfix technology to permanently trap and mineralize CO_2 within two years (Pogge von Strandmann et al., 2019). CO_2-trapping mechanisms include **structural trapping**, wherein CO_2 is stored below a caprock or sealing formation (such as in supercritical or traditional CCS), **residual trapping** - or capillary trapping - in pore space, **solubility trapping** of CO_2 as it dissolves in formation water, and **mineral trapping** as carbonate precipitation occurs (Figure 1, (Snæbjörnsdóttir et al., 2020). The Carbfix technology promotes mineral carbonation via dissolution of CO_2 into water before or during its injection. Since the injected CO_2-charged fluid is acidic, it is strongly undersaturated with respect to the primary and secondary minerals of the reservoir rocks (Clark et al., 2018) promoting dissolution which releases cations (Ca^{2+}, Mg^{2+}, Fe^{2+}) and gradually increases the pH, resulting in the bulk of the CO_2 being permanently transformed to carbonate minerals in less than two years (Pogge von Strandmann et al., 2019).

This method of CO_2 storage eliminates the risk of leakage since the CO_2-charged water is denser than surrounding formation water and immediately achieves solubility trapping with mineral trapping occurring just months or years later, effectively reducing the possibility of leakage and

ensuring its security, permanence, and sustainability. There is a significant difference between the Carbfix method and other CCS projects in the removal of the requirement for a cap rock and the reliance on the integrity of the seal, which is fundamental to supercritical CO_2 storage. This has led to high public acceptance of previous CO_2 mineral storage projects using the Carbfix method.

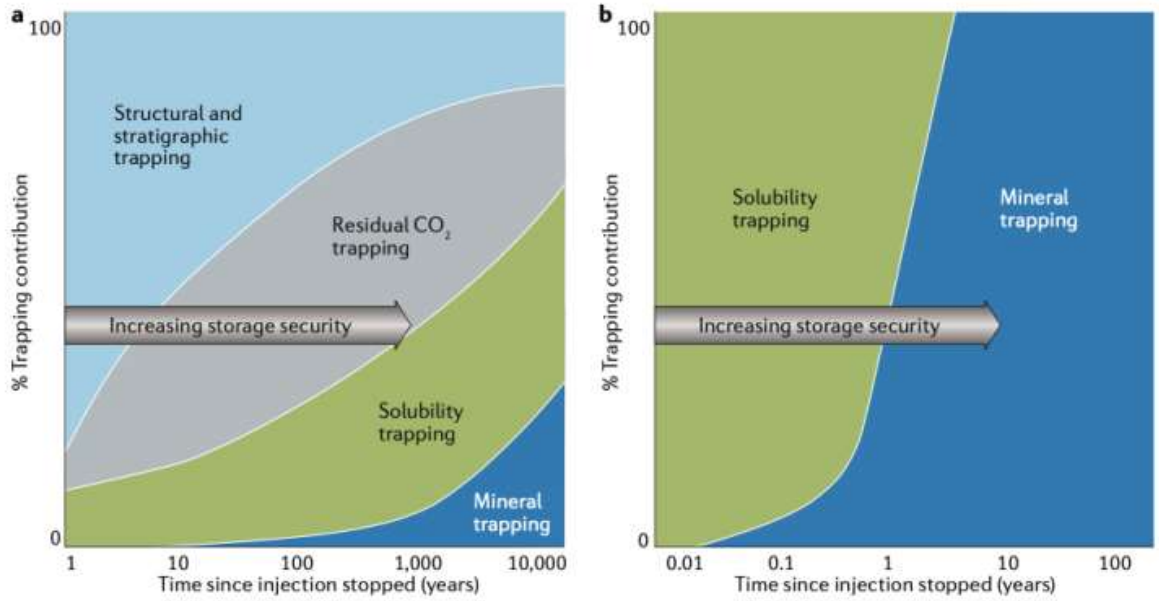

Figure 1: Comparison of CO_2-trapping mechanisms for (a) supercritical and (b) dissolved CO_2 injections. Contribution of trapping mechanisms gradually changes over time for both conventional and mineral storage. In mineralization storage, immediate solubility trapping occurs as the CO_2-charged fluid is denser than formation water and tends to sink. Over the month-year time scale the CO_2 is mineralized, leading to increased storage security on geologic time scales via permanent mineralization (Figure 1; Snæbjörnsdóttir et al., 2020).

Carbfix conducted the first pilot injections of carbon dioxide (CO_2) and mixtures of CO_2 and hydrogen sulfide (H_2S) in 2012 into the basaltic subsurface formations at the Þrengsli site in SW-Iceland (Snæbjörnsdóttir et al., 2017). The site, the Carbfix1 site, is a subfield of the Hellisheiði Geothermal Field, where geothermal energy is harvested at the Hellisheiði Geothermal Power Plant. The rapid mineralization of the injected gases of these injection experiments was confirmed via geochemical sampling (Matter et al., 2016; Pogge von Strandmann et al., 2019; Snæbjörnsdóttir et al., 2017), geochemical modelling (Snæbjörnsdóttir et al., 2018), as well as reservoir scale transport modelling (Aradóttir et al., 2012) The results proved the suitability of basalts for mineral storage of CO_2 (Matter et al., 2016), resulting in the upscaling of the project in 2014 with capture of CO_2 and H_2S from the Hellisheidi Geothermal Power Plant and injection into a hotter geothermal reservoir at the Carbfix2 injection site (I. Gunnarsson et al., 2018; Sigfússon et al., 2018).

The injection of CO_2 and H_2S has been an integral part of the operations at the power plant since 2014, with over 80,000 tCO_2 injected to date. The operation has been scaled up stepwise since commission and, at current rates, about 12,000 tonnes of CO_2 and about 6,000 tonnes of H_2S are injected annually (Sigfússon et al., 2018). These non-condensable gases are captured directly from the power plant exhaust stream through a scrubbing process where the gases are dissolved into pure condensate from the power plant's turbines. The resulting CO_2-H_2S-charged fluid is then piped towards the Carbfix2 injection site at the Húsmúli reinjection site and injected to about ~700 m depth into the fractured basaltic reservoir at temperatures of ~250°C. As the low-pH fluid initially interacts with rocks near the wellbore, dissolution occurs and contributes metal cations to

the fluid. Further away from the well, the pH shifts and precipitation occurs – thus, to date there are no signs of decreasing system injectivity since the start of injections in 2014. At present, >50% of the injected carbon is fixed as carbonate minerals within months of its injection (Clark et al., 2018; I. Gunnarsson et al., 2018).

3 Favorable conditions at Hellisheidi

The bedrock characteristics at Hellisheiði indicate extremely favorable conditions for CO_2 mineral storage with the storage reservoir consisting of highly reactive, basaltic rocks which have been demonstrated to achieve CO_2 mineralization within years from injection (Clark et al., 2018; I. Gunnarsson et al., 2018). The basaltic formations at the site are geologically young, porous and permeable, providing pathways for the migrating fluids and access to mineral surfaces that contribute cations to the mineralization, and space for the carbonate precipitates. Both pilot and commercial-scale CO_2 injection has been demonstrated at Hellisheiði - within the intermediate system (Carbfix1) and the deep geothermal system (Carbfix2). Three key aspects must be included in a reservoir model that influences fluid-rock interactions and thus the potential mineralization:

1) Lithology and mineralogy – favorable geochemical composition (mafic & ultramafic > felsic rocks), abundant mafic minerals (olivine > pyroxene > feldspar)
2) Origin of permeability - permeable and fractured rock to provide the pathways for the injection fluid, access to surfaces for fluid-rock interaction, and sufficient pore and fracture volume for the mineralization process.
3) Alteration - secondary minerals that may influence the mineralization process or flow patterns (e.g., porosity decline with increased alteration extent)

3.1 Lithology and mineralogy

A simplified stratigraphic sequence at Hellisheiði can be described as follows (see e.g., Alfredsson et al., 2013; Snæbjörnsdóttir et al., 2018):

- Surface to 100-150m: A sequence of aquifer-bearing fine-grained basaltic lava flows.
- 150 to 400m: A hyaloclastite formation containing glassy basaltic tuff layers, consisting of consolidated volcanic ash. This formation also contains (1) layers of breccia consisting of consolidated volcanic ash and poorly crystallized basalt-fragments, and (2) poorly crystallized basalts including pillow lavas.
- 400 m to 1300m: succession of olivine tholeiitic basalt and hyaloclastic sequences from alternating glacial-interglacial periods.
- Below 1300m: altered crystalline rock heavily intruded by low viscosity magmas – “base” formation of the Hengill volcano, formed prior to the onset of central volcanic activity.

Alfredsson et al., 2013 analyzed fifty rock samples from just below the surface down to 1200 m for major and trace elements. The variation with depth of selected element is shown in Figure 2. The sum of the concentrations of the major divalent cation oxides CaO, MgO, and FeO, ranged from 25 to 33% of the rocks. The silica compositions, as plotted in Figure 2d range from about 45 to 49% SiO_2. The overall chemical composition range spans from picrite to tholeiite (Maaløe & Jakobsson, 1980). The majority of the rocks are of olivine tholeiite composition and often contain plagioclase phenocrysts in both glassy and crystalline formations (Snæbjörnsdóttir et al., 2018). Intrusive rocks become more common below ~500 m below sea level (mbsl) and dominant below ~1300 mbsl in the crystalline basement (Snæbjörnsdóttir et al., 2018).

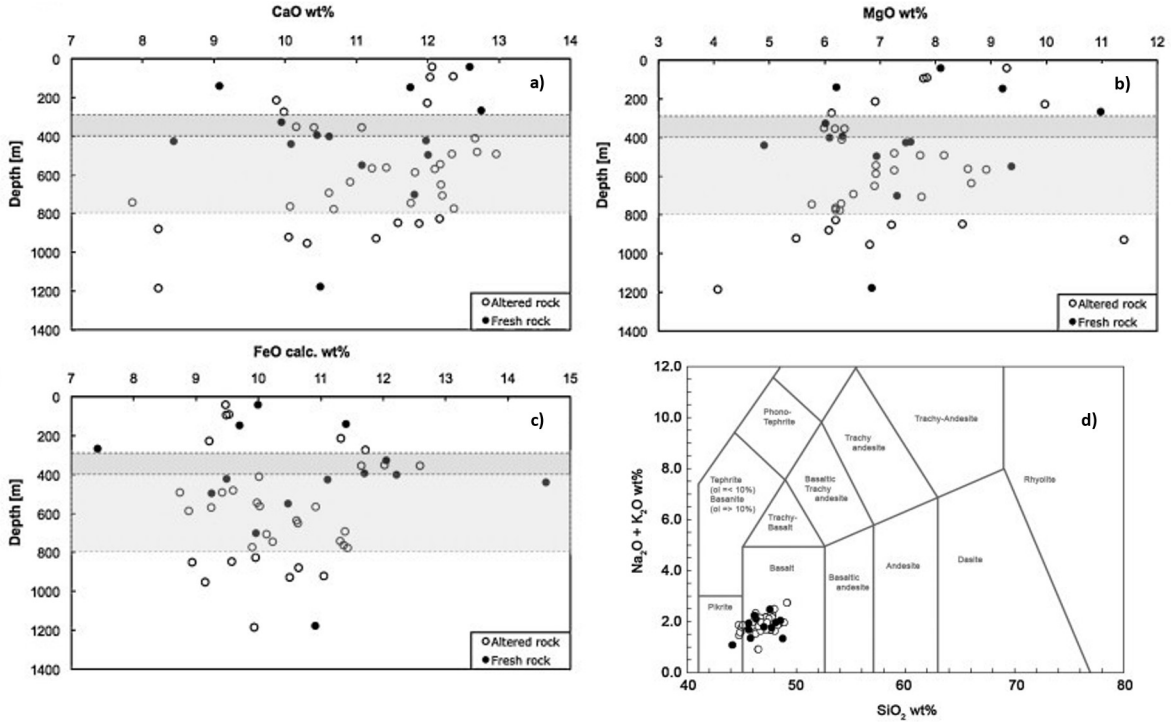

Figure 2: Chemical composition of rocks at Hellisheidi as a function of depth in wells HN-1, HN-2, HN-4, HK-31, and HK-26. a) CaO wt%, b) MgO wt%, c) FeO calc. wt%; dark gray shaded area represents the upper hyaloclastite formation and the light-gray area the target injection zone of Carbfix1 at Þrengsli. d) TAS diagram showing predominantly basalt and picrite composition for rocks at Hellisheidi. (Figures adapted from Alfredsson et al., 2013).

3.2 Origin of permeability

Studies have been done on permeability and porosity of Icelandic rock samples and they include samples consistent with the geological setting of the shallow subsurface beneath the Carbfix site (e.g., Frolova et al., 2005a; Sigurðsson et al., 2000; Sigurðsson & Stefánsson, 1994).

However, in volcanic tectonically active settings such as Hellisheiði, fracture permeability and porosity are usually dominant and may overprint the primary lithological values. Permeability anomalies can usually be of lithostratigraphic nature at the contact zones between units or structural nature due to faults and fractures. At Hellisheiði both are found and are characteristic of the intermediate and deep systems.

– Origin of permeability in the Intermediate system

The stratigraphical boundaries between the succession of interglacial lavas and hyaloclastite formations show very high permeability. Large aquifers or permeable layers in wells in Iceland occur preferentially along boundaries between accumulative volcanic units in analogue systems (Franzson, 1988, 2000; Helgadóttir et al., 2010). These are dominant in Iceland in the first 800 m of the subsurface.

– Origin of permeability in the deep system

The permeability in the deep system at the Hellisheiði site is structurally controlled and affiliated with intrusive bodies and sub-vertical faults following a NNE orientation (Franzson, 1988). The highest temperatures in the deep geothermal field and the most productive wells at Hellisheiði are predominantly located along large rifting faults trending NNE along the extension zone and the two postglacial eruptive fissures. Similarly, sharp boundaries in the formation temperature parallel to the rifting direction are found at Hellisheiði (G. Gunnarsson et al., 2011). Modelling studies have

showed that a structural control of the geothermal resource at Hellisheiði is consistent with the data available (G. Gunnarsson et al., 2011). Below ~1000 m, intrusive rocks are believed to be sources of permeability due to fracture creation during their emplacement (Franzson, 1988, 1998)

3.3 Alteration

In geothermal environments such as the Hellisheiði field, primary minerals tend to alter to secondary minerals that are more stable at the high temperatures encountered within a geothermal system. The formation of these alteration minerals is usually dependent on the temperature, permeability, pressure, fluid composition, initial composition of the rock and the duration of the hydrothermal activity (Lagat, 2009). As the hydrothermal fluid flows through the rock, it alters the composition of the rocks by adding, removing or redistributing components. The sequence of the alteration minerals indicates a progressive increase in alteration temperature with depth, spanning the smectite-zeolite alteration zone down to 800–1000 m depth (Franzson et al., 2008; Kristmannsdóttir & Tómasson, 1978; Snæbjörnsdóttir et al., 2018). Quartz starts forming at about >180 °C, and smectites become interlayered with chlorite, forming **mixed layer clays** at temperatures around >200 °C (Figure 3). The high temperature hydrothermal alteration is characterized by the formation of chlorite and epidote above 230-250 °C. Epidote becomes more abundant along with prehnite and actinolite at temperatures above 280 °C (Figure 3).

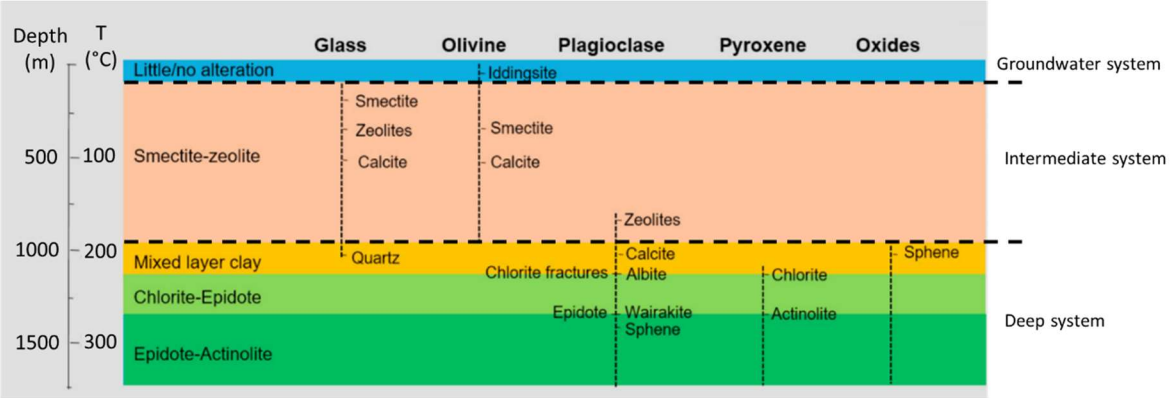

Figure 3: The alteration zones and the breakdown of the primary phases. Also shown are the approximated depth ranges of the shallow groundwater system, the intermediate system and the deep system. The figure is adapted from Snæbjörnsdóttir et al., 2018.

Studies on Icelandic bedrock show that porosity and permeability generally decrease with progressive alteration, gradual burial, and/or increasing rock age since these processes result in the pore space being filled with secondary minerals (Neuhoff et al., 1999). Analysis of the alteration state of the injection site rocks at Carbfix1 (analogous to the intermediate system) is presented in Figure 4 below (Alfredsson et al., 2013).

At the depth of the CO_2 injection (~500 m) the alteration stage is low, with the main alteration minerals being low temperature zeolites and clays. Microscopic and XRD analysis show that the major alteration minerals are pore filling Ca–Mg–Fe–smectite, Ca-rich zeolites and calcite.

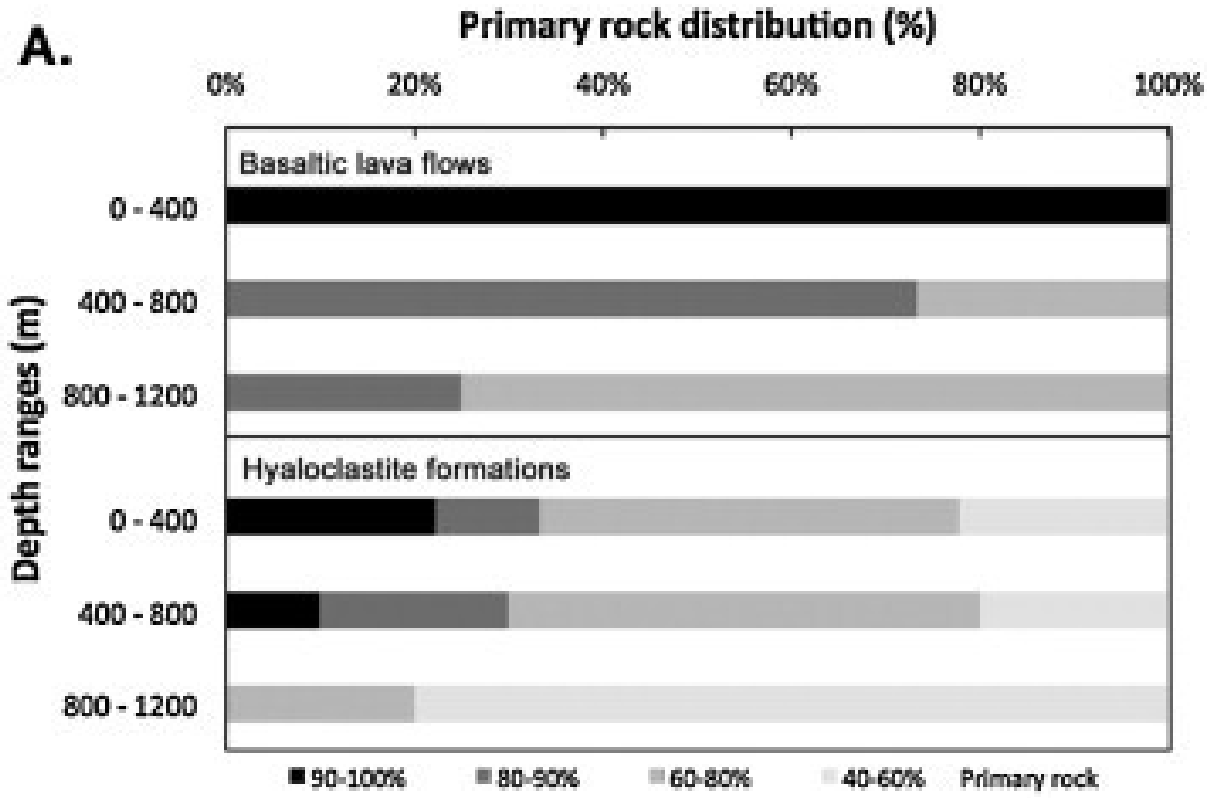

Figure 4: Distribution of calculated unaltered primary rock content of the lava flows and the hyaloclastites at the Carbfix1 study site at selected depths (Alfredsson et al., 2013; Fig. 8a)

4 Conceptual model of Hellisheiði

A three-dimensional conceptual model of the Hellisheiði geothermal system was developed in the Leapfrog Geothermal software in 2016 using surface data, well data, well logging data, geophysical data, laboratory analysis and desktop studies (Gunnarsdóttir & Poux, 2016). This project was part of the combined efforts of OR (Orkuveita Reykjavíkur), Carbfix, and ÍSOR to refine, expand, and deepen the understanding of the Hellisheiði geothermal field and surrounding areas. The data were used to prepare several 3D models of the area: lithological, structural, alteration, temperature and resistivity. These models can be combined and visualized in parallel to provide an integrated view of the subsurface geology and abundance of data encountered at Hellisheiði (Gunnarsdóttir & Poux, 2016).

Building on this work, an extended and refined geological and alteration model of Hellisheiði was developed in 2022 to support the Environmental Impact Assessment (EIA) by expanding the existing models and incorporating updated data that can inform scientists, regulators, and stakeholders of potential impacts from expanded CO_2 injections at Hellisheiði.

The objectives for this model update include:

1) Expanding the existing geologic (Jarðfræðilíkan) and alteration model (Ummyndunarlíkan) to cover a wider area around the Hellisheiði geothermal field (Figure 5).
    a. New boundaries of the model should cover the planned Geothermal Resource Park, including existing and planned geothermal wells (HE-series, HN-series), groundwater wells affected (HK-series, KH-series, HU-series), and new planned Carbfix injection wells (HC-series: planned injection wells, HM-series: planned

monitoring wells, HW-series: planned water supply wells) *Note: naming conventions are tentative and may be updated in the future.*

2) Visualizing how planned wells and the expansion of Carbfix operations related to other subsurface features (wells, faults, geothermal/intermediate system boundary, etc.).
3) Incorporating new data into the model and updating existing data as available.
4) Utilizing the expanded geologic and alteration model to produce cross sections and figures to visualize and communicate the complexity of the geothermal system and potential impacts of expanded CO_2 injections in the area.
5) Building an integrated TOUGH2 reservoir model combining the geologic model, alteration model, and location of intermediate/geothermal system boundary (defined as the low resistivity boundary of the mixed layer clay (MLC) alteration zone).
6) Improving communication and correlation between geologic models based on field data and reservoir models for simulation of injection schemes and assessment of potential impacts.

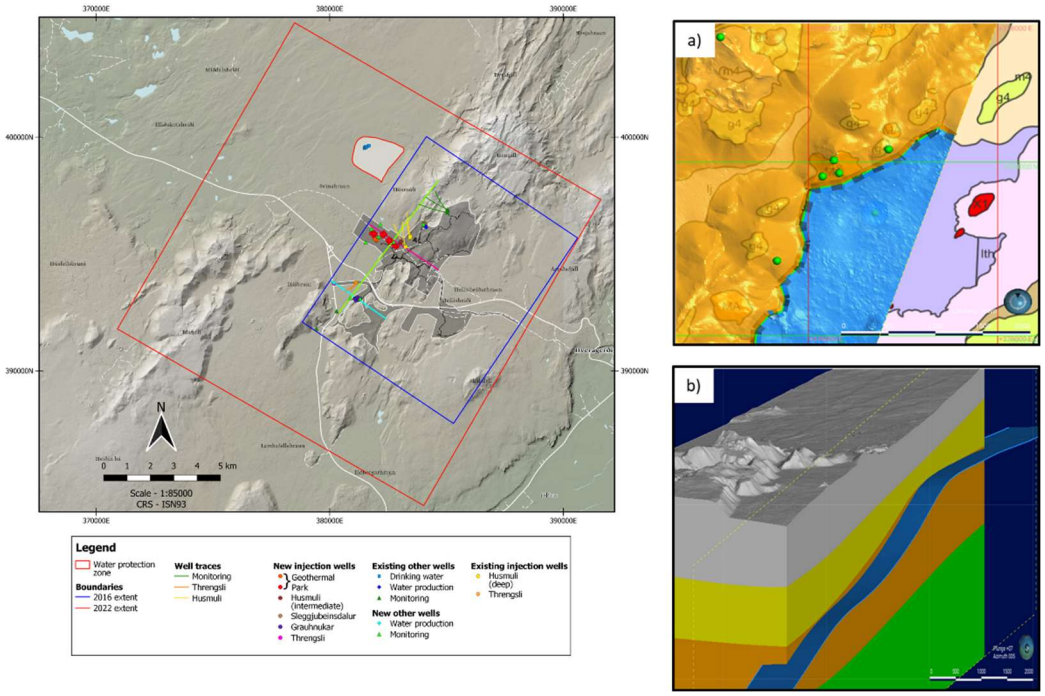

Figure 5: Extents of the geological model (left) and workflow for updating geologic and alteration models (right). Both the original Leapfrog model 2016 (in blue) and extended model 2022 (in red) is shown with existing wells, well traces, and locations of cross-sections (select sections shown in section 3 of ÍSOR specialist report) produced from Leapfrog model. Due to the lack of exploration and geophysical data outside of the central Hengill system, the geologic a) and alteration models b) were manually edited based on geologic interpretations and imported resistivity data (blue surface in 7b) (right).

4.1 Modelling update

4.1.1 Extension of boundaries

The area selected for the expanded model is rectangularly shaped and has an orientation of NE-SW, following the orientation of the previous model and the TOUGH grid created in PyTOUGH for the EIA. The previous model covered an area of 74.55 km^2, whereas the expanded dimensions are approximately 15.17 by 15.05 km, which corresponds to an area of approximately 228.31 km^2. The expanded modelling efforts have increased the area covered near Hellisheiði by approximately 153.76 km^2. The boundaries of the expanded model were selected primarily to cover the extents

of the TOUGH grid generated for reservoir simulation and to incorporate all geothermal, groundwater, existing and planned Carbfix wells (see for location of planned and existing Carbfix wells). Only the geologic and alteration models were extended to this new area due to the lack of data (e.g., temperature, resistivity, structure) outside of the previous model extent.

4.1.2 Import of new data

The large volume of geoscientific data incorporated into the previous Leapfrog model is described in the appendix of the 2016 report by Gunnarsdóttir and Poux and includes surface data, well data, well logging data, geophysical data, and data from laboratory and desktop studies. All new and existing data in the project are referenced in the GCS ISN 1993 geographic coordinate system in meters. New or updated data sources are listed below:

Surface data:

- DEM grid (updated extents to match new model boundaries)
    - Source: Landmælingar Íslands DEM, ISN93 zone 57/58
- Aerial picture (updated extents to match new model boundaries)
    - Source: Google Earth
- Well locations (updated to include and show HU, HK, KH, and Carbfix (HC, HM, HW) wells)
    - Appended HU-07, HU-08, HU-09 to well set (Source: Orkustofnun borehole register)
    - Appended planned Carbfix well series (HC-01 to HC-36, HW-01, HM-01 to HM-08)
- Geological map (updated from ÍSOR's web map to cover wider extent)
    - Used to edit surface lava flow and hyaloclastite boundaries
        - Source: ÍSOR Jarðfræðikort 1:100.000 web map

Geophysical data:

- Seismicity data (used to correlate seismic events with injections, geologic structures)
    - Point data from over 40 seismic stations part of the EU-funded COSEISMIQ project (1.12.2018 – 20.08.2021)
        - Source: ÍSOR
    - Point data from Orka náttúrunnar network (10.2016 – 06.2022)
        - Source: ÍSOR
- Resistivity data (used to determine depth to top of low-resistivity boundary that separates intermediate and deep geothermal systems)
    - 1D TEM resistivity sounding measurements
    - Source: ÍSOR/OR

Flow models:

- TOUGH model grids (2)
    - 152,979 block model, oriented 30° NE-SW in parallel with main structural orientation
    - 96,424 block model, oriented 30° NE-SW in parallel with main structural orientation
        - Source: generated, rotated, and optimized using PyTOUGH
- TOUGH simulation outputs from different scenarios

4.1.3 Model workflow and assumptions

The detailed modelling workflow for building the geologic, structural, alteration, and numerical models can be found in the 2016 report by Gunnarsdóttir and Poux, but an adapted version is shown below that incorporates updates made within the scope of this project. The Leapfrog model is a living model and will be continuously updated as new data becomes available (e.g., from new drilling, exploration, geophysical surveys, monitoring campaigns).

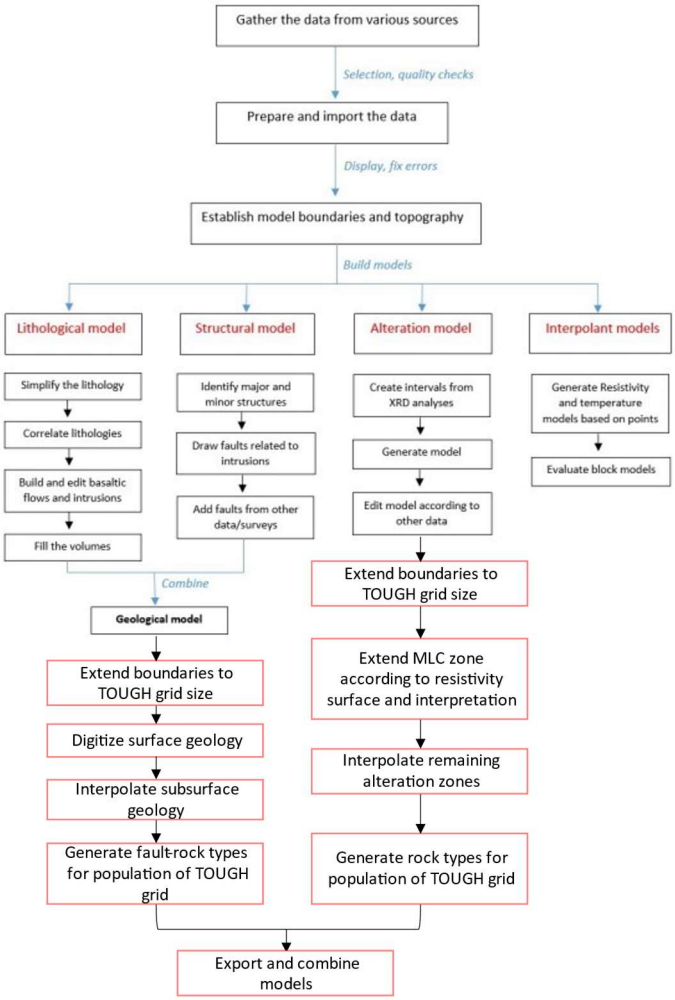

Figure 6: Workflow of the project. Adapted from Gunnarsdóttir & Poux, 2016 to include updates (shown in red) made within the scope of the 2022 modelling update.

The main updates made to the model include the previously mentioned boundary extension, surface mapping of geologic boundaries outside the original model extent, extension of alteration model surfaces following the temperature and resistivity surfaces, and population of imported TOUGH grids with rock types generated from the Leapfrog model (Figure 6). The workflow was designed to expand the applicability of the pre-existing geologic and alteration models for use in reservoir simulation, streamline development of reservoir simulations, and improve the connection between conceptual and reservoir models.

The geologic model simplifies and groups lithologies from the well logs as follows: hyaloclastite (basaltic breccia, tuff, and glassy basalt), basaltic lava flows (fine to coarse-grained basalt), and intrusive basalt (basalts linked to mapped fractures and surface fissure eruptions).

It is assumed that any volumes not built as basalt flows, intrusions, or the basement formation are filled by hyaloclastite. Hyaloclastite formations dominate the stratigraphy in the Hengill system, particularly under areas of high relief such as Skarðsmýrarfjall Mountain (Snæbjörnsdóttir et al., 2018). It is challenging to correlate basalt flows between wells where thicknesses can vary from a few meters to several hundreds of meters thick. The majority of well data is located within the pre-existing model boundaries near the main geothermal production and injection areas of Hellisheiði (Figure 5). Similarly for the alteration model, the primary data that built the alteration zones (XRD, drill cutting analysis, desktop studies) are concentrated around Hellisheiði and manually

interpreted following the resistivity and temperature structures on the boundaries of the model. Thus, the building of geologic formations beyond the existing model required interpretation and validation by the modeler and should be taken as preliminary.

For the geologic model shown in Figure 5a), ÍSOR's 1:100.000 scale geologic map was imported and used to digitize contacts between hyaloclastite and basalt flows at the surface. These basalt flows were then manually edited using points and polylines (shown in green) to reflect a similar thickness to previously modelled lava flows and the topography that channels lava flows from the higher elevations of the hyaloclastite ridges to the depressions formed in the valleys between them.

Figure 5.b) shows the alteration model, where the blue surface represents the low-resistivity surface generated from the imported 1D TEM point measurements. This surface was used to extend the boundaries and edit the shape of the MLC surface, resulting in a close correlation between the modelled low-resistivity MLC layer and the 1D TEM surface.

No adjustments were made to the structural model within the scope of this project, but two primary structures are included in the original model: NE-SW trending faults related to dilationary rifting and the main fissure zone near Hengill and a transform component in the eastern part related to the South Iceland Seismic Zone (Franzson et al., 2010). For the scope of this project, only the main NE-SW faults were included for reservoir modeling as they are the primary structural control in the area.

The final result of the updated model is shown in Figure 7 below.

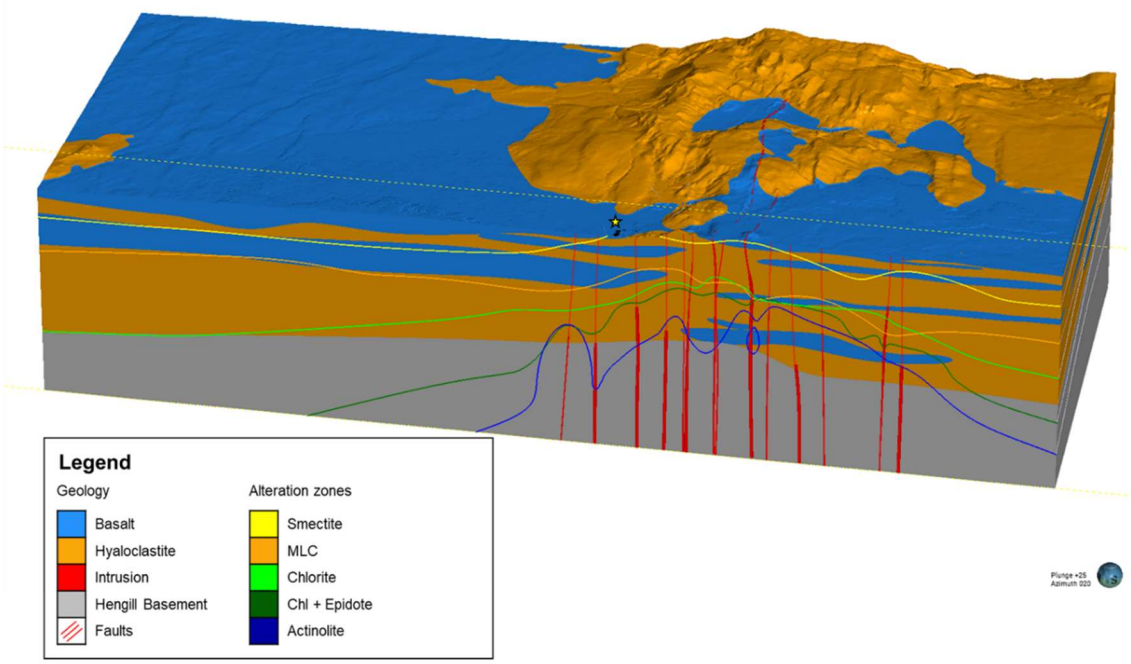

Figure 7: Final expanded geologic, alteration, and structural models. The final updated geologic, alteration, and structural models are products of iterative updates to the conceptual model and understanding of the Hellisheiði system by scientists and modelers from ÍSOR, Orkuveita Reykjavíkur, and Carbfix. The final Leapfrog model shown here is sliced towards the NW to show the main characteristics through the center of Hellisheiði power station (black outline, gold star marker). The faults shown as slightly transparent red planes extend from the basement to the surface according to mapped structures (Árnason & Magnússon, 2001; Khodayar et al., 2013; Kristinsson & Þorbergsson, 2016). Thicker red planar volumes correspond to interpreted intrusions correlated to fault locations and effusive surface eruptions mapped in ÍSOR's 1:100.000 geologic map. Alteration zone boundaries represent the top of the relevant alteration zone.

4.2 Storage capacity estimates

Storage capacity at Hellisheiði is generally controlled by the availability of divalent metal cations, however the porosity, permeability, partial pressure of CO_2, and temperature play a role in the overall success of mineralization (Snæbjörnsdóttir et al., 2014). Methods for estimation of storage capacity in basaltic reservoirs described by (Gislason et al., 2010; Goldberg et al., 2008; Snæbjörnsdóttir et al., 2014) form the basis of the following storage capacity estimations. The combined geologic and alteration model generated in Leapfrog was used as the base model for the storage potential, with physical boundaries defined by the reservoir extent, depth of injection, and upper temperature limit of carbonate precipitation. This resulted in a clipped model that represents the storage reservoir (herein referred to as the storage capacity model - Figure 9). This storage capacity estimation does not reflect the mineralization or storage potential of specific injection scenarios, but rather the overall volumetric storage potential of the Hellisheiði storage site based on all possible injection scenarios modelled here and the physical constraints for carbon mineralization.

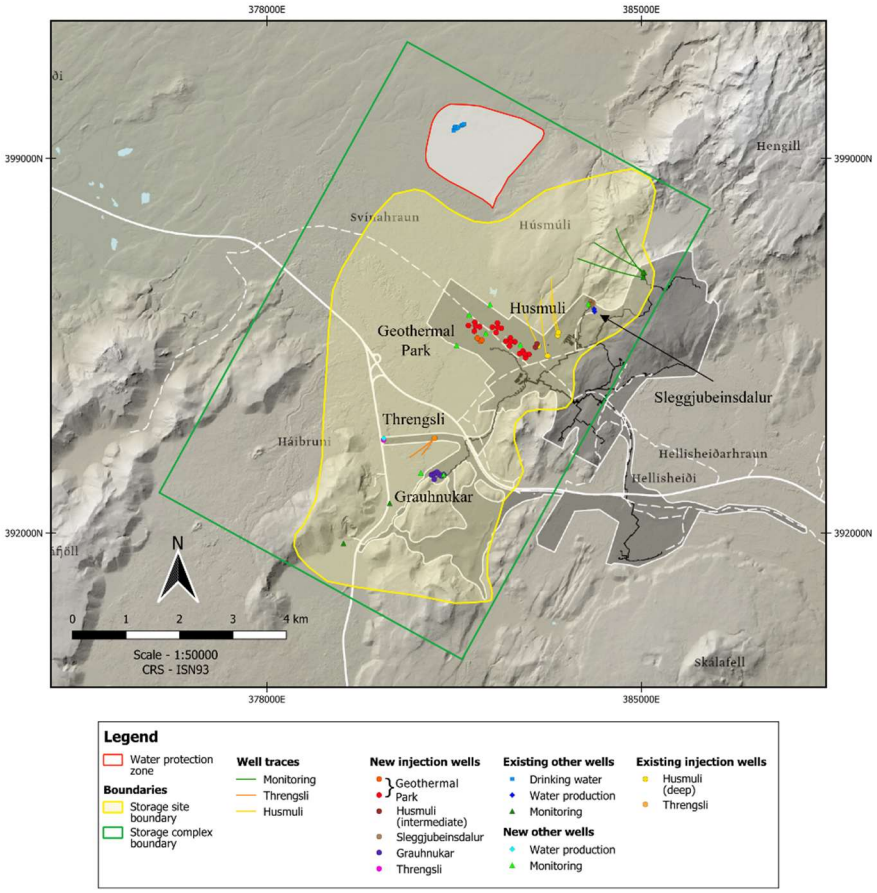

Figure 8: Map of storage reservoir and storage complex boundaries. Extents of the storage reservoir determined by simulation results presented in section 7. Storage reservoir boundary (yellow) was used to clip the lateral extents of the storage capacity model in Figure 9b. Locations of existing and planned wells for Carbfix injection operations in Hellisheiði, water production and monitoring wells, and boundaries of the defined industrial area (grey shaded area) and Engidalur water protection zone (red hashed area).

4.2.1 Assumptions

4.2.1.1 Storage reservoir boundary

Storage capacity estimates for the modelled area are confined to the bounds of the storage reservoir shown in Figure 8. This polygon shown in yellow includes the maximum possible extent of the CO_2 from all injection scenarios plus a buffer area to incorporate the uncertainty of modelling. This boundary served as the lateral extents of the clipped storage capacity model shown in Figure 9b.

4.2.1.2 Depth

The minimum depth for injection of CO_2 using the Carbfix method is dictated by the dissolution of CO_2 – the CO_2 must be dissolved at a minimum pressure of 25 bar, which is roughly 250 m below the water table. Regardless of whether the CO_2 is dissolved at the surface and injected under pressure (Carbfix2) or dissolved down-hole (Carbfix1), the ideal depth of injection is below 350 m to ensure solubility trapping and eliminate the risk of the CO_2 degassing (Snæbjörnsdóttir et al., 2014). This minimum depth of injection serves as the upper boundary for the storage capacity model shown in Figure 9b and excludes any volume between this depth and the surface of the combined geologic/alteration model.

4.2.1.3 Temperature

Carbon mineralization has been demonstrated at ambient temperatures (~35°C) at Hellisheidi during pilot injections at Carbfix1 in 2012 (Matter et al., 2016) and temperatures >250°C at Carbfix2 (Clark et al., 2020). Increased temperature has been shown to enhance dissolution and release of cations from glassy basalt and contributes to the overall mineralization rate. The lower boundary for mineral storge in basalt is dictated by the geothermal gradient, and thus the depth of the injection well and reservoir. The thermodynamic stability of carbonates is limited at temperatures > 300°C but can vary in natural conditions. In the Hengill geothermal area, calcite has been observed in drill cuttings at all depths except where the temperature is > 280°C (Fridleifsson, 1991; Larsson et al., 2002). For the storage capacity estimation, the combined model (Figure 8c) was clipped to the 280°C temperature contour and serves as the lower boundary of the storage capacity model since carbonates are not likely to form at temperatures above this.

4.2.1.4 Cation availability

Carbon mineralization requires available divalent metal cations, including Ca^{2+}, Mg^{2+}, and Fe^{2+}, that can combine with CO_2 to form carbonate minerals such as calcite ($CaCO_3$), dolomite ($CaMg(CO_3)_2$), magnesite ($MgCO_3$), siderite ($FeCO_3$), and Ca-Mg and Mg-Fe carbonate solid solutions (Snæbjörnsdóttir et al., 2014). The availability of these cations can be enhanced by promoting the dissolution of Ca,Mg,Fe-rich silicate rocks like basalt (Gislason et al., 2010). The stratigraphy at Hellisheiði is dominated by basaltic lavas and glassy hyaloclastites with abundant cation exchange capacity, thus the storage capacity estimation method assumes favorable rock composition to supply cations and mineralize carbon.

4.2.1.5 Porosity and Permeability

The combined geologic and alteration model generated in Leapfrog was used as the basis for the storage reservoir model to incorporate the variation in porosity with alteration degree. Studies on the permeability and porosity of Icelandic bedrock show that porosity and permeability generally decrease with progressive alteration, gradual burial and increasing rock age as pore space becomes filled by secondary minerals (Frolova et al., 2005; Snæbjörnsdóttir et al., 2014). The

average porosity of rock types in the model are listed in Table 1 as reported by core measurements and experiments on Icelandic reservoir rocks (Frolova et al., 2005; Stefánsson et al., 1997). The Hengill basement was assigned constant low porosity corresponding to reflect its deep burial and significant alteration extent (Snæbjörnsdóttir et al., 2018).

Table 1: Model volumes and average porosity values used for storage potential estimation, reflecting porosity decrease with increased alteration. Most of the average (total) porosity values come from core measurements done on Icelandic rock samples by Stefánsson et al., 1997. Where available (basalt lavas and smectite zone hyaloclastite), specific alteration zone porosities were assigned from published literature. Where specific alteration zone porosities were unavailable, the average value was modified by the corresponding scaling factor in **Table 6**. The Hengill basement was assigned constant low porosity associated with its deep burial and highly altered state. References: (1) Stefánsson et al., 1997 (2) Frolova et al., 2005 (3) Snæbjörnsdóttir et al., 2018.

Rock Types	Model Volumes	Volume (km^3)	Average Porosity (%)	Reference
Innskot (intrusions - correlated to faults)	Innskot, All volumes	2.2	3.68%	(1)*
	Innskot, No Clay	0.0	3.68%	(1)*
	Innskot, Smectite	0.1	2.94%	(1)*
	Innskot, MLC	0.1	0.37%	(1)*
	Innskot, Chlorite	0.1	2.21%	(1)*
	Innskot, Chlorite + epidote	0.4	2.21%	(1)*
	Innskot, Actinolite	1.5	1.84%	(1)*
Moberg (hyaloclastite)	Moberg, All volumes	39.2	29.69%	(1)*
	Moberg, No Clay	1.1	29.69%	(1)*
	Moberg, Smectite	8.2	21.00%	(2)
	Moberg, MLC	11.8	2.97%	(1)*
	Moberg, Chlorite	9.4	17.81%	(1)*
	Moberg, Chlorite + epidote	4.4	17.81%	(1)*
	Moberg, Actinolite	4.3	14.85%	(1)*
Basalt	Basalt, All volumes	12.7	8.09%	(1)***
	Basalt, No Clay	0.7	17.50%	(1)**
	Basalt, Smectite	8.4	6.69%	(1)***
	Basalt, MLC	1.2	0.67%	(1)***
	Basalt, Chlorite	0.4	6.13%	(1)***
	Basalt, Chlorite + epidote	0.3	6.13%	(1)***
	Basalt, Actinolite	1.7	5.00%	(1)*
Hengill Basement	Hengill basement, All volumes	21.2	4.00%	(3)
	Hengill basement, No Clay	0.0	4.00%	(3)
	Hengill basement, Smectite	0.0	4.00%	(3)
	Hengill basement, MLC	0.0	4.00%	(3)
	Hengill basement, Chlorite	5.5	4.00%	(3)
	Hengill basement, Chlorite + epidote	5.7	4.00%	(3)
	Hengill basement, Actinolite	10.0	4.00%	(3)

* - average X scaling factors (table 6)
** - average + 1 standard deviation
*** - average from table 5 in Stefánsson et al., 1997

4.3 Theoretical CO_2 storage capacity of Hellisheiði

The general methodology for calculating CO_2 storage potential via mineralization involves calculating the volume of feasible rocks in the defined storage reservoir, calculating the pore volume available, and assuming a fixed proportion of carbonates that can mineralize in this pore volume. Here, we describe the minimum theoretical potential as the pore volume determined from the porosity assumptions in Table 1.and 10% filled with calcite (Gislason et al., 2010) and the maximum theoretical potential assuming 100% of the available pore volume is filled with calcite (Goldberg et al., 2008). Because the storage potential estimation is based on multiple assumptions

(porosity, alteration degree/scaling factors, modelled volumes, % of porosity filled, etc.), the theoretical storage capacity estimates presented here represent the maximum potential of all rocks in the defined storage reservoir without considering specific injection scenarios. Storage capacity estimates based on specific injection scenario simulations are presented in Table 9 and Table 10. For each scenario, two storage potentials are calculated by applying the average porosity for a specific rocktype to all volumes and using the variable porosities defined in Table 1. With the underlying assumptions, the theoretical storage capacity of the modelled area ranges from 0.84 $GtCO_2$ (minimum variable porosity) to 15.8 $GtCO_2$ (maximum average porosity). Assuming the minimum storage capacity estimate (scenario 1) of 0.84 $GtCO_2$, and the planned injection capacity of 406,000 tCO_2/year (up to 359,000 tCO_2 into intermediate system + 47,000 tCO_2 into deep system), it would take over 2,000 years to be completely filled by carbonate mineralization.

Table 2: Theoretical storage capacity of the modelled area at Hellisheiði. Range of storage capacity estimates based on published methods (Goldberg et al., 2008; Gislason et al., 2010).

			Volume	Porosity	Carbonates	Storage Potential			
	Scenario	Notes	km^3	%	%	$MtCO_2$ (average porosity)	$MtCO_2$ (variable porosity)	$GtCO_2$ (average porosity)	$GtCO_2$ (variable porosity)
1	Gislason et al., 2010	*Minimum - All carbonates as calcite*	75.26	see Table 1	10%	1577.87	835.74	1.58	**0.84**
2	Goldberg et al., 2008	*Maximum - All carbonates as calcite*	75.26	see Table 1	100%	15778.73	8357.43	15.78	**8.36**

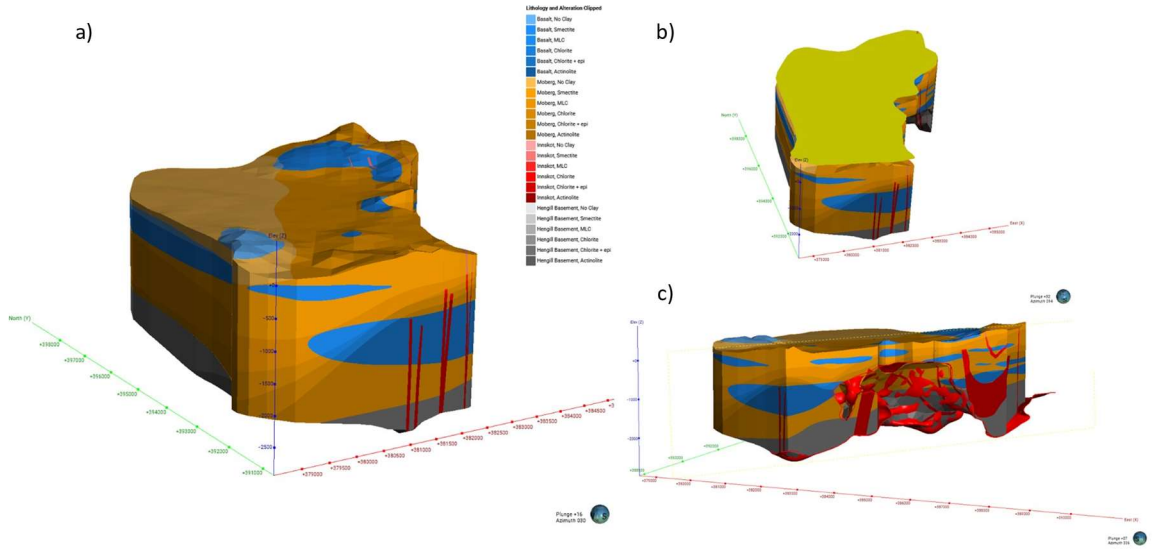

Figure 9: Storage capacity model. 9a) Clipped geologic/alteration model showing the combined models. Increased alteration intensity is represented by darker shades of the corresponding lithology color. 9b) Yellow storage reservoir boundary shown above clipped model to show the intermediate steps to clip the model by the lateral extent of the reservoir and the depth constraint (-350 masl). 9c) Side view showing the 280°C temperature contour (red surface) that was used to exclude model volumes outside of the thermodynamic stability of calcite.

5 Modeling scenarios: Injected amount and injection sites

Figure 10 shows existing and planned well locations for the Carbfix injection operations in Hellisheiði as well as existing and planned water production and monitoring wells. The location of planned wells is preliminary and may change. The following subchapters describe the current CO_2 injection scheme and the modeled injection scenarios for the purpose of the EIA.

5.1 Geological storage in the intermediate system

5.1.1 Scenario considered

The three main scenarios are considered in this work namely:

- Scenario 1: full reinjection of up to 355,000 tCO_2/yr into the intermediate system within the Geothermal Park and up to 4,000 tCO_2/yr into the intermediate system at Þrengsli
- Scenario 2: reinjection of up to 155,000 tCO_2/yr into the intermediate system at the Geothermal Park, up to 200,000 tCO_2/yr into the intermediate system at Gráuhnúkar, and up to 4,000 tCO_2/yr into the intermediate system at Þrengsli
- Scenario 3: reinjection of up to 130,000 tCO_2/yr into the intermediate system at the Geothermal Park, up to 200,000 tCO_2/yr into the intermediate system at Gráuhnúkar, and up to 29,000 tCO_2/yr into the intermediate system at Þrengsli.

These have been chosen to assess the impact of large-scale injection operations at the Geothermal Park and at Gráuhnúkar and are depicted visually in Figure 10.

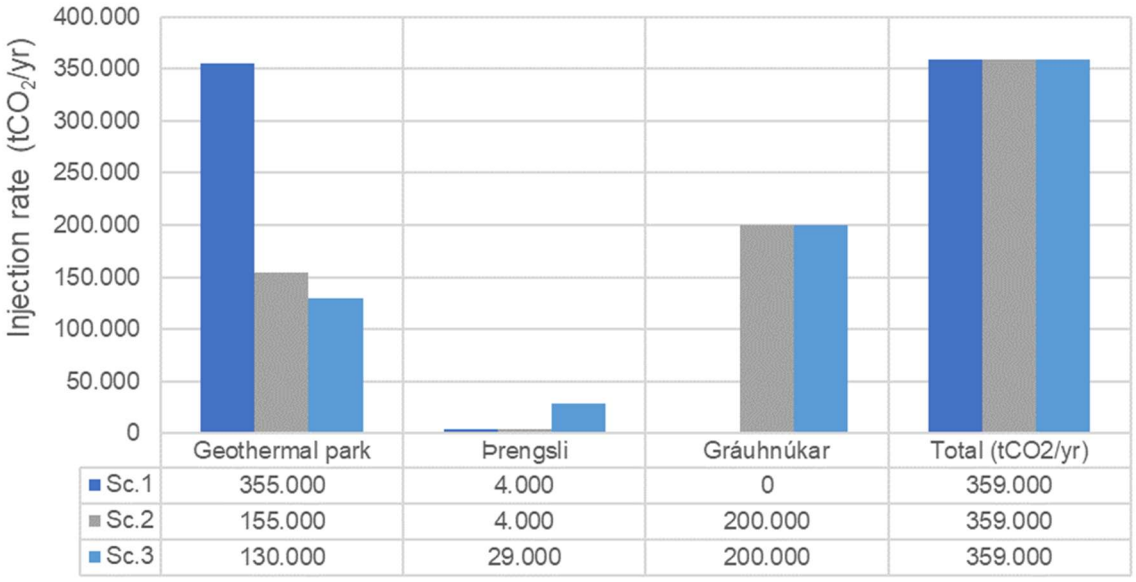

Figure 10: Primary injection scenarios considered in the modeling work.

In addition, two variations of Scenario 1 have been included to investigate the impact of injecting CO_2 in the intermediate system at different injection sites in the vicinity on the Geothermal Park. These scenarios are depicted visually in Figure 11 and include:

- Scenario 1b: include injection of up to 50,000 tCO_2/yr in two wells located at the Husmuli – intermediate site and,
- Scenario 1c: include injection of up to 50,000 tCO_2/yr in two wells at Sleggjubeinsdalur in addition to the 50,000 tCO_2/yr in the Húsmúli – intermediate site from scenario 1b (Figure 10)

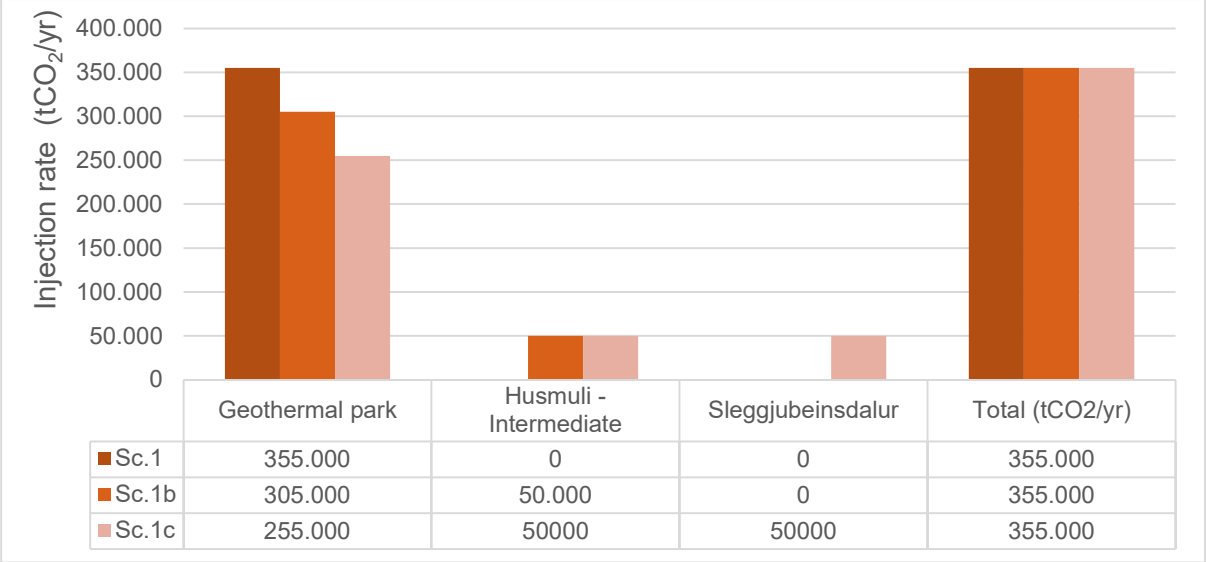

	Geothermal park	Husmuli - Intermediate	Sleggjubeinsdalur	Total (tCO2/yr)
Sc.1	355.000	0	0	355.000
Sc.1b	305.000	50.000	0	355.000
Sc.1c	255.000	50000	50000	355.000

Figure 11: Additional injection scenarios considered in the modeling work.

5.1.2 Injection wells

- A maximum of 36 new injection wells (HC-01 to HC-36) have been included in the model in the Geothermal Park (Scenario 1, 2, 3), Gráuhnúkar (Scenario 2, 3), and Þrengsli (Scenario 3). The maximum number of wells in use is 22.
- Two existing injection HN-02 and HN-04 is also included in the model.

5.1.3 Water production

Water production from shallow groundwater is included in the model. On one hand production wells specifically intended to produce water for the CO_2 injection plans are included and on the other hand, ON Power´s current cold water production wells for the thermal plant and other use are included.

Nine production wells (HU-wells) are located in the Engidalur valley where ON Power produces cold water. The largest portion of the water is used for hot water production, but it is also used for cooling purposes in the power plant, as a cold-water source for the Geothermal Park and as drinking water in the area. The Engidalur production area is also the emergency drinking water production area for the capital region. ON Power has a permit to produce 2000 L/s of water from Engidalur. The annual average production in 2021 was ~900 L/s but production will increase up to 2000 L/s in coming years with expansions of the thermal plant in Hellisheiði and other uses.

5.1.4 Model assumptions

- The CO_2 can be injected in a gaseous or dissolved form, however the model assumes that it is fully dissolved prior to entry into reservoir.
- The water/CO_2 ratio is equal to 25/1.
- The injection temperature is 20ºC.
- A maximum of 25,000 tCO_2/yr per well which represents an injection rate of ~20 kg/s.
- Four feedzones for each new injection well (HC wells) and the injection of the dissolved CO_2 is distributed evenly over the feedzones.

Table 3: CO_2 injection well, feedzones depth and contribution. For all new wells (HC wells), four feedzones were included in the model. However, these will be updated once the wells are drilled and feedzones are logged.

Wells	Feedzones depth (masl)	Contribution (%)
HN-02	-266	1
HN-04	-144	1
HC wells	-100, -200, -300, -400	0.25, 0.25, 0.25, 0.25,

5.2 Geological storage in the deep system

5.2.1 Scenario considered

Current CO_2 injection into the deep geothermal system at the Húsmúli site is approximately 12,000 tCO_2/yr. In 2025 this will be increased to 47,000 tCO_2/yr with the commissioning of the Silverstone capture plant. The CO_2 and H_2S captured are sourced from the same geothermal reservoir and therefore there is no overall increase in CO_2 and H_2S in the deep geothermal system.

No further injection into the deep system is planned.

Three different injection strategies are included to discuss the fate of the injected CO_2 and potential impact on the geothermal reservoir and resource:

- Scenario 1: CO_2 (and H_2S) injection in HN-16
- Scenario 2: CO_2 (and H_2S) injection in HN-16 and HN-14
- Scenario 3: CO_2 (and H_2S) injection in HN-16, HN-14, HN-12, and HN-09

5.2.2 Injection wells

- Injection wells: HN-09, HN-12, HN-14, HN-16

5.2.3 Water production

Geothermal fluid production from the geothermal wells located within the area considered are included.

- Monitoring wells: HE-31, HE-48, HE-44
- Geothermal wells: HE-31, HE-48, HE-44, HE-33, HE-46, HE-05

5.2.4 Model assumptions

- The water/CO_2 ratio is equal to 25/1.
- The injection temperature is 20ºC.

Table 4: CO_2 injection well, feedzones depth and contribution.

Wells	Feedzones depth (masl)	Contribution (%)
HN-09	-1202, -1333, -1496, -1906, -2230	0.143, 0.143, 0.214, 0.214, 0.143

HN-12	-364, -1459	0.4, 0.6
HN-14	-989, -1452	0.375, 0.625
HN-16	-712, -990, -1380, -1520, -1601	0.25, 0.125, 0.25, 0.25, 0.125

6 Material and method

The numerical simulations are carried out with a finite volume code, TOUGH2 (Transport Of Unsaturated Groundwater and Heat). TOUGH2 is a multiphase flow and transport simulation program for fractured and porous media (Pruess, 1991). The TOUGH suite of codes is widely used for geothermal applications and is for example used for the reservoir management of the Hengill geothermal system (G. Gunnarsson et al., 2011). The TOUGH2 simulator as implemented in forward mode in the iTOUGH2 program (Finsterle, 2007) was used to iteratively solve the governing equations.

6.1 Governing equations

The governing equations solved by TOUGH2 describe the conservation of mass and energy in the system. The change in mass/energy in a given subdomain V_n resulting from fluxes across enclosing surface A_n is represented as:

$$\frac{d}{dt}\int_{Vn} M^K dV_n = \int_{An} F^K \cdot dA_n + \int_{Vn} q^K dV_n \qquad \text{Eqn. 1}$$

where M^K represents the mass or energy per unit volume of the component κ. $F^K.dA_n$ is the flux of component κ into V_n normal to surface A_n. q^K denotes sinks and sources. Eqn. 1 expresses that the rate of change of fluid mass in V_n is equal to the net inflow across the surface of V_n plus net gain from the fluid sources. Advective flux is defined for each component κ:

$$F^K|_{adv} = \sum_\beta X_\beta^k F_\beta \qquad \text{Eqn. 2}$$

and individual phase flux is given by Darcy's law:

$$F_\beta = \rho_\beta u_\beta = -K\frac{K_{r\beta}\rho_\beta}{\mu_\beta}(\nabla P_\beta - \rho_\beta g) \qquad \text{Eqn. 3}$$

where F_β is the flux of phase β, ρ_β is the density of phase β, u_β is the Darcy velocity in phase β. K is the absolute permeability, $K_{r\beta}$ is the relative permeability of phase β, μ_β is the viscosity of phase β, P_β is the sum of the pressure of a reference phase and the capillary pressure and g is the vector of gravitational acceleration. Transport is controlled by advection and dispersion was not included in this modelling work. Molecular diffusion was included in the modelling framework because while the transport is dominated by the high advection velocities within the fracture network at the injection site, matrix diffusion may be an important process in retarding movement of solutes and attenuating their concentrations (Walter, 1982). Diffusive flux is written as being proportional to the gradient in the concentration of the diffusing component (Fick's law):

$$f = -d\nabla C \qquad \text{Eqn. 4}$$

where d is an effective diffusivity, which in general will depend on properties of the diffusing component, the pore fluid, and the porous medium and C the concentration variable. Heat transfer is controlled conduction and convection solved in the following equation for both heat flux.

$$F^{NK+1} = -\lambda \nabla \mathrm{T} + \sum_{\beta} h_{\beta} F_{\beta}$$ Eqn. 5

with λ as thermal conductivity and h_{β} is the specific enthalpy in phase β. Description of thermodynamic conditions assumes local equilibrium of all phases. TOUGH2 uses an integral finite difference (IFD) method for space discretization, and first-order fully implicit time differencing. The resulting strongly coupled, nonlinear algebraic equations are solved simultaneously using Newton-Raphson iterations for each time step. Time steps can be automatically adjusted during a simulation run, depending on the convergence rate of the iteration process. The IFD method avoids any reference to a global system of coordinates and is applicable to regular or irregular discretization in one, two, and three dimensions. The IFD method also makes it possible, to implement double- and multiple-porosity methods for fractured media.

6.2 MINC formulation

Multiple Interacting Continua (MINC) is a method used to model fluid and heat flow in fractured media (Pruess & Narasimhan, 1982, 1985). The concept is based on the notion that changes in fluid pressures, temperatures, phase compositions, etc. due to the presence of sinks and sources (production and injection wells) will propagate rapidly through the fracture system while invading the tight matrix blocks only slowly. In the MINC approach the fractured porous reservoir is divided into several computational volume elements: fractures and nested matrix blocks. Fractures blocks are inter-connected and represent the fracture network. Each set of nested matrix blocks is connected to a fracture block and changes in matrix conditions will (locally) be controlled by the distance from the fractures. Fluid and heat flow from the fractures into the matrix blocks, or from the matrix blocks into the fractures, can then be modelled employing one-dimensional strings of nested grid blocks. This approach is well adapted to approximate fracture flow in a porous medium.

7 Reservoir modelling – Transport Model

7.1 Reservoir modelling workflow

Reservoir modelling plays an important role in the reservoir management of the mineral storage operations at Hellisheiði as it provides tools to predict and optimize the long-term management of the injection of dissolved CO_2 and contributes to the safe application of this carbon storage method. Comparison between the observed and modelled behavior of the subsurface CO_2 transport and mineralization is an integral part of the verification process as part of conformance monitoring. The ability to model the fate of the injected CO_2 as well as to quantify the amount of CO_2 that can be mineralized is also beneficial to increase the overall confidence in the effective permanent storage of CO_2. The formations are fresh and permeable, ensuring flow paths for the injected CO_2-charged fluid and reactive surfaces contributing to the mineralization process.

Two reservoir models were developed to simulate the injection of CO_2 in the intermediate system and the deep geothermal system. In the following section we will present the model assumption, characteristics, and results for both models.

The workflow developed consists of:

1. A conceptual model of the system, describing the main physical processes.

2. Description of the numerical grid is provided.
   The grids used are irregular with different levels of refinement, ranging from large blocks at the outskirts of the model to smaller blocks at the injection site(s) (Figure 13). This configuration decreases the computational cost of the simulation while preserving a high level of detail in the area of interest. The multi-scale heterogeneity in the reservoir can be

represented by a finer grid by assigning individual blocks with a corresponding rock-type. In particular, a finer grid enables the model to include the individual structural features such as faults allowing the modelling of discrete flow paths for the geothermal fluid. Local refinement of the grid is carried out by performing a Delaunay triangulation of the transition zone in which blocks of intermediate size is created (A. E. Croucher & O'Sullivan, 2013). The connections are usually not orthogonal and may introduce mass balance errors in the IFD solution. This is addressed by optimizing the connection angle block geometry using a non-linear least squares optimization formulation at the transition zone between blocks.

3. Geological representation and permeability field.
   The subsurface geology described in the geological model (4. Conceptual model of Hellisheiði) is represented in the numerical model by defining a rock-type for each geological unit which populates the three-dimensional array of blocks that covers the model area (Figure 13). The rock-type parameters represent the properties of each geological unit. Distinct hydrogeological parameters (permeability, porosity, density, conductivity, etc.) are then assigned to each rock-type to represent the characteristic of each unit. This represents the single porosity model and introduces the heterogeneity and anisotropy for specific units (e.g., faults).

4. Representation of flow process – MINC approach
   Flow through a basaltic sequence is controlled by the fractures found within the reservoir. The fractures provide the high permeability conduits for the transport of fluid while the rock matrix has low permeability. This has been confirmed by tracer tests conducted at Hellisheiði and neighboring Nesjavellir geothermal fields (Kristjánsson et al., 2016). This can be represented by applying a Multiple Interacting Continua (MINC) approach to discretize the grid into three continua: one fracture block and two nested matrix blocks.

   Fracture volume proportion for each block was then defined and partitioning of the single porosity mesh into three computational volume elements to create a triple-porosity grid was generated using the MINC function in the PyTOUGH library (A. Croucher, 2015). The fracture porosity was chosen such that effective porosity of the dual porosity model is the same as the porosity of the single porosity model (Eqn. 6):

$$\theta_{eff} = \theta_f V_f + \theta_m (1 - V_f), \qquad \text{Eqn. 6}$$

   Where θ_{eff}, θ_f, and θ_m are the effective, fracture, and matrix porosities and V_f is the fraction of the total block volume occupied by the fractures.

5. Boundary Conditions were defined for each model.

6. Initial conditions for both models were extracted from the numerical model of the Hengill geothermal resource (G. Gunnarsson et al., 2011). This model is developed and maintained by Reykjavik Energy and simulates the production from Hellisheiði and Nesjavellir geothermal fields for resource management purposes (G. Gunnarsson et al., 2011). The Hengill model covers a larger area and the grid is coarser than the grid developed in this study (Figure 13). The values were interpolated using a spatial three-dimensional Delaunay triangulation.

7.2 Reservoir model of the intermediate system at Hellisheiði

Reservoir models were developed to represent the injection of CO_2 into the Intermediate system at Hellisheiði. The model extends from the top surface of the groundwater to -2500 masl within the deep geothermal system. In the following section, the models are described and the results from the scenarios (section 5.1) are shown.

7.2.1 Conceptual Model of the intermediate system

- The flow within the intermediate system is controlled by contact zones of basaltic layers and hyaloclastite units. These boundaries are glassy, porous and highly permeable.

- Hyaloclastite formations are found down to ~ 400 m, below which are basalts and tuffs that extend beyond the depth of planned injections in the intermediate system at ~ 800 m.
- This hyaloclastite formation is thought to act as a cap that contains the intermediate system. In these areas groundwater is found at depths ranging from 50-100 m.
- Temperature ranges from 50°C to 200°C at depths of 300-700 m.
- At depth ranges between 350-750 m smectite-zeolite alteration is common. Smectite, calcite, ca-rich zeolites and iron oxide are found in the intermediate system. The bottom of the intermediate system is demarcated by the low-resistivity boundary of the mixed-layer clay zone.

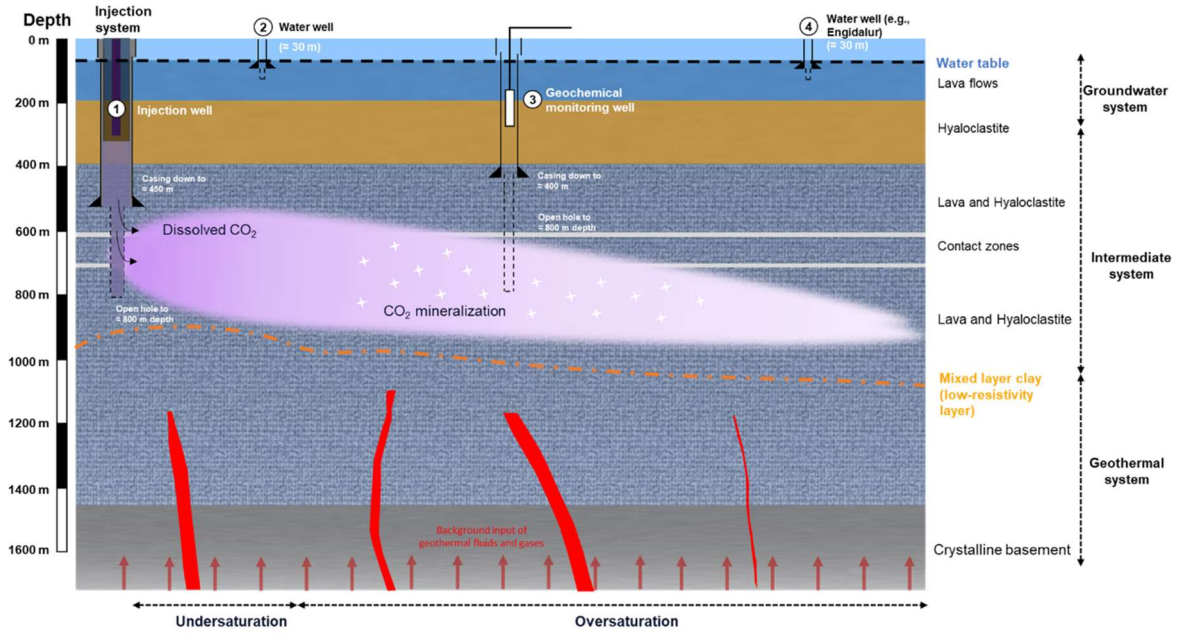

Figure 12: Conceptual model of the intermediate system at Hellisheiði. CO_2 is dissolved in water and injected into wells that are cased to ~ 400 m and open hole down to ~ 800 m (1). Water is produced from shallow water wells (2) and from cooling towers at Hellisheiði power plant. Flow of CO_2 in the intermediate system is predicted to be confined below by a low-permeability mixed-layer-clay (MLC) layer and separated from the groundwater system above by dense hyaloclastite formations. Geochemical monitoring wells (3) will be placed between the injection site and sensitive environmental areas such as the Engidalur water protection zone (4) to ensure no significant impact from CO_2 injections.

7.2.2 Grid Structure

The three-dimensional model covers an area of 400 km^2 (20 km × 20 km) and is large enough to encompass the geological storage reservoir (Figure 13). The grid used is irregular with four levels of refinement; blocks range from 1 km by 1 km at the outskirts of the model to 62.5 m by 62.5 m at the injection site(s). This configuration decreases the computational cost of the simulation while preserving a high level of detail in the geological storage reservoir.

The model is made up of 68 layers ranging from 400 masl to -2500 masl and with a thickness comprised between 100 m and 25 m. A minimum thickness of 25 m was assigned to reservoir depth between the casing depth (400 m) and bottom depth (800 m). The water table fluctuates and has been at different elevations over the time span that the model covers (from 1972). Fluctuations in water table elevation cause shifts in the location of water divides in the Hellisheiði Power Plant area. Vatnaskil extracted water level contours from the model at two different times to illustrate this difference in groundwater divides, May 1980 when the divides close to the power plant lie far north

and July 1994 when they lie far south. For simplification purposes, the top of the model was set to follow the top of the water table for the 1994 groundwater levels (Vatnaskil, 2021).

It is noted the groundwater levels used from 1994 are well calibrated with the available data from the groundwater wells, with the exception of the future development area of the Geothermal Park. The top surface of the groundwater used is approximately 50 meters lower than the measured groundwater level. This impacts the water height above the intermediate system. Therefore, around the Geothermal Park, the current model will underestimate by approximately 5 bar the resulting hydrostatic pressure which may otherwise provide additional confining pressure support on the intermediate system.

7.2.3 Geology and Permeability Field

The multi-scale heterogeneity in the reservoir is represented by assigning individual blocks with a corresponding rock-type. The distribution of the rock-type is based on the geological model described in section 4 (Figure 13).

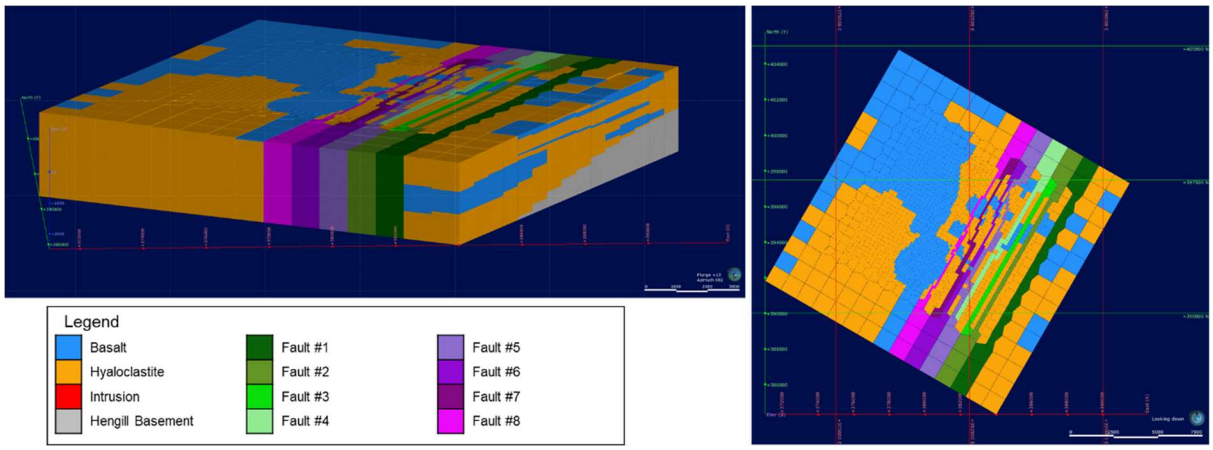

Figure 13: Rock-type distribution (lithology and faults) as implemented in the numerical model.

The rock-type parameters represent the properties of each geological unit: basalt sequence, hyaloclastites, dyke intrusions, crystalline basement, faults (Table 5). Contact zones between lithological units are represented by a distinct rock-type. They represent the contact zones between lithological units in which the feedzones in the groundwater and intermediate systems are mostly found.

Table 5: Permeability and porosity values for the rock-types defined in the single porosity model. Rock grain density (ρr) is set at 2,600kg/m3, rock grain specific heat (Cp) is 900 kJ/kg.K, and formation heat conductivity under fully liquid-saturated conditions (κr) is 1.5 W/m.K.

	Porosity (%)	Permeability (millidarcy)		
		k_1	k_2	k_3
Basalt	10	0.5		0.1
Hyaloclastite	20	0.1		0.02
Intrusion	5	0.01		0.01
Fault	10	0.0005	0.0001	12

Contact zone 1	15	5000	1000
Contact zone 2	12	50	10
Contact zone 3	12	1	0.5
Contact zone 4	12	100	50

The impact of the alteration state on the subsurface lithologies was included by assigning a factor to the permeability and porosity values. This scaling factor is based on the decline in porosity with varying degrees of alteration described by Stefánsson et al., 1997.

Table 6: Scaling factor for porosity and permeability as a function of alteration type.

Alteration	Porosity	Permeability
- *Fresh*	1	1
- *Smectite*	0.8	0.8
- *Mixed layer clay*	0.1	0.01
- *Chlorite-epidote*	0.6	0.6
- *Chlorite-actinolite*	0.5	0.5

7.2.4 Representation of Flow Process

Fractures characteristics in the intermediate system is currently not well constrained therefore four realizations are modelled with the fracture volume fraction ranging from 15 to 40% of the total block volume for each scenario. The matrix was assigned a low porosity fixed at 2.5%.

Table 7: Model realizations for varying fracture volume fractions. Matrix permeability is isotropic where $k_1=k_2=k_3$.

Model realization	Volume fractions			Matrix porosity (%)	Matrix permeability (k_1,k_2,k_3) millidarcy
	Fracture	Matrix 1	Matrix 1		
A	0.15	0.1	0.75	2.5	0.1
B	0.2	0.1	0.7		
C	0.3	0.1	0.6		
D	0.4	0.1	0.5		

7.2.5 Boundary Conditions

A Dirichlet boundary condition is applied to the top boundary by assigning atmospheric conditions at the top surface (1 bar, 5°C). The atmosphere is therefore considered as an open boundary condition and fluid can flow in and out of the system. An annual rainfall of 4,000 mm in the area with an infiltration rate of 60% is represented by cold water injected into the top of the model (Figure 14). All the side boundaries are assumed to be closed, i.e., no heat or mass is coming into or going out of the system. This approximation is valid provided the side boundaries are located sufficiently far from the active system. A conductive flow of heat of 80 mW/m^2 is applied at the bottom of the

model to represent the natural geothermal gradient at the site. Net mass flow under natural conditions is only through the top and bottom. The bottom layer has low permeability, but it is high enough to allow a limited amount of fluid to flow in and out, thereby considering the interaction with the deeper parts of the system. Mass of the injected fluid is set to ~1 kg/s per element, and the enthalpy is set to ~1,400 kJ/kg, which corresponds to temperature of ~310ºC.

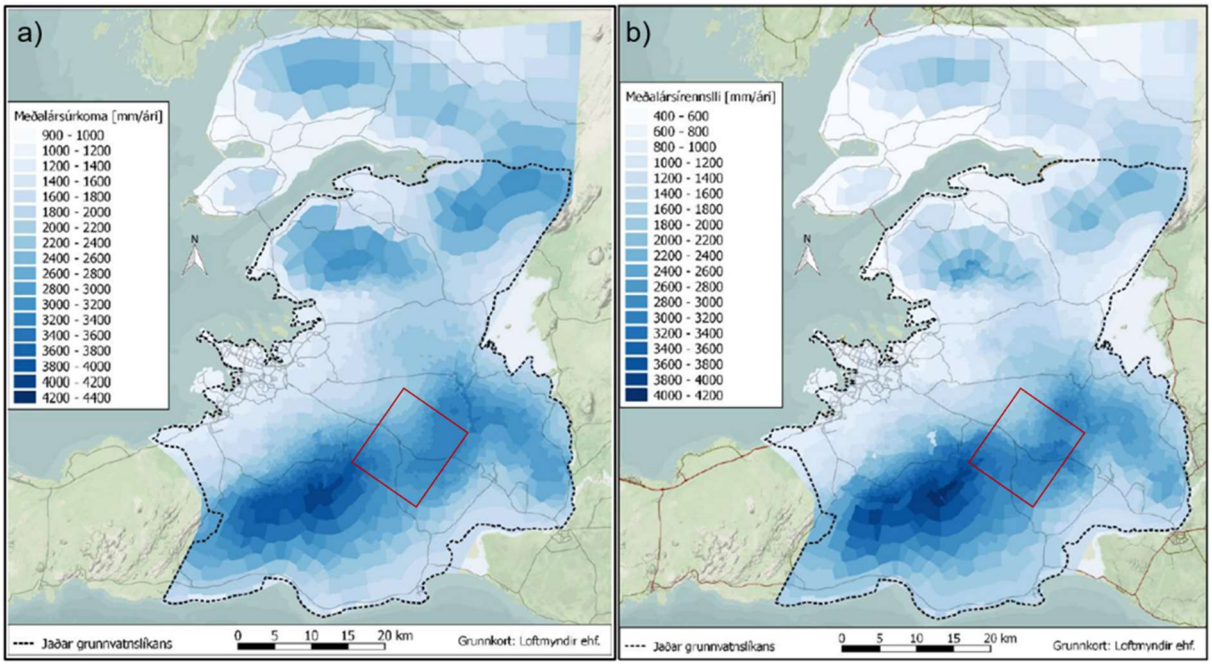

Figure 14: Rainfall and infiltration model of the capital area. a) Estimated annual average precipitation in mm/year and b) estimated annual average infiltration in mm/year (Vatnaskil, 2019). The areal extent of the geological model is indicated by the red box.

7.2.6 Initial Conditions

The initial conditions (temperature, pressure and gas saturation) for the reservoir models were extracted from the numerical model of the Hengill geothermal resource which covers a larger area (G. Gunnarsson et al., 2011). This model is developed and maintained by Reykjavik Energy and simulates the production from Hellisheiði and Nesjavellir geothermal fields for resource management purposes (G. Gunnarsson et al., 2011). The values were interpolated using a spatial three-dimensional Delaunay triangulation and assigned to the new grid (Figure 15).

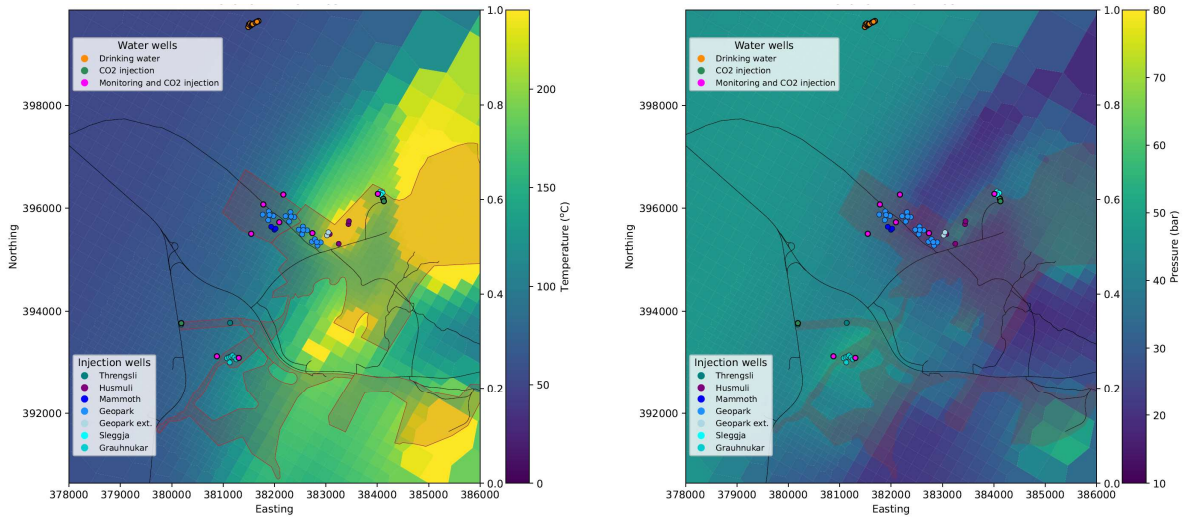

Figure 15: Temperature (left) and pressure (right) distribution of the baseline condition of the Intermediate system (260 masl) used as initial conditions for the scenario forecasts.

7.3 Reservoir model of the deep system at Hellisheiði

Reservoir models were developed to represent the injection of CO_2 into the deep geothermal system at the Húsmúli site at Hellisheiði. A full description of the model that was calibrated against tracer tests can be found in (Ratouis et al., 2022). In the following section, a short summary of relevant model parameters and the results from the different scenarios (section 5.2) are shown.

7.3.1 Tracer tests

A comprehensive tracer test was conducted in 2013 at the Húsmúli reinjection site to define the hydrological flow paths and to provide data to evaluate the risk of thermal breakthrough between injection and production wells (Kristjánsson et al., 2016). The tracer test involved the injection of different naphthalene sulfonic acid (NTS) tracers into three different injection wells located in the Húsmúli reinjection area (Kristjánsson et al., 2016).

In addition, in 2014 at the start of the Carbfix 2 injection, a thermally stable inert tracer was added to the gas-charged water to monitor the fate of the dissolved gases after their injection in HN-16. It enables the quantification of the mineralization of the injected CO_2 and H_2S by mass balance calculations of the injected CO_2 (Clark et al., 2018; I. Gunnarsson et al., 2018). This was followed by a slug tracer test in HN16 in 2018 to monitor any changes to the flow path during the Carbfix injection from 2014 to 2018. The timing of the peak is consistent between the 2013 and 2018, showing that the maximum and average velocities of the main fractures between the injection and the monitoring wells have remained unchanged (*Carbfix 2, Deliverable 3.2*, 2020).

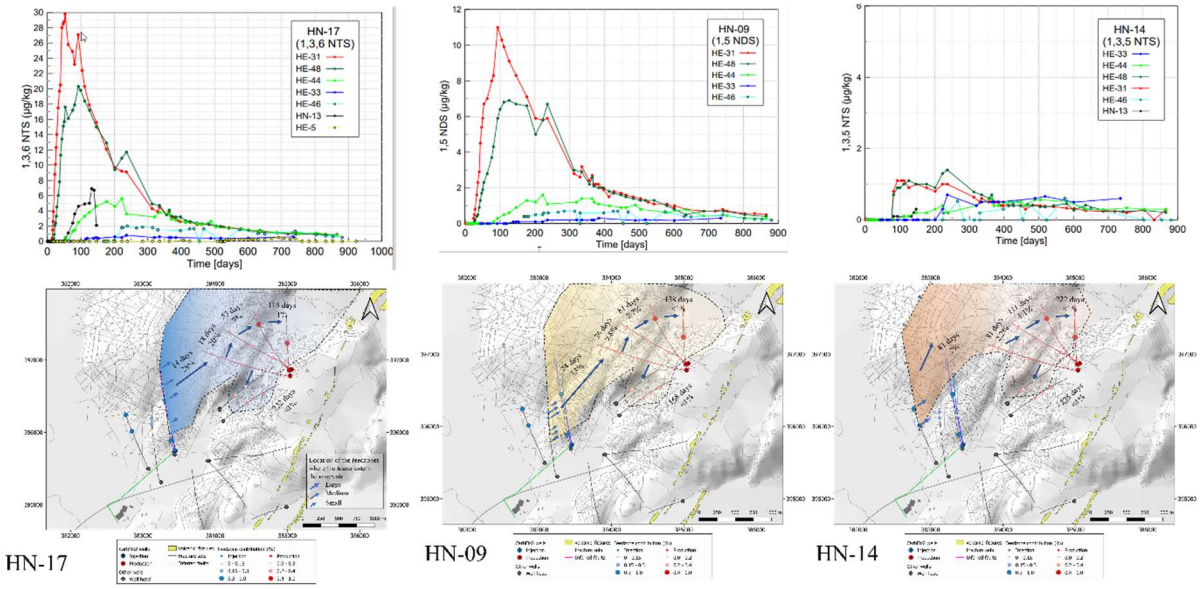

Figure 16: 2013 tracer tests and interpretations

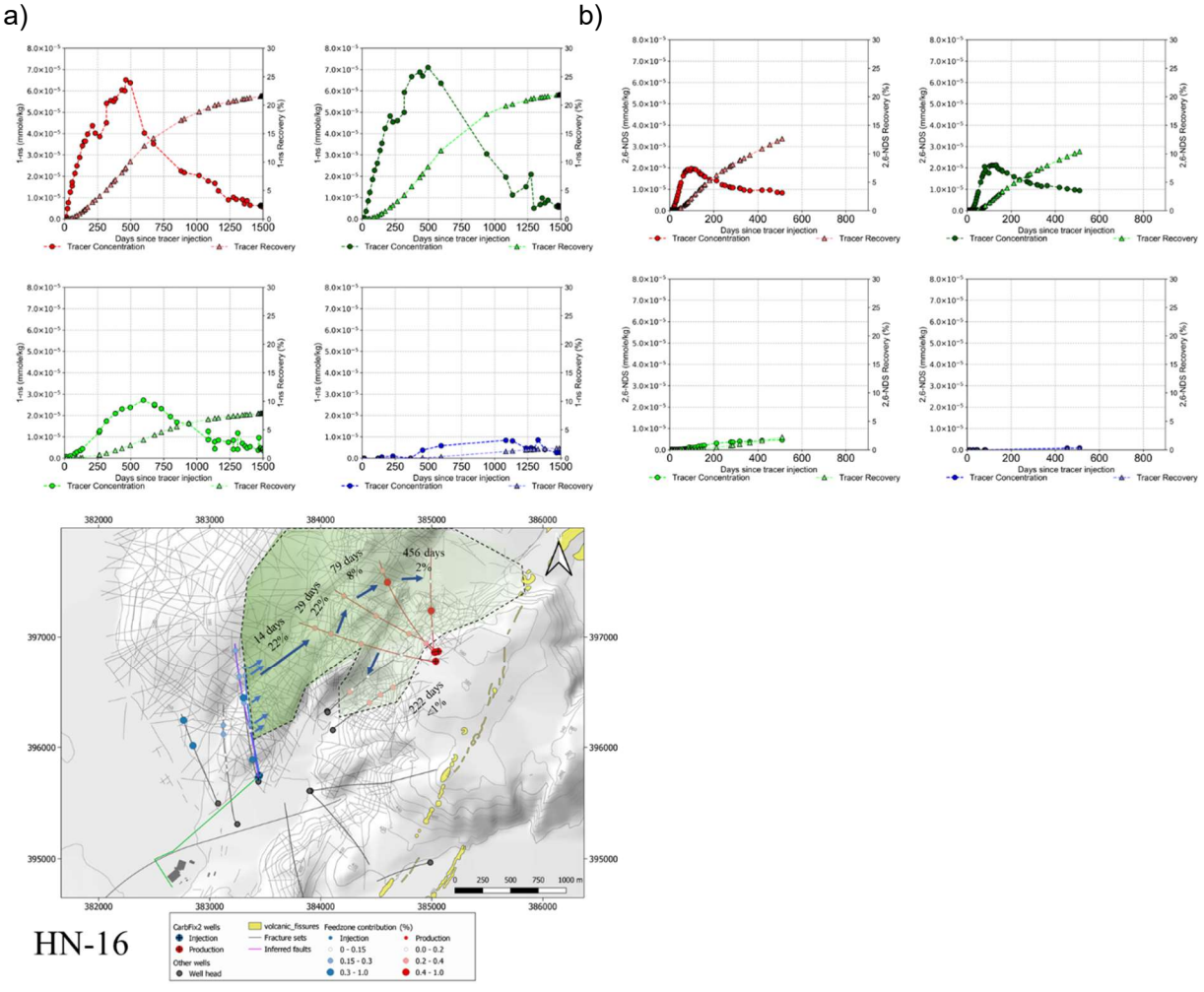

Figure 17: 2014 and 2018 HN-16 tracer tests. Above are recovery curves for tracer test in a) 2014 and b) 2018.

7.3.2 Conceptual Model of the deep system

Large faults are believed to control the flow at Húsmúli by providing favorable conduits along the length of the fault and impeding the flow across the fault face. This is substantiated by surface fault mapping, televiewer, and tracer recovery in the monitoring wells and lack of tracer return in wells located south of the area indicates a strongly anisotropic permeability structure at Húsmúli (Kristjánsson et al. 2016). The conceptual model includes tectonic configurations identified by Khodayar et al. (2015) and NNE trending faults identified at the surface in the vicinity of the Húsmúli re-injection site (Gunnarsdóttir & Poux, 2016). The conceptual model is described in (Ratouis et al., 2022)

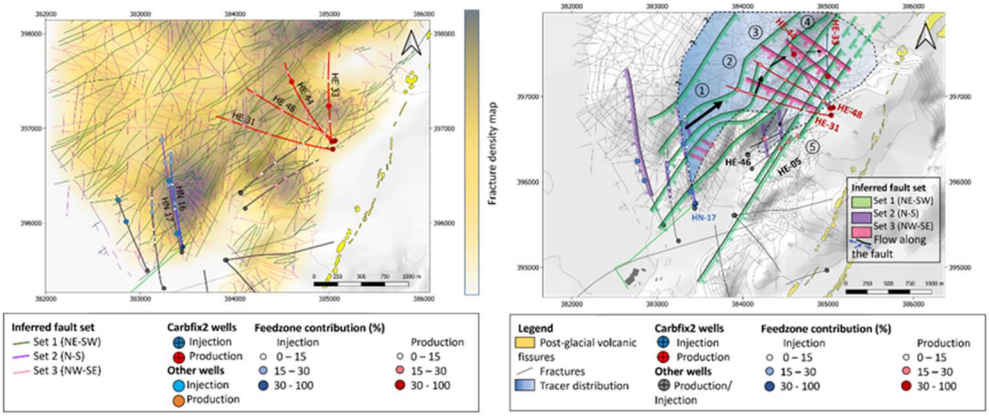

Figure 18: Fracture trace and density map at the Húsmúli site (left). Conceptual model - Aerial map of the conceptual model of the flow paths at the Húsmúli re-injection site (right). The figure shows the main transport routes of the tracer injected into well HN-17 (black arrows) and tracer distribution (peak value %). The travel time (first arrival) from the reinjection well to production well and the recovery at the end of the tracer test are as follows: HE-31: 14 days, 22% (1); HE-48: 29 days, 22% (2);HE-44: 79 days, 8% (3);HE-33: 456 days,2% (4);HE-46: 222 days, <1% (5);HE-05: No tracer recovered.

7.3.3 Grid Structure

The model developed in this study is a three-dimensional model centered on the Húsmúli re-injection zone and the nearby Skarðsmýrarfjall production zone (Figure 18). The model covers an area of 42 km^2 (6 km x 8 km) and the lateral extent of the model was set large enough to encompass the flow paths between Húsmúli and Skarðsmýrarfjall while avoiding boundary effects (Figure 19).

The model is made up of 68 layers ranging from 400 masl to -2500 masl and with a thickness comprised between 100 m and 25 m. Layers with a high feedzone density were set to have a minimum thickness of 25 m (Figure 19). The present model in its single porosity configuration has a total of 81,600 active blocks and 242,808 connections. The grid was rotated and aligned along an NE direction parallel to the rift and some of the large NE faults found in Húsmúli (Figure 18).

7.3.4 Geology and Permeability Field

The multi-scale heterogeneity in the reservoir is represented by assigning individual blocks with a corresponding rock-type. The distribution of the rock type is based on the geological model described in section 4 (Figure 19).

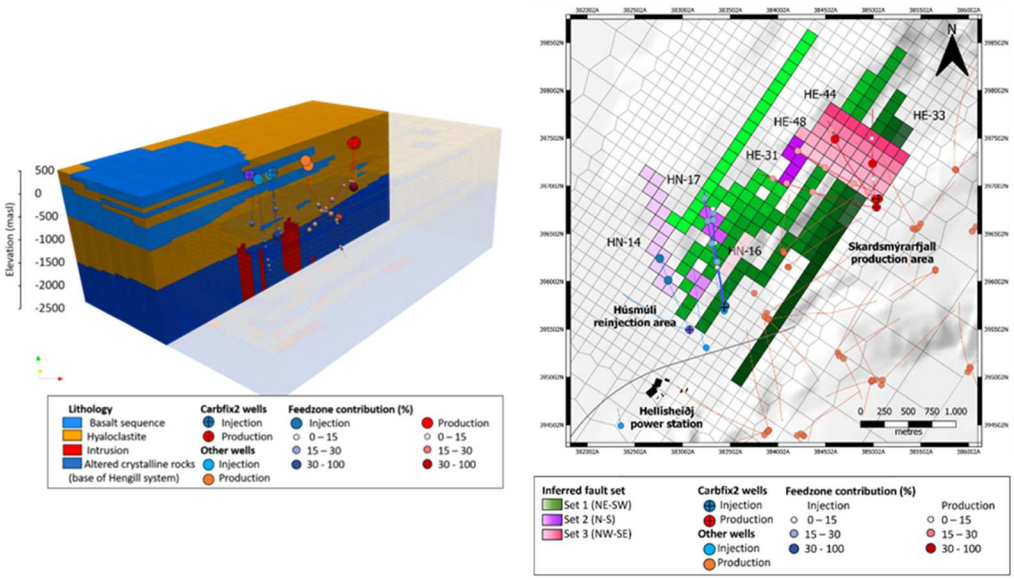

Figure 19: Three-dimensional view of the numerical grid (left). Rock-type distribution of the tectonic features in the numerical model (right). Injection wells are shown in blue and production/monitoring wells in red as well as the respective feedzones.

The rock-type parameters represent the properties of each geological unit: basalt sequence, hyaloclastites, dyke intrusions, faults, and cap rock. The rock-types are characterized by horizontal isotropy, in which the permeability in the x (k1) and y (k2) direction are equal. Individual tectonic structures based on the conceptual model were then explicitly represented (Figure 19). This introduces anisotropy in the model and reflects the tectonic controls on the flow paths at Húsmúli.

The model was calibrated using results from the tracer tests conducted at the Húsmúli site in 2013 and 2014 (Ratouis et al., 2022).

7.3.5 Representation of Flow Process

The current model for the deep geothermal system considers a single porosity approach. Tracer tests conducted at Húsmúli suggest that the main flow occurs through the fracture system (Figure 18) leading to rapid tracer return at the monitoring wells in Skarðsmýrarfjall. The MINC approach can effectively simulate the nested flow in fracture and matrix blocks that control transport in the deep geothermal system. Table 8 below shows the fracture and matrix block parameters used to model the injection of CO_2 into the deep geothermal system at Húsmúli and will serve as the basis for future updates to the model to incorporate fracture and matrix flow (Ratouis et al., 2022).

Table 8: Fracture and matrix properties for rock-types in Húsmúli from Ratouis et al., 2022.

	Fracture				Matrix			
	k_1	k_2	k_3	ϕ	k_1	k_2	k_3	ϕ
Faults set 1	200–5000	5	10–500	0.1	0.1	0.1	0.1	0.1
Faults set 2	100–5000	10–100	10–200	0.1				
Faults set 3	50–150	10–20	10–50	0.1				
Basalt	5–10	5–10	0.5–2	0.1				
	- fresh	100	100	20	0.1			
	- outer	0.05–0.1	0.05–0.1	0.005–0.02	0.1			
Hyaloclastite	15–50	15–50	2–10	0.1				
	- fresh	100	100	20	0.1			
	- outer	0.05–0.1	0.05–0.1	0.005–0.02	0.1			
Intrusion	1–5	1–5	2–10	0.1				
	- fresh	100	100	20	0.01			
	- outer	0.01–0.05	0.01–0.05	0.02–0.1	0.1			
Caprock	1	1	1	0.1				

7.3.6 Boundary Conditions

The water table at Hellisheiði is shallow and located a few tens' of meters below the surface. The cold-groundwater surface is not connected hydraulically to the geothermal systems due to the presence of a self-sealing mixed clay layer (G. Gunnarsson et al., 2011) and fluid injections impose negligible fluid pressure changes at shallow depth. Therefore, the top of the model was set to a Dirichlet boundary condition (fixed pressure) and elevation was set to the top of the water table. The lateral boundaries to the NW, SW, and SE have been set as closed boundaries. The regional flow suggests very limited flow from these directions and no boundary feedback was observed on the edge of the model domain (negligible pressure changes) during simulation. A fixed pressure boundary condition was applied to the blocks located at the northern edge of the grid to allow for natural recharge as the regional flow suggests. The bottom layer of the model has been set as a closed boundary.

7.3.7 Initial Conditions

The initial conditions (temperature, pressure and gas saturation) for the reservoir models were extracted from the numerical model of the Hengill geothermal resource which covers a larger area (G. Gunnarsson et al., 2011). This model is developed and maintained by Reykjavik Energy and simulates the production from Hellisheiði and Nesjavellir geothermal fields for resource management purposes (G. Gunnarsson et al., 2011). The values were interpolated using a spatial three-dimensional Delaunay triangulation and assigned to the new grid (Ratouis et al., 2022).

7.4 CO_2 Injection Modelling Results

7.4.1 Intermediate system

This section presents the results of the simulations of each injection scenario. Unless specified otherwise, the results are shown for case B (fracture volume fraction 0.2).

Table 9: Scenario modelling results for CO_2 injection into the intermediate system. Maximum CO_2 concentration presented as % CO_2 content ($kgCO_2/kgH_2O$) in the liquid phase, average areal extent in intermediate system (-100 to -600 masl) and maximum areal extent in intermediate system determined from maximum extent of area with significant CO_2 concentration (>0.1%), maximum volume of rock (km^3) determined from volume of rock that interacts with CO_2 in the models, maximum theoretical storage estimates calculated by the maximum volume of rock, porosity (according to Table 6) and density of carbonates minerals (2,711 kg/m^3; at 25.2°C), and CO_2 containment in the intermediate reservoir evaluated by calculating the pressure difference of the reservoir and partial pressure of CO_2.

Scenario	Average areal extent (km^2)	Maximum areal extent (km^2)	Maximum CO_2 concentration (%)	Maximum volume of rock (km^3)	Storage estimates ($MtCO_2$)	CO_2 containment in the Intermediate reservoir
1	7.2	9.6	1.64	2.19	923	✓
1b	7.3	9.7	1.65	2.21	933	✓
1c	4.6	6.5	1.1	1.16	516	✓
2	8.6	11.6	1.4	2.12	896	✓
3	8.1	11.1	1.3	1.97	829	✓

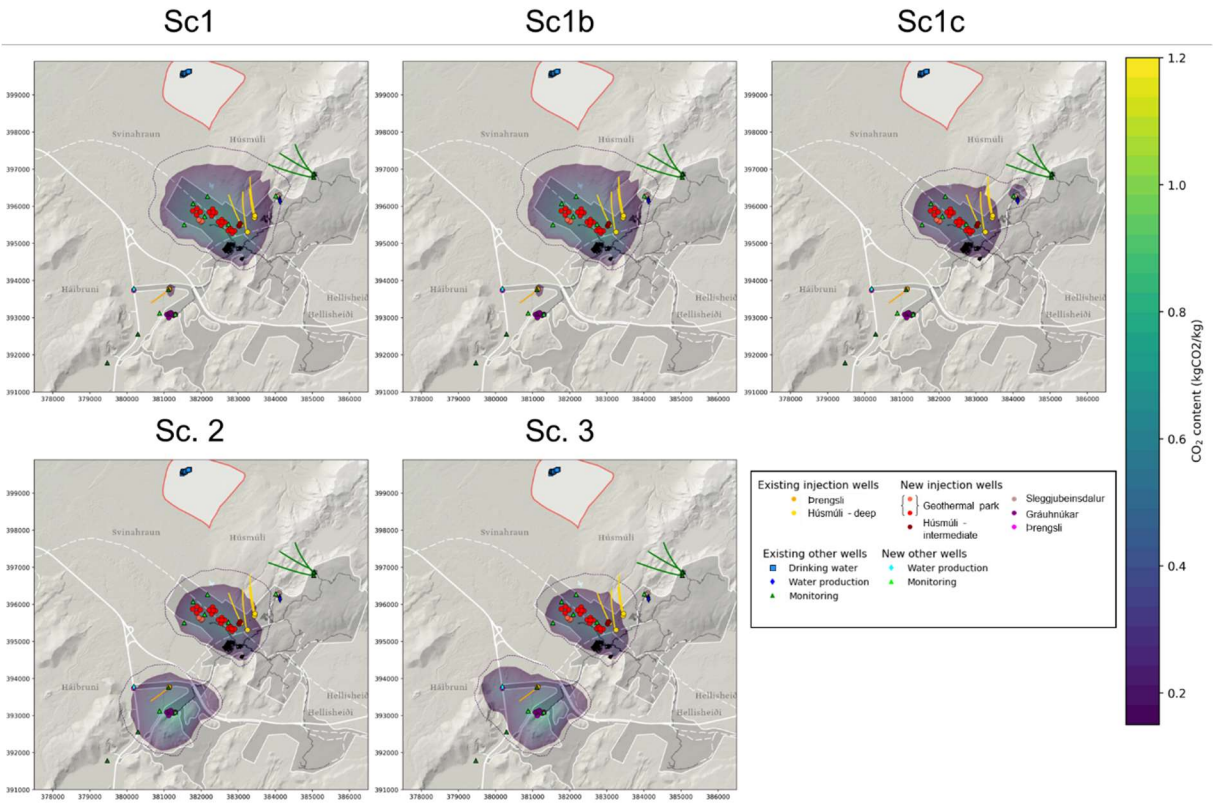

Figure 20: Areal view of the modelled CO_2 content in the storage reservoir after 30 years. The filled contours represent the average CO_2 content in the intermediate reservoir (-100 to -600 masl) and the outside contour represents the maximum extent (layer 30: -380 masl).

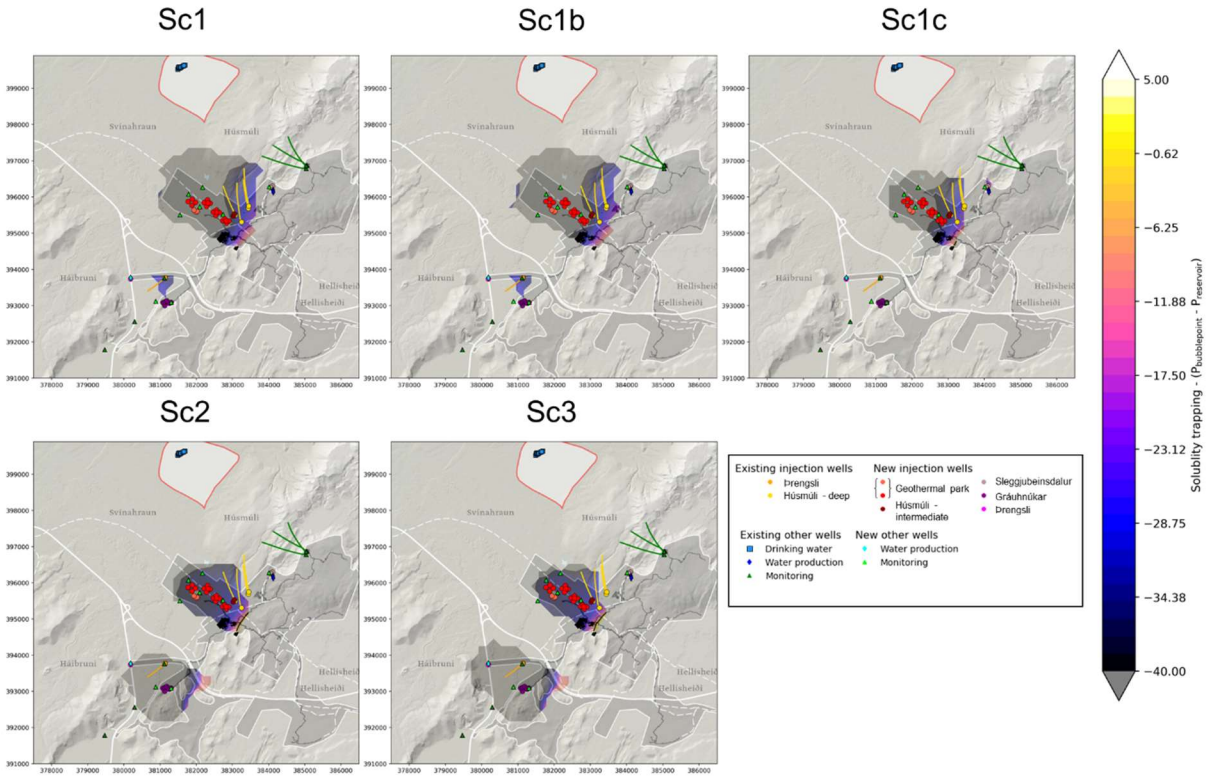

Figure 21: Areal view of the modelled solubility trapping in the storage reservoir after 30 years. The filled contours represent the average CO_2 content in the intermediate reservoir (-100 to -600 masl).

Figure 20 shows the maximum CO_2 extent for scenarios 1, 1b,1 c, 2, and 3 in the intermediate systems. Figure 21 shows the CO_2 solubility trapping for scenarios 1, 1b, 1c, 2, and 3 in the intermediate systems. It is calculated as the difference between the pressure at which the first bubble of CO_2 (P_{bubble}) will appear and the modelled reservoir pressure ($P_{reservoir}$). P_{bubble} is dependent on CO_2 concentration and temperature and the solubilities have been generated following Duan & Sun, 2003.

- For Scenario 1 (355,000 tCO_2/yr injection in the Geothermal Park and 4,000 tCO_2/yr injection in Þrengsli), the maximum areal extent is 9.6 km^2 with a maximum of 1.64% CO_2 per unit of fluid within the Intermediate system and corresponds to a volume of ~ 2.19 km^3. The solubility trapping of the CO_2 ($P_{bubblepoint}$ - $P_{reservoir}$<0) is ensured for Sc1, however due to higher temperature toward the East, a small portion of the reservoir may experience $P_{bubblepoint}$ - $P_{reservoir}$ within 2 bar.
- For Scenario 1b (40,000 tCO_2/yr injection for Mammoth, 265,000 tCO_2/yr injection in the Geothermal park and 50,000 tCO2/yr at the Husmuli – intermediate site), the maximum areal extent is 9.7 km^2 with a maximum of 1.65% CO_2 per unit of fluid within the Intermediate system and corresponds to a volume of ~ 2.21 km^3. The solubility trapping of the CO_2 ($P_{bubblepoint}$ - $P_{reservoir}$<0) is ensured for Sc1b, however due to higher temperature toward the East, a portion of the reservoir may experience $P_{bubblepoint}$ - $P_{reservoir}$ within 2 bar.
- For Scenario 1c (40,000 tCO_2/yr injection for Mammoth, 215,000 tCO_2/yr injection in the Geothermal Park, 50,000 tCO_2/yr at the Husmuli – intermediate site, and 50,000 tCO_2/yr in Sleggjubeinsdalur), the maximum areal extent is 6.5 km^2 with a maximum of 1.1% CO_2 per unit of fluid within the Intermediate system and corresponds to a volume of ~ 1.16 km^3. The solubility trapping of the CO_2 ($P_{bubblepoint}$ - $P_{reservoir}$<0) is ensured for Sc1c, however due to higher temperature toward the East, a small portion of the reservoir may experience $P_{bubblepoint}$ - $P_{reservoir}$ within 2 bar.
- For Scenario 2 (155,000 tCO_2/yr injection in the Geothermal Park, 200,000 tCO_2/yr in Gráuhnúkar, and 4,000 tCO_2/yr in Þrengsli), the maximum areal extent is 11.6 km^2 with a maximum of 1.4% CO_2 per unit of fluid within the Intermediate system and corresponds to a volume of ~ 2.12 km^3. The solubility trapping of the CO_2 ($P_{bubblepoint}$ - $P_{reservoir}$<0) is ensured for Sc2, however due to higher temperature toward the East, a small portion of the reservoir may experience $P_{bubblepoint}$ - $P_{reservoir}$ within 2 bar.
- For Scenario 3 (130,000 tCO_2/yr injection in the Geothermal Park, 200,000 tCO_2/yr in Gráuhnúkar, and 29,000 tCO_2/yr in Þrengsli), the maximum areal extent is 11.1 km^2 with a maximum of 1.3% CO2 per unit of fluid within the Intermediate system and corresponds to a volume of ~ 1.97 km^3. The solubility trapping of the CO_2 ($P_{bubblepoint}$ - $P_{reservoir}$<0) is ensured for Sc3, however due to higher temperature toward the East, a small portion of the reservoir may experience $P_{bubblepoint}$ - $P_{reservoir}$ within 2 bar.

Additional results are discussed below and figures presented in Annex 1 – Modelling results – Intermediate system and for the three systems that comprise the geological storage complex 5, 10, 20, and 30 years after the injection starts:

– Groundwater system at a depth of 75 masl – model layer 15
– Intermediate system at a depth of - 380 masl – model layer 30
– Geothermal system at a depth of - 1000 masl – model layer 50

and include:

- Movement of dissolved CO_2 and concentration contours showing the maximum extent of the dissolved CO_2 – here referred to as CO_2 plume, and the area affected by the injection. The CO_2 content ($kgCO_2/kgH_2O$) is presented as a percentage of the CO_2 present in the liquid phase in the model block.
- Effectiveness of the solubility trapping is expressed as the difference between the modelled reservoir pressure ($P_{reservoir}$) and bubble point pressure of CO_2 ($P_{bubblepoint}$). To ensure solubility trapping, the reservoir pressure shall be at least 5 bara higher than the pressure at which the first bubble of CO_2 will appear.
- Temperature and pressure impact of the injection around the injection sites ($\Delta_{T,\ T0}$ $\Delta_{P,\ P0}$) including potential hydraulic interference between wells.

7.4.1.1 Scenario 1

The results from Sc1 show that, with no reactions occurring, the extent of the dissolved CO_2 plume is located outside the protection zone of Engidalur after 30 years of injection. Concentrations of CO_2 in the geothermal park are up to ~1.64% per unit of fluid after 30 years and all CO_2 is modelled to remain solubility trapped in the reservoir (Figure 30). The maximum areal extent of CO_2 in Sc1 covers 9.6 km^2 and a maximum rock volume of ~2.19 km^3 interacts with CO_2 in the model, indicating the potential to mineralize up to 923 $MtCO_2$ (Figure 29). The maximum extent of the CO_2 plume in this scenario reaches within ~0.5 km of the Engidalur water protection zone, but at greater depths than the groundwater system. Local temperature reduction is expected in the close vicinity of the injection site as the injected fluid is colder than the formation water (Figure 31).

7.4.1.2 Scenario 1b

Sc1b shows very similar results to Sc1, with only slightly larger maximum areal extent of the dissolved CO_2 plume (~9.7 km^2) and a maximum of ~1.65% CO_2 per unit of fluid after 30 years (Figure 32). Under this scenario, a maximum rock volume of ~2.21 km^3 interacts with the injected CO_2 and has the potential to mineralize up to 933 $MtCO_2$. This scenario represents the maximum extent of the dissolved CO_2 plume and potential mineralization capacity of all modelled scenarios. No CO_2 is modelled to flow into the groundwater system and all CO_2 is modelled to remain solubility trapped within the intermediate system (Figure 33). Pressure and temperature impacts of Sc1b are similar to Sc1 (Figure 34). The only difference in the extent and migration of CO_2 is due to the additional injection into the Husmuli – intermediate site.

7.4.1.3 Scenario 1c

Sc1c shows significantly different results to Sc1 and Sc1b, primarily because of the diversification of injection locations between the Geothermal Park and Sleggjubeinsdalur. The dissolved CO_2 plume does not extend as far from the injection site towards the Engidalur water protection zone. In this scenario, the maximum areal extent of the dissolved CO_2 plume reaches ~6.5 km^2 and concentrations of CO_2 of up to 1.1% per unit of fluid after 30 years (Figure 35). The maximum volume of rock interacting with CO_2 in this scenario is ~1.16 km^3, with the potential to mineralize up to 516 $MtCO_2$. No CO_2 is modelled to flow into the groundwater system and all CO_2 is modelled to remain solubility trapped within the intermediate system (Figure 36). Pressure and temperature impacts of Sc1c are similar to Sc1 and Sc1b (Figure 37), but noticeably less significant due to the use of injection wells in Sleggjubeinsdalur as well as the Geothermal Park.

7.4.1.4 Scenario 2

Sc2 shows significantly different results to all variations of Sc1, primarily because of the diversification of injection locations between the Geothermal Park and Grauhnukar. This scenario presents the greatest maximum areal extent of all scenarios (11.6 km^2), but a lower maximum

volume than Sc1 and 1b (2.12 km^3). Figure 38 shows that no CO_2 flows into the groundwater system or accumulates around the injection area. Similarly, no CO_2 is found within the deep geothermal system. Additionally, all CO_2 is modelled to remain solubility trapped based on the pressure difference of the reservoir and partial pressure of CO_2 (Figure 39). The temperature impact from the model shows a slight cooling effect near the injection site in the Geothermal Park and in Gráuhnúkar. The pressure front associated with injecting large volumes of fluid builds up mostly near the injection sites at Gráuhnúkar with some noticeable increase near the Geothermal Park (Figure 40).

7.4.1.5 Scenario 3

Sc3 shows significantly different results to all variations of Sc1, primarily because of the diversification of injection locations in Grauhnukar and increased injection capacity at Þrengsli. This scenario presents the second greatest maximum areal extent of all scenarios (11.1 km^2), but a lower maximum volume (1.97 km^3) than all other scenarios except Sc1c. Figure 41 shows that no CO_2 flows into the groundwater system or accumulates around the injection area. Similarly, no CO_2 is found within the deep geothermal system. Additionally, all CO_2 is modelled to remain solubility trapped based on the pressure difference of the reservoir and partial pressure of CO_2 (Figure 42). The temperature impact from the model shows a slight cooling effect near the injection site in the Geothermal Park, Gráuhnúkar, and Þrengsli. The pressure front associated with injecting large volumes of fluid builds up mostly near the injection sites at Gráuhnúkar and Þrengsli with some noticeable increase near the Geothermal Park (Figure 43).

7.4.2 Deep geothermal system

This section presents the results of the simulations of each injection scenario.

Table 10: Scenario modelling results for CO_2 injection into the deep system. Maximum CO_2 concentration presented as % CO_2 content ($kgCO_2/kgH_2O$) in the liquid phase, average and maximum areal extent in the deep system (-1000 to -2000 masl) determined from maximum extent of area with significant CO_2 concentration (>0.1%), maximum volume of rock (km^3) determined from volume of rock that interacts with CO_2 in the models, maximum theoretical storage estimates calculated by the maximum volume of rock and density of carbonates minerals (2,711 kg/m^3; at 25.2°C), and CO_2 containment in the intermediate reservoir evaluated by calculating the pressure difference of the reservoir and partial pressure of CO_2.

Scenario	Average areal extent (km^2)	Maximum areal extent (km^2)	Maximum CO_2 concentration (%)	Maximum volume of rock (km^3)	Storage estimates ($MtCO_2$)	CO_2 containment in the Intermediate reservoir
1	5.9	6.2	0.3	5.4	650	✓
2	9.5	10.4	0.05	10.0	1,200	✓
3	11.1	11.8	0.17	12.0	1,400	✓

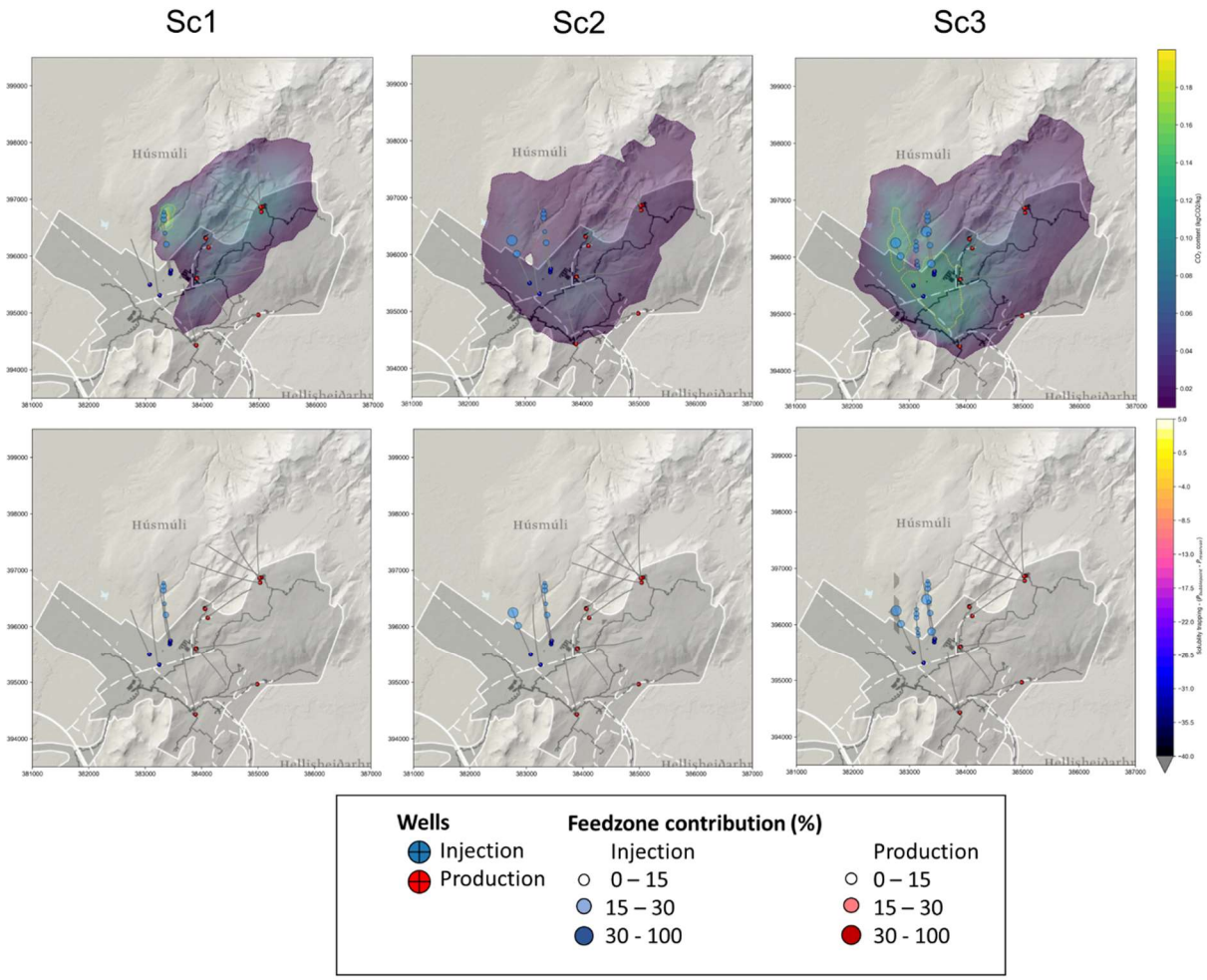

Figure 22: Areal view of the modelled CO_2 content (top) and solubility criteria (bottom) in the storage reservoir after 30 years. The filled contours represent the average CO_2 content in the deep system (-1000 to -2000 masl). In all scenarios, the storage reservoir pressure is more than 40 bar higher than the bubble point pressure which reflects why no results appear on the figure. Sc3 shows a slight decrease from this trend, but still maintains a significant pressure buffer that ensures the security of solubility trapping.

Figure 22Figure 20 shows the maximum CO_2 extent and CO_2 solubility trapping for scenarios 1,1b,1c,2, and 3 in the intermediate systems. The CO_2 solubility trapping is calculated as the difference between the pressure at which the first bubble of CO_2 (P_{bubble}) will appear and the modelled reservoir pressure ($P_{reservoir}$). P_{bubble} is dependent on CO_2 concentration and temperature and the solubilities have been generated following Duan & Sun, 2003.

- For Scenario 1 the maximum areal extent is 6.2 km^2 with a maximum of 0.3% CO_2 per unit of fluid within the deep system and corresponds to a volume of ~ 5.4 km^3. The solubility trapping of the CO_2 ($P_{bubblepoint}$ - $P_{reservoir}$<0) is ensured for Sc1 and there is over 40 bar additional to ensure solubility trapping.
- For Scenario 2 the maximum areal extent is 10.4 km^2 with a maximum of 0.05% CO_2 per unit of fluid within the deep system and corresponds to a volume of ~ 10.0 km^3. The solubility trapping of the CO_2 ($P_{bubblepoint}$ - $P_{reservoir}$<0) is is ensured for Sc2 and there is over 40 bar additional to ensure solubility trapping.
- For Scenario 3 the maximum areal extent is 11.8 km^2 with a maximum of 0.17% CO_2 per unit of fluid within the deep system and corresponds to a volume of ~ 12.0 km^3. The

solubility trapping of the CO_2 ($P_{bubblepoint}$ - $P_{reservoir}$<0) is is ensured for Sc3 and there is over 40 bar additional to ensure solubility trapping.

Additional results are discussed below and figures presented in Annex 2 – Modelling results – Deep geothermal system and for the three depth that comprise the geological storage complex 5, 10, 20, and 30 years after the injection starts:

- -100 masl – model layer 5
- - 1000 masl – model layer 30
- - 1600 masl – model layer 47

The results are presented 5, 10, 20, and 30 years after the injection starts and include:

- the migration of CO_2 and concentration contours showing the maximum extent of the dissolved CO_2 plume and the area affected by the injection. The CO_2 content ($kgCO_2/kgH_2O$) is presented as a percentage of the CO_2 present in the liquid phase the model block.
- Effectiveness of the solubility trapping is expressed as the difference between the modelled reservoir pressure ($P_{reservoir}$) and bubble point pressure of CO_2 ($P_{bubblepoint}$). To ensure solubility trapping, the reservoir pressure shall be at least 5 bara higher than the pressure at which the first bubble of CO_2 will appear.
- Temperature and pressure impact of the injection around the injection sites ($\Delta_{T,T0}$ $\Delta_{P,P0}$) including potential hydraulic interference between wells.

7.4.2.1 Scenario 1

Figure 44 shows the CO_2 distribution as a function of time in the different systems of the geological storage complex. It shows that for Scenario 1 (47,000 tCO_2/yr injection in Húsmúli in HN-16) no CO_2 flows into the groundwater system or accumulates around the injection area at -100 masl. In the deeper layers (-1000 and -1600 masl), CO_2 migrates to the NE following the Húsmúli structural controls. All CO_2 is modelled to remain solubility trapped based on the pressure difference of the reservoir and bubble point pressure of CO_2 (Figure 45).

The temperature impact from the model shows a slight cooling effect near the injection site in the Húsmúli reinjection area as well as a pressure front surrounding the area (Figure 46). These impacts observed in the model would be present regardless of CO_2 injections, since condensate from the power plant operations are required to be reinjected under the operational license.

7.4.2.2 Scenario 2

Figure 47 shows the CO_2 distribution as a function of time in the different systems of the geological storage complex. It shows that for Scenario 2 (47,000 tCO_2/yr injection in Húsmúli in HN-16 and HN-14) no CO_2 flows into the groundwater system or accumulates around the injection area at -100 masl. In the deeper layers (-1000 and -1600 masl), CO_2 migrates to the NE following the Húsmúli structural controls. All CO_2 is modelled to remain solubility trapped based on the pressure difference of the reservoir and partial pressure of CO_2. (Figure 48).

The temperature impact from the model shows a slight cooling effect near the injection site in the Húsmúli reinjection area as well as a pressure front surrounding the area (Figure 49). These impacts observed in the model would be present regardless of CO_2 injections, since condensate from the power plant operations are required to be reinjected under the operational license.

7.4.2.3 Scenario 3

Figure 50 shows the CO_2 distribution as a function of time in the different systems of the geological storage complex. It shows that for Scenario 2 (47,000 tCO_2/yr injection in Húsmúli in HN-16 and HN-14) no CO_2 flows into the groundwater system or accumulates around the injection area at -100 masl. In the deeper layers (-1000 and -1600 masl), CO_2 migrates to the NE following the Húsmúli structural controls. All CO_2 is modelled to remain solubility trapped based on the pressure difference of the reservoir and partial pressure of CO_2 (Figure 51).

The temperature impact from the model shows a slight cooling effect near the injection site in the Húsmúli reinjection area as well as a pressure front surrounding the area (Figure 52). These impacts observed in the model would be present regardless of CO_2 injections, since condensate from the power plant operations are required to be reinjected under the operational license.

8 Environmental Impact of CO_2 injection

The transport model developed represents a non-reactive transport of the CO_2-charged fluid through the reservoir and hence, predicts the maximum potential impact that the injection may have in the system for a theoretical worst-case scenario in which no mineralization occurs.

8.1 Impact of injection into the Intermediate system at Hellisheiði

8.1.1 Impact on the intermediate system

Figure 23 shows a comparison between Sc1, Sc2 and Sc3 for the intermediate system (-380 masl) after 30 years with regards to maximum extent of the plume, solubility trapping and difference in temperature and pressure.

The average areal extent (extent of dissolved CO_2 plume averaged for all layers from -100 to -600 masl) of modelled CO_2 injection scenarios shown in Table 9 indicates that in all scenarios, the CO_2 does not enter the main area of concern, the Engidalur water protection zone. Even in the worst-case scenario (Sc1 or Sc1b), the maximum extent of CO_2 is modelled to extend to ~ 0.5 km from the protection zone, but never enters it. All scenarios show that the effectiveness of the solubility trapping is always maintained as bubble point pressure of CO_2 ($P_{bubblepoint}$) is below modelled reservoir pressure. It can be noted that on the eastern edge of the storage reservoir, while the simulated solubility trapping is ensured, the pressure buffer falls within 2 bar. Additional work can be conducted to i) improve the model and to address the discrepancies (up to 5 bar) between the groundwater surface level as discussed in 7.2.2 and ii) further constrain temperatures in the eastern part of the storage reservoir. The preliminary modelling results highlight that the intermediate system is a good candidate for a large-scale injection of dissolved CO_2. Local temperature reduction is expected in proximity to the injection site since the injected fluid is colder than the formation water. The pressure impact extends towards the edge of the Engidalur area but is only present in the deeper layer (-380 masl) and only faintly appears in the groundwater or deep systems. Since there are no production wells for the geothermal power plant or water production wells in the intermediate system, the temperature and pressure impacts are not of significant concern.

The extent of the CO_2 plume and its migration towards Engidalur shows that there may be a need for monitoring wells penetrating the intermediate system further away from the injection sites in the direction of Engidalur to ensure the safety of the water protection area and to verify modeling results. However, a situation where the CO_2 reaches the max extent indicated at -380 masl is

unlikely since mineralization will take place along the way. The deepest water production well in the Engidalur area (HU-03; feeding depth: 120 m, TVD: 280 m, bottom hole depth: -39 masl) does not extend to the depth of layer 30 (-380 masl), indicating the possible impacts under this scenario are completely separated from the shallow groundwater system and will not interact.

The storage potential under scenario 1b (maximum extent and volume) indicates a preliminary theoretical potential to mineralize up to 933 $MtCO_2$. Thus, the positive environmental impact of avoiding emissions from Hellisheiði or permanently mineralizing atmospheric emissions outweighs any possible adverse impacts of injection in the intermediate system.

8.1.2 Impact on the groundwater system and water supply

Figure 24 shows a comparison between Sc1, Sc2 and Sc3 for the groundwater system (75 masl) after 30 years with regards to maximum extent of the plume, solubility trapping and difference in temperature and pressure. All scenarios show that no CO_2 enters the groundwater system and thus that the CO_2 containment is fully achieved.

None of the scenarios show an impact on the Engidalur water production area with 30 years of injection. However, due to the migration direction of the CO_2 plume and its migration towards Engidalur, and due to uncertainties in modeling in general, there is a need for monitoring wells further away from the injection sites in the direction of Engidalur, both shallow and into the intermediate system, to ensure the safety of the water protection area and to verify modeling results.

Currently the modeling work assumes an annual uptake rate of 900 L/s from Engidalur based on the actual production rate. However as previously mentioned, ON Power has a permit for 2000 L/s uptake while the annual uptake in 2021 was around 900 L/s. Updates to the modelled scenarios shall be made if the production from Engidalur would increase to the maximum permitted values.

8.1.3 Impact on the geothermal system and geothermal fluid production

Figure 24Figure 25 shows a comparison between Sc1, Sc2 and Sc3 for the geothermal system (-1000 masl) after 30 years with regards to maximum extent of the plume, solubility trapping and difference in temperature and pressure. All scenarios show that no CO_2 enters the geothermal system from the intermediate system and thus the CO_2 containment is fully achieved.

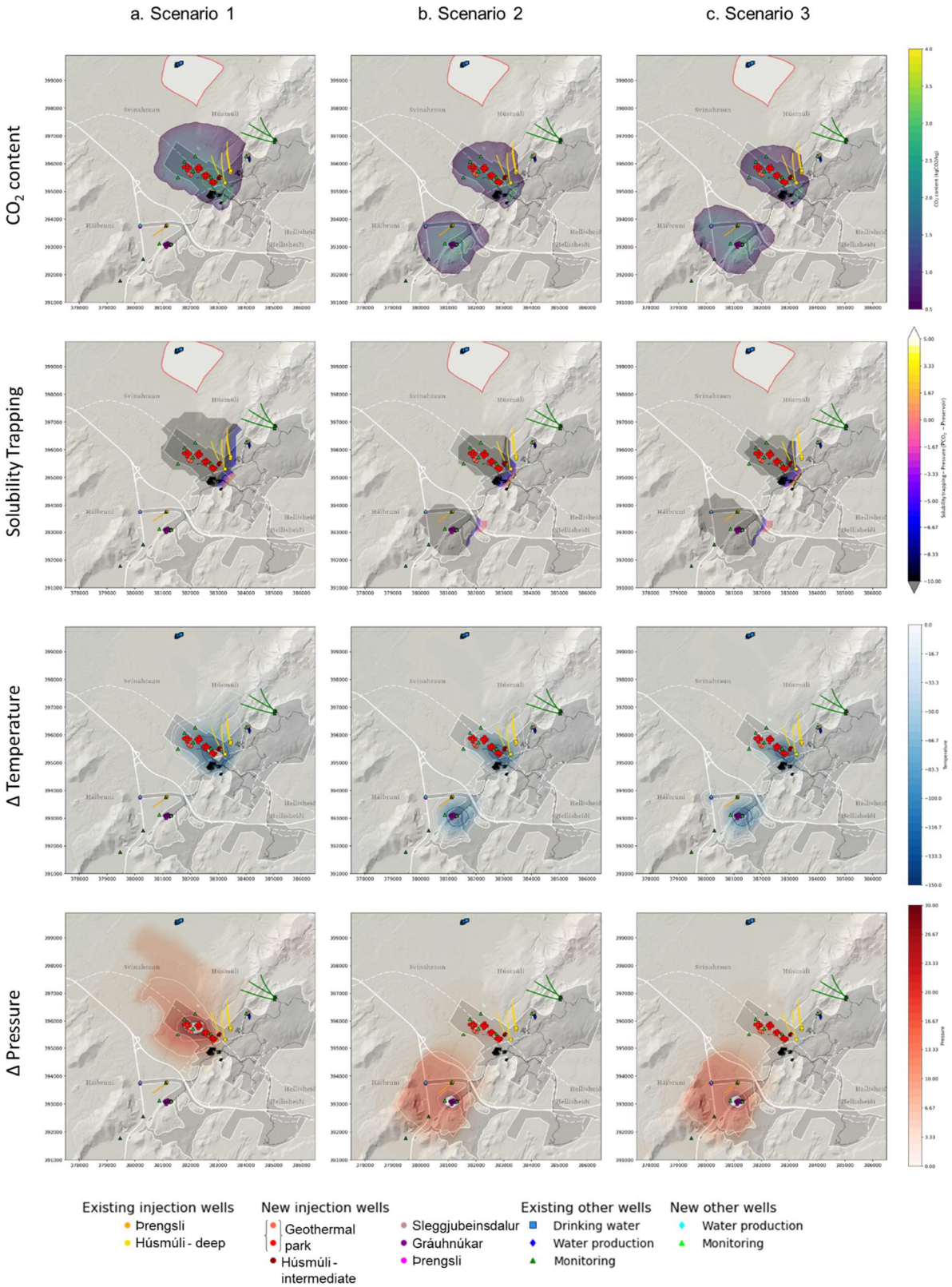

Figure 23: A comparison between Sc1, Sc2 and Sc3 for the intermediate system (-380 masl) after 30 years of injection with regards to maximum extent of the CO_2 plume, solubility trapping and difference in temperature and pressure.

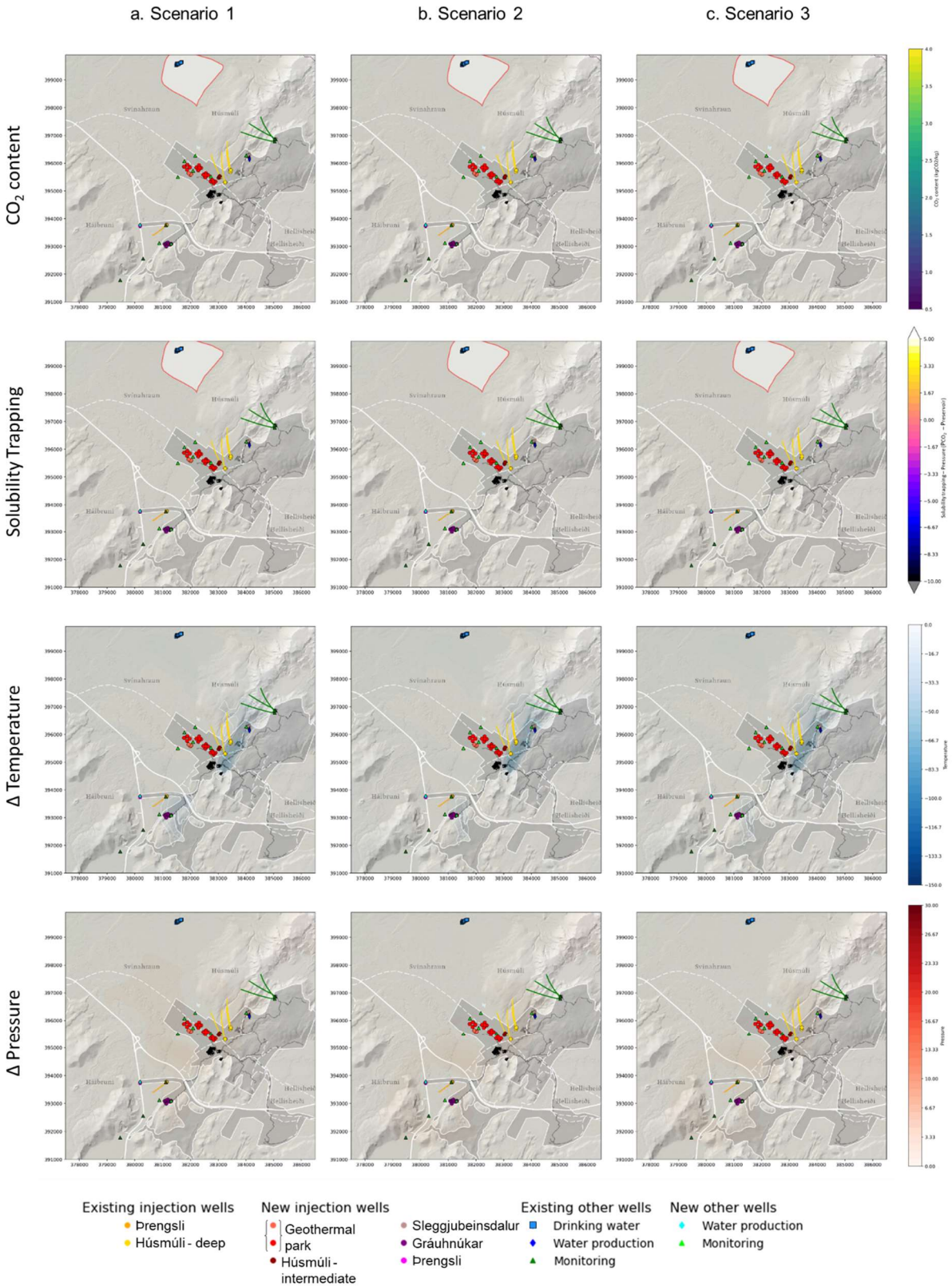

Figure 24: A comparison between Sc1, Sc2 and Sc3 for the shallow groundwater system (75 m asl) after 30 years of injection in the intermediate system with regards to maximum extent of the CO_2 plume, solubility trapping and difference in temperature and pressure.

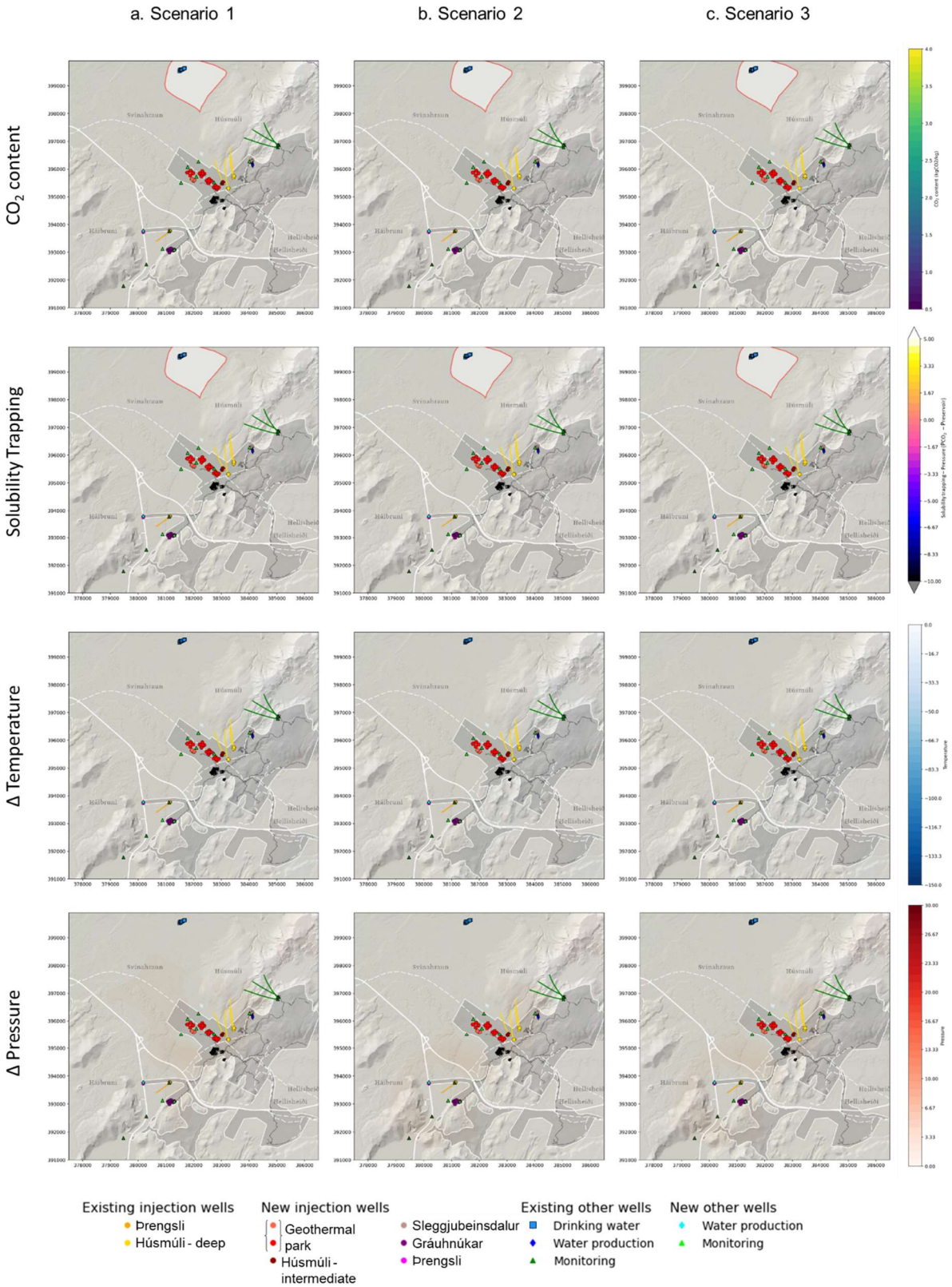

Figure 25: A comparison between Sc1, Sc2 and Sc3 for the deep system (-1000 masl) after 30 years of injection in the intermediate system with regards to maximum extent of the CO_2 plume, solubility trapping and difference in temperature and pressure.

8.2 Impact of injection into the deep system at Hellisheiði

Figure 26 and Figure 28 shows a comparison between Sc1, Sc2 and Sc3 for the deep system (-1000 and -1600 masl) after 30 years with regards to maximum extent of the plume, solubility trapping and difference in temperature and pressure.

The results for all three scenarios show that CO_2 is contained within the deep groundwater system and that solubility trapping is always maintained. As such, these results also highlight the fact that H_2S will benefit from the solubility trapping mechanism, and along with the CO_2, will be retained in the system where they naturally originated. If no reaction occurs, the CO_2 plume will travel from the Húsmúli injection area mainly following the fault system, towards the NE part of the reservoir.

The maximum extent is reached in Sc1. Yet, concentrations of CO_2 in the areas of interest are less than ~1% per unit of fluid after 30 years, emphasizing the negligible effect of the injection operations on the overall reservoir fluid composition. No particular migration of the CO_2 plume is modelled towards Engidalur, showing that there is no need for deep monitoring wells further away from the injection sites in the direction of the water protection area. The maximum extent of the CO_2 is greater in the deeper layer (-1600 masl) of the geothermal system when compared to the shallower layer (-1000 masl) as shown in Figure 26.

A weak pressure increase of up to 5 bars is recorded in Sc1 and Sc3, located ~1 km South from the injection site. In Sc2, the pressure increase can be considered insignificant (<1 bar). This slight pressure increase would not be considered a risk for induced seismicity and Hjörleifsdóttir et al., 2021 have reported that seismicity in Húsmúli is not induced by condensate injection or the injection of CO_2.

8.2.1 Impact on the groundwater system and water supply

The model results shown for Sc1, Sc2 and Sc3 at shallow depths (-100 masl) show no CO_2 at noticeable concentrations. Regardless of injection scenario, no CO_2 migrates upwards towards the groundwater system above this depth (Figure 44, Figure 47, Figure 50).

Furthermore, it is evident that the low-permeability mixed-layer-clay (MLC) layer that forms a clay cap on the geothermal system would prevent upward migration of injected gases, just as it does for geothermal fluids. Thus, the injection of CO_2 and H_2S into the deep geothermal system would have no impact on the groundwater system or water supply wells in the area of review. Even in the worst-case scenario, no CO_2 is present near the Engidalur water production area at a depth of -100 masl, which is below the depth of the deepest water production well (HU-03: -39 masl) and justifies the conclusion that there will be no impact on the groundwater system from injections into the deep geothermal system.

8.2.2 Impact on the intermediate system

In all scenarios modelled for the upper intermediate system (-100 masl), no CO_2 is present in significant concentrations (Figure 44, Figure 47, Figure 50). No CO_2 is modelled to migrated into the intermediate system due to the presence of a low-permeability clay cap demarcated by the low-resistivity mixed-layer-clay (MLC) alteration zone. This layer provides added security between the injections into the deep geothermal system and the shallower intermediate and groundwater systems.

8.2.3 Impact on the geothermal system and geothermal fluid production

A slight temperature reduction is seen in the close vicinity of the injection site, in particular in Sc1 and Sc3, as the injected fluid is colder than the formation water. Such temperature change occurs much slower than changes in tracer concentration along the flow path, meaning that such a cooling process does not significantly impact the thermal conditions of the surrounding rocks.

Based on the flow patterns of injections at Húsmúli (NE-trending), the maximum possible impact on the geothermal system and production may occur at the Skarðsmýrarfjall production area. Therefore, Sc1 represents the maximum possible impact of increased CO_2 concentrations in the Skarðsmýrarfjall production area due to the proximity of injection well HN-16 and production wells HE-31, HE-48, and HE-44. Rapid tracer returns into these production wells was documented by Ratouis et al., 2022 with HE-31 seeing tracer returns in approximately 15 days after tracer injection, followed by 18 and 60 days for HE-48 and HE-44, respectively. Both HE-31 and HE-48 saw tracer recovery rates of 22% while HE-44 saw recovery of 8% of tracers injected in the 2014 tracer test. Assuming injection of 47,000 tCO_2/year into HN-16 in Sc1 and the field tracer recovery rates, we may see up to ~10,340 tCO_2/year back into HE-31 and HE-48, and up to ~3,760 tCO_2/year back into HE-44 – assuming the worst-case scenario where no mineralization occurs.

Previous modelling of long-term injections into Húsmúli showed that HE-31, located closest to HN-16, could see enthalpy declines by 2030 that would render the well insufficient (< 900 $kJ \cdot kg^{-1}$) for electricity generation with current technology (Ratouis et al., 2022). The reinjection of condensate and brine may already reduce the lifespan of HE-31 to within the next 10 years, so the additional injection of CO_2 in Sc1 will not change the long-term future of this well. However, monitoring efforts should focus on wells HE-48 and HE-44 to better understand the potential impact of increased CO_2 injection into Húsmúli on power generation from these wells.

In general, all the presented model simulations identify minor changes in the deep system at Hellisheiði due to the injection operations, suggesting that the power production, as well as the composition of the background fluids in the reservoir formations will not be affected in the long-term (30 yrs.).

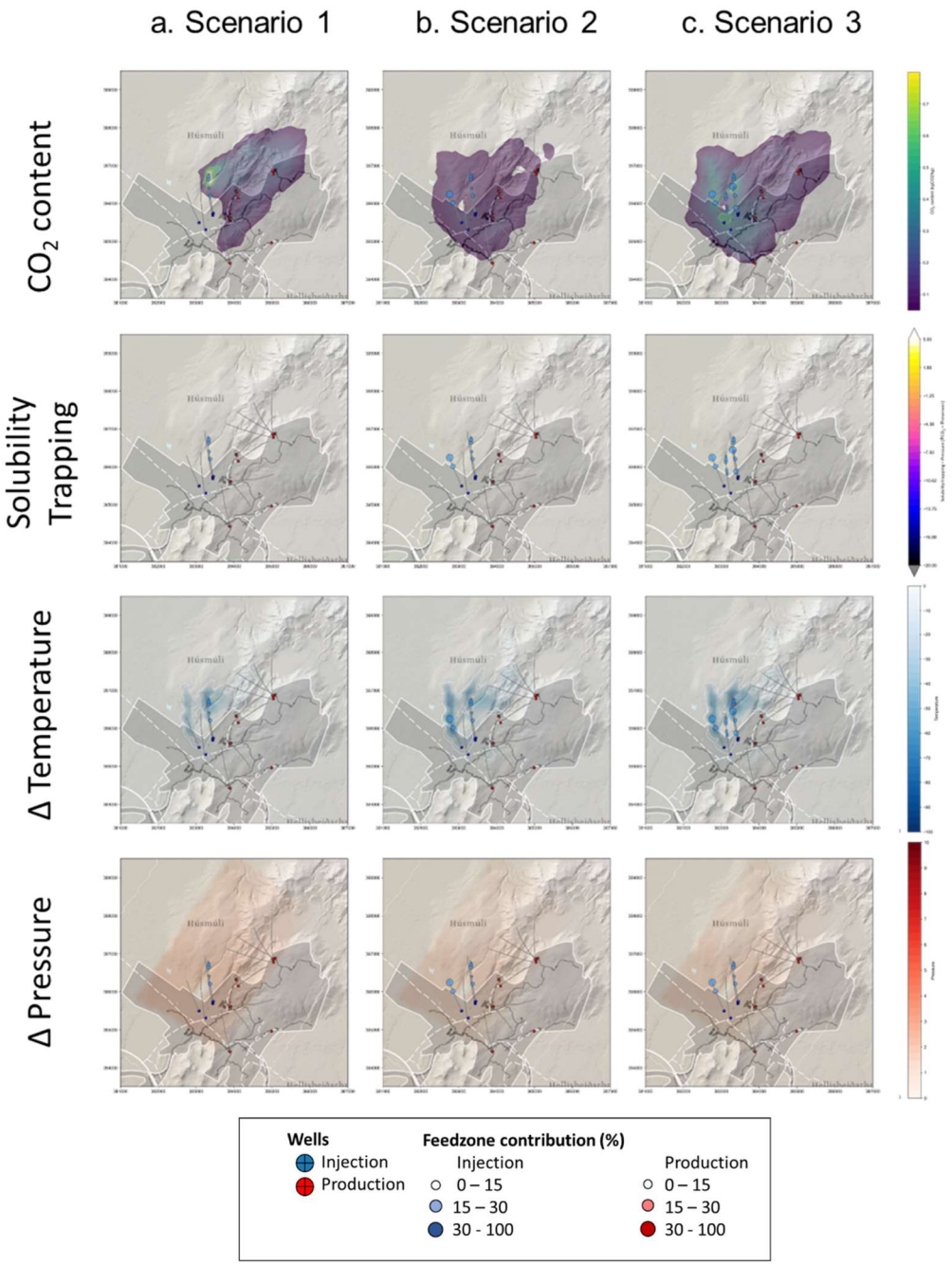

Figure 26: A comparison between Sc1, Sc2 and Sc3 in the deep system (-1600 masl) after 30 years of injection into the deep system with regards to maximum extent of the CO_2 plume (CO_2 content), solubility trapping, and difference in temperature and pressure.

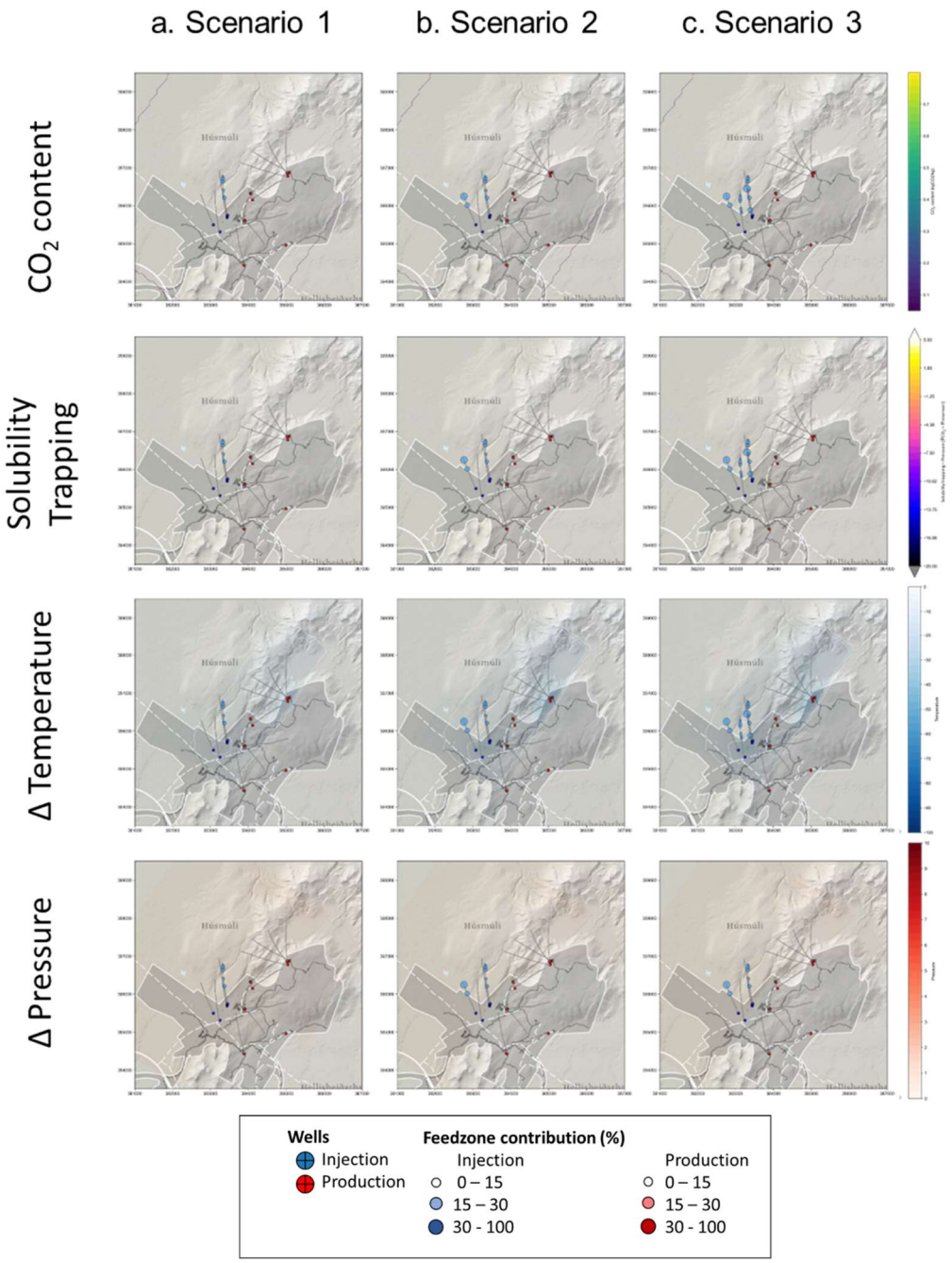

Figure 27: A comparison between Sc1, Sc2 and Sc3 above the deep system (-100 masl) after 30 years of injection into the deep system with regards to maximum extent of the CO_2 plume (CO_2 content), solubility trapping, and difference in temperature and pressure.

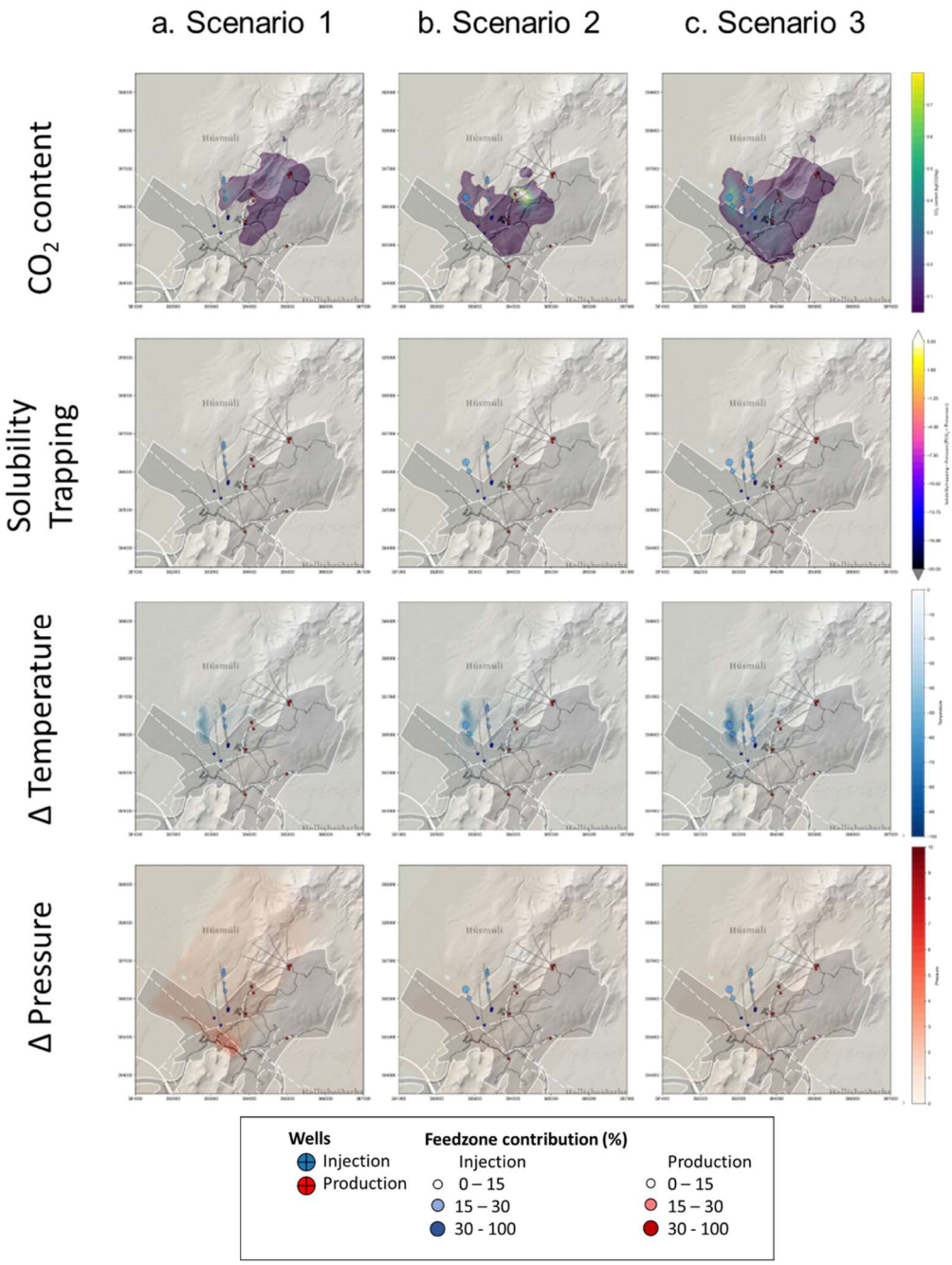

Figure 28: A comparison between Sc1, Sc2 and Sc3 in the deep system (-1000 masl) after 30 years of injection into the deep system with regards to maximum extent of the CO_2 plume (CO_2 content), solubility trapping, and difference in temperature and pressure.

9 References

Alfredsson, H. A., Oelkers, E. H., Hardarsson, B. S., Franzson, H., Gunnlaugsson, E., & Gislason, S. R. (2013). The geology and water chemistry of the Hellisheidi, SW-Iceland carbon storage site. *International Journal of Greenhouse Gas Control*, *12*, 399–418. https://doi.org/10.1016/j.ijggc.2012.11.019

Aradóttir, E. S. P., Sonnenthal, E. L., Björnsson, G., & Jónsson, H. (2012). Multidimensional reactive transport modeling of CO2 mineral sequestration in basalts at the Hellisheidi geothermal field, Iceland. *International Journal of Greenhouse Gas Control*, *9*, 24–40. https://doi.org/10.1016/j.ijggc.2012.02.006

Árnason, K., & Magnússon, I. Þ. (2001). *Jarðhiti við Hengil og á Hellisheiði: Niðurstöður viðnámsmælinga* (OS-2001/091). Orkustofnun.

Clark, D. E., Gunnarsson, I., Aradóttir, E. S., Þ. Arnarson, M., Þorgeirsson, Þ. A., Sigurðardóttir, S. S., Sigfússon, B., Snæbjörnsdóttir, S. Ó., Oelkers, E. H., & Gíslason, S. R. (2018). The chemistry and potential reactivity of the CO2-H2S charged injected waters at the basaltic CarbFix2 site, Iceland. *Energy Procedia*, *146*, 121–128. https://doi.org/10.1016/j.egypro.2018.07.016

Clark, D. E., Oelkers, E. H., Gunnarsson, I., Sigfússon, B., Snæbjörnsdóttir, S. Ó., Aradóttir, E. S., & Gíslason, S. R. (2020). CarbFix2: CO2 and H2S mineralization during 3.5 years of continuous injection into basaltic rocks at more than 250 °C. *Geochimica et Cosmochimica Acta*, *279*, 45–66. https://doi.org/10.1016/j.gca.2020.03.039

Croucher, A. (2015, November). *Recent developments in the PyTOUGH scripting library for TOUGH2 simulations*. https://researchspace.auckland.ac.nz/handle/2292/28102

Croucher, A. E., & O'Sullivan, M. J. (2013). Approaches to local grid refinement in TOUGH2 models. *Proceedings of the 33rd New Zealand Geothermal, Workshop, Auckland, New Zealand*.

Finsterle, S. (2007). *iTOUGH2 User's Guide. (LBNL-40040).* (User Guide. (LBNL-40040)). Lawrence Berkeley National Laboratory.

Franzson, H. (1988). *Nesjavellir: Permeability in geothermal reservoir (in Icelandic) OS-88046/JHD-09,*. Reykjavik; Energy Authority of Iceland.

Franzson, H. (1998). *The Nesjavellir high-temperature field, SW-Iceland, reservoir geology. Proceedings 19th Annual PNOC-EDC Geothermal Conference, Manilla, Phillippines,*. 13–20.

Franzson, H. (2000). *HYDROTHERMAL EVOLUTION OF THE NESJAVELLIR HIGH-TEMPERATURE SYSTEM, ICELAND*.

Franzson, H., Gunnlaugsson, E., Árnason, K., Steingrímsson, B., & Harðarson, B. S. (2010). The Hengill Geothermal System, Conceptual Model and Thermal Evolution. *In Proceedings World Geothermal Congress 2010.*, 9.

Franzson, H., Zierenberg, R., & Schiffman, P. (2008). Chemical transport in geothermal systems in Iceland: Evidence from hydrothermal alteration. *Journal of Volcanology and Geothermal Research*, *173*(3), 217–229. https://doi.org/10.1016/j.jvolgeores.2008.01.027

Fridleifsson, G. (1991). Hydrothermal systems and associated alteration in Iceland. *Chishitsu Chosajo Hokoku (Report, Geological Survey of Japan); (Japan)*, *277*. https://www.osti.gov/etdeweb/biblio/7075527

Frolova, J., Ladygin, V., Franzson, H., Sigurdsson, O., Stefánsson, V., & Shustrov, V. (2005). Petrophysical Properties of Fresh to Mildly Altered Hyaloclasitie Tuffs. *Proceedings of the World Geothermal Conference. Antalya, Turkey*.

Gislason, S. R., Wolff-Boenisch, D., Stefansson, A., Oelkers, E. H., Gunnlaugsson, E., Sigurdardottir, H., Sigfusson, B., Broecker, W. S., Matter, J. M., Stute, M., Axelsson, G., & Fridriksson, T. (2010). Mineral sequestration of carbon dioxide in basalt: A pre-injection overview of the CarbFix project. *International Journal of Greenhouse Gas Control*, *4*(3), 537–545. https://doi.org/10.1016/j.ijggc.2009.11.013

Goldberg, D. S., Takahashi, T., & Slagle, A. L. (2008). Carbon dioxide sequestration in deep-sea basalt. *Proceedings of the National Academy of Sciences*, *105*(29), 9920–9925. https://doi.org/10.1073/pnas.0804397105

Gunnarsdóttir, S., & Poux, B. (2016). *3D Modelling of Hellisheiði Geothermal Field using Leapfrog: Data, Workflow and Preliminary Models.* (ÍSOR-2016/039; p. 22). ÍSOR.

Gunnarsson, G., Arnaldsson, A., & Oddsdóttir, A. L. (2011). Model Simulations of the Hengill Area, Southwestern Iceland. *Transport in Porous Media*, *90*(1), 3–22. https://doi.org/10.1007/s11242-010-9629-1

Gunnarsson, I., Aradóttir, E. S., Oelkers, E. H., Clark, D. E., Arnarson, M. Þ., Sigfússon, B., Snæbjörnsdóttir, S. Ó., Matter, J. M., Stute, M., Júlíusson, B. M., & Gíslason, S. R. (2018). The rapid and cost-effective capture and subsurface mineral storage of carbon and sulfur at the CarbFix2 site. *International Journal of Greenhouse Gas Control*, *79*, 117–126. https://doi.org/10.1016/j.ijggc.2018.08.014

Helgadóttir, H. M., Sn, S. Ó., Harðarson, B. S., Einarsson, G. M., & Franzson, H. (2010). *Geology and Hydrothermal Alteration in the Reservoir of the Hellisheiði High Temperature System, SW-Iceland*. 10.

Hjörleifsdóttir, V., Ingvarsson, G., Ratouis, T., Gunnarsson, G., Snæbjörnsdóttir, S. ?sk, & Sigfússon, B. (2021). Ten years of induced earthquakes in the Húsmúli CO2 injection site, Hellisheidi, Iceland. In *Sixth International Conference on Engineering Geophysics, Virtual, 25?28 October 2021* (pp. 96–100). Society of Exploration Geophysicists. https://doi.org/10.1190/iceg2021-027.1

Khodayar, M., Axelsson, G., & Steingrímsson, B. (2013). *Fracture analysis from aerial imageries and correlation with triggered earthquakes by injection at Húsmúli, Hengill, South Iceland.* (Report ÍSOR-2013/008). Iceland GeoSurvey.

Kristinsson, S., & Þorbergsson, A. (2016). *Endurskoðun sprungukorts á Hengilssvæðinu* (Report ÍSOR-16019). Iceland GeoSurvey.

Kristjánsson, B. R., Axelsson, G., Gunnarsson, G., Gunnarsson, I., & Óskarsson, F. (2016). Comprehensive Tracer Testing in the Hellisheidi Geothermal Field in SW-Iceland 2013-14. *Proceedings, 41st Workshop on Geothermal Reservoir Engineering. Stanford, California.*, 20.

Kristmannsdóttir, H., & Tómasson, J. (1978). Zeolite zones in geothermal areas in Iceland. Natural Zeolites: Occurrence, Properties, Use. *Pergamon Press, Elmsford, New York*.

Lagat, J. (2009). Hydrothermal alteration mineralogy in geothermal fields with case examples from Olkaria domes geothermal field, Kenya. *Short Course IV on Exploration for Geothermal Resources*, 24.

Larsson, D., Grönvold, K., Oskarsson, N., & Gunnlaugsson, E. (2002). Hydrothermal alteration of plagioclase and growth of secondary feldspar in the Hengill Volcanic Centre, SW Iceland. *Journal of Volcanology and Geothermal Research*, *114*(3), 275–290. https://doi.org/10.1016/S0377-0273(01)00267-0

Maaløe, S., & Jakobsson, S. P. (1980). The PT phase relations of a primary oceanite from the Reykjanes peninsula, Iceland. *Lithos*, *13*(3), 237–246. https://doi.org/10.1016/0024-4937(80)90069-9

Matter, J. M., Stute, M., Snæbjörnsdottir, S. Ó., Oelkers, E. H., Gislason, S. R., Aradottir, E. S., Sigfusson, B., Gunnarsson, I., Sigurdardottir, H., Gunnlaugsson, E., Axelsson, G., Alfredsson, H. A., Wolff-Boenisch, D., Mesfin, K., Taya, D. F. de la R., Hall, J., Dideriksen, K., & Broecker, W. S. (2016). Rapid carbon mineralization for permanent disposal of anthropogenic carbon dioxide emissions. *Science*, *352*(6291), 1312–1314. https://doi.org/10.1126/science.aad8132

Neuhoff, P. S., Friðriksson, Þ., Arnórsson, S., & Bird, D. K. (1999). Porosity evolution and mineral paragenesis during low-grade metamorphism of basaltic lavas at Teigarhorn, eastern Iceland. *American Journal of Science*, *299*(6), 467–501. https://doi.org/10.2475/ajs.299.6.467

Nugraha, R., O'Sullivan, J., O'Sullivan, M., & Abdurachman, F. (2022, February 9). *Geothermal Modelling: Industry Standard Practices*.

Pogge von Strandmann, P. A. E., Burton, K. W., Snæbjörnsdóttir, S. O., Sigfússon, B., Aradóttir, E. S., Gunnarsson, I., Alfredsson, H. A., Mesfin, K. G., Oelkers, E. H., & Gislason, S. R. (2019). Rapid CO2 mineralisation into calcite at the CarbFix storage site quantified using

calcium isotopes. *Nature Communications*, *10*(1), Article 1. https://doi.org/10.1038/s41467-019-10003-8

Pruess, K. (1991). *TOUGH2: A general-purpose numerical simulator for multiphase fluid and heat flow* (User Guide. LBL-29400, 5212064; p. LBL-29400, 5212064). Lawrence Berkeley National Laboratory. https://doi.org/10.2172/5212064

Pruess, K., & Narasimhan, T. N. (1982). On fluid reserves and the production of superheated steam from fractured, vapor-dominated geothermal reservoirs. *Journal of Geophysical Research*, *87*(B11), 9329. https://doi.org/10.1029/JB087iB11p09329

Pruess, K., & Narasimhan, T. N. (1985). A Practical Method for Modeling Fluid and Heat Flow in Fractured Porous Media. *Society of Petroleum Engineers Journal*, *25*(01), 14–26. https://doi.org/10.2118/10509-PA

Ratouis, T. M. P., Snæbjörnsdóttir, S. Ó., Voigt, M. J., Sigfússon, B., Gunnarsson, G., Aradóttir, E. S., & Hjörleifsdóttir, V. (2022). Carbfix 2: A transport model of long-term CO2 and H2S injection into basaltic rocks at Hellisheidi, SW-Iceland. *International Journal of Greenhouse Gas Control*, *114*, 103586. https://doi.org/10.1016/j.ijggc.2022.103586

Sigfússon, B., Arnarson, M. Þ., Snæbjörnsdóttir, S. Ó., Karlsdóttir, M. R., Aradóttir, E. S., & Gunnarsson, I. (2018). Reducing emissions of carbon dioxide and hydrogen sulphide at Hellisheidi power plant in 2014-2017 and the role of CarbFix in achieving the 2040 Iceland climate goals. *Energy Procedia*, *146*, 135–145. https://doi.org/10.1016/j.egypro.2018.07.018

Sigurðsson, Ó., Guðmundsson, Á., Friðleifsson, G. Ó., Franzson, H., Guðlaugsson, S. Þ., & Stefánsson, V. (2000). Database on igneous rock properties in Icelandic geothermal systems, status and unexpected results. *In: Proceedings of the World Geothermal Congress 2000, Kyushu-Tohoku, Japan, 28 May – 10 June 2000.*, 2881–2886.

Sigurðsson, Ó., & Stefánsson, V. (1994). *Forðafræðistuðlar – Mælingar á bergsýnum [Reservoir properties – Sample Measurements]. Report OS-94049/JHD-28 B*. Reykjavík: Orkustofnun.

Snæbjörnsdóttir, S. Ó., Oelkers, E. H., Mesfin, K., Aradóttir, E. S., Dideriksen, K., Gunnarsson, I., Gunnlaugsson, E., Matter, J. M., Stute, M., & Gislason, S. R. (2017). The chemistry and saturation states of subsurface fluids during the in situ mineralisation of CO2 and H2S at the CarbFix site in SW-Iceland. *International Journal of Greenhouse Gas Control*, *58*, 87–102. https://doi.org/10.1016/j.ijggc.2017.01.007

Snæbjörnsdóttir, S. Ó., Sigfússon, B., Marieni, C., Goldberg, D., Gislason, S. R., & Oelkers, E. H. (2020). Carbon dioxide storage through mineral carbonation. *Nature Reviews Earth & Environment*, *1*(2), 90–102. https://doi.org/10.1038/s43017-019-0011-8

Snæbjörnsdóttir, S. Ó., Tómasdóttir, S., Sigfússon, B., Aradóttir, E. S., Gunnarsson, G., Niemi, A., Basirat, F., Dessirier, B., Gislason, S. R., Oelkers, E. H., & Franzson, H. (2018). The geology and hydrology of the CarbFix2 site, SW-Iceland. *Energy Procedia*, *146*, 146–157. https://doi.org/10.1016/j.egypro.2018.07.019

Snæbjörnsdóttir, S. Ó., Wiese, F., Fridriksson, T., Ármansson, H., Einarsson, G. M., & Gislason, S. R. (2014). CO2 storage potential of basaltic rocks in Iceland and the oceanic ridges. *Energy Procedia*, *63*, 4585–4600. https://doi.org/10.1016/j.egypro.2014.11.491

Stefánsson, V., Sigurðsson, Ó., Guðmundsson, Á., Franzson, H., Friðleifsson, G., & Tulinius, H. (1997). Core measurements and geothermal modelling. *Second Nordic Symposium on Petrophysics*, 199–220.

Vatnaskil. (2019). *Capital area. Annual revision of flow model 2019* (19.13). Vatnaskil.

Vatnaskil. (2021). *Capital area. Annual revision of flow model 2021* (21.10). Vatnaskil.

Walter, G. R. (1982). *Theoretical and Experimental Determination of Matrix Diffusion and Related Solute Transport Properties of Fractured Tuffs From the Nevada Test §ite*. 137.

Wiese, F., Fridriksson, T., & Ármannsson, H. (2008). CO2 Fixation by Calcite in High-temperature Geothermal Systems in Iceland. *ÍSOR Report ÍSOR-2008/003*.

10 Annex 1 – Modelling results – Intermediate system

10.1 Scenario 1

– *CO_2 content – maximum extent of the storage reservoir*

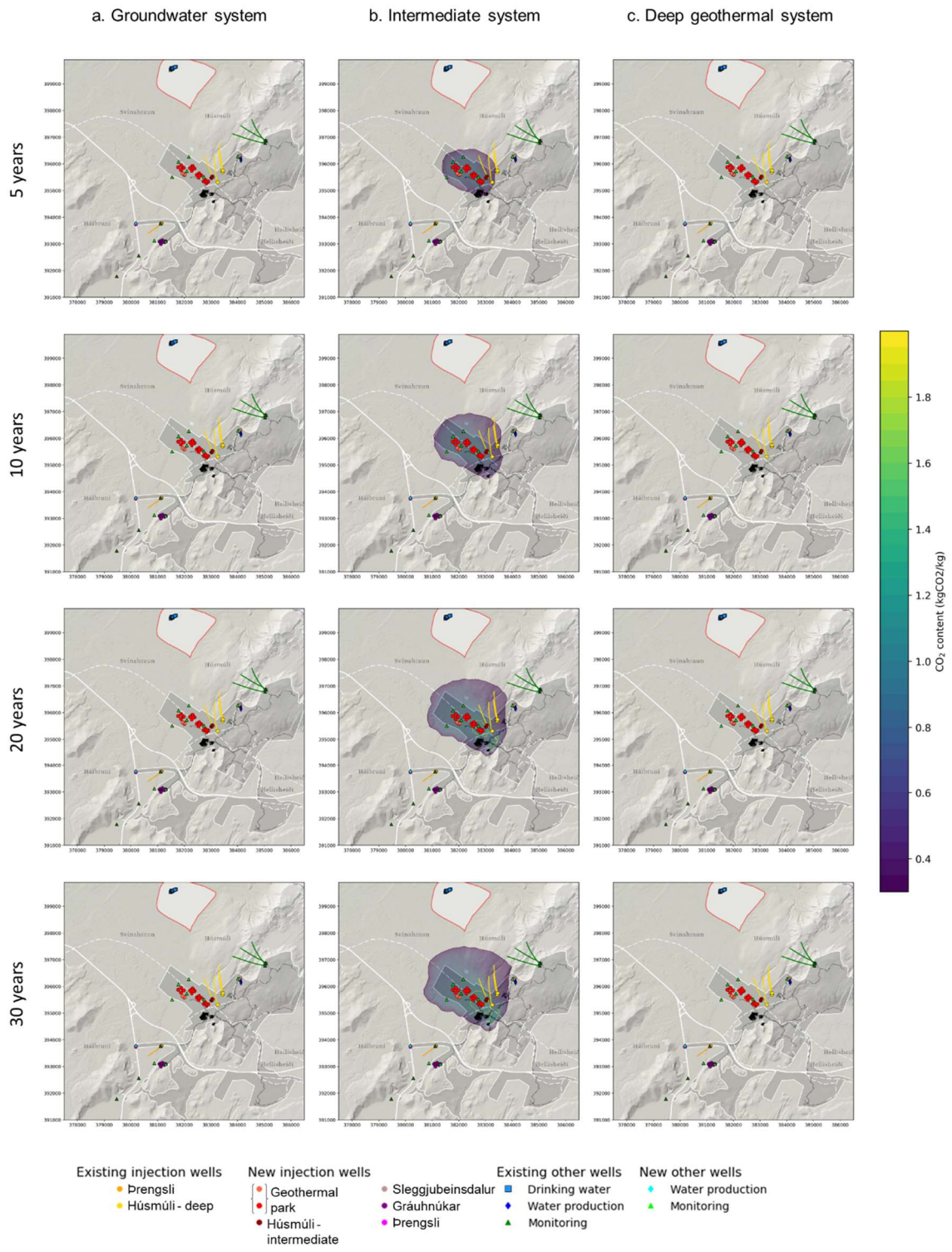

Figure 29: Scenario 1: Areal view of the modelled CO_2 content in the storage reservoir after 5, 10, 20, and 30 years in the groundwater, intermediate, and geothermal systems.

– *Solubility trapping condition – Storage security*

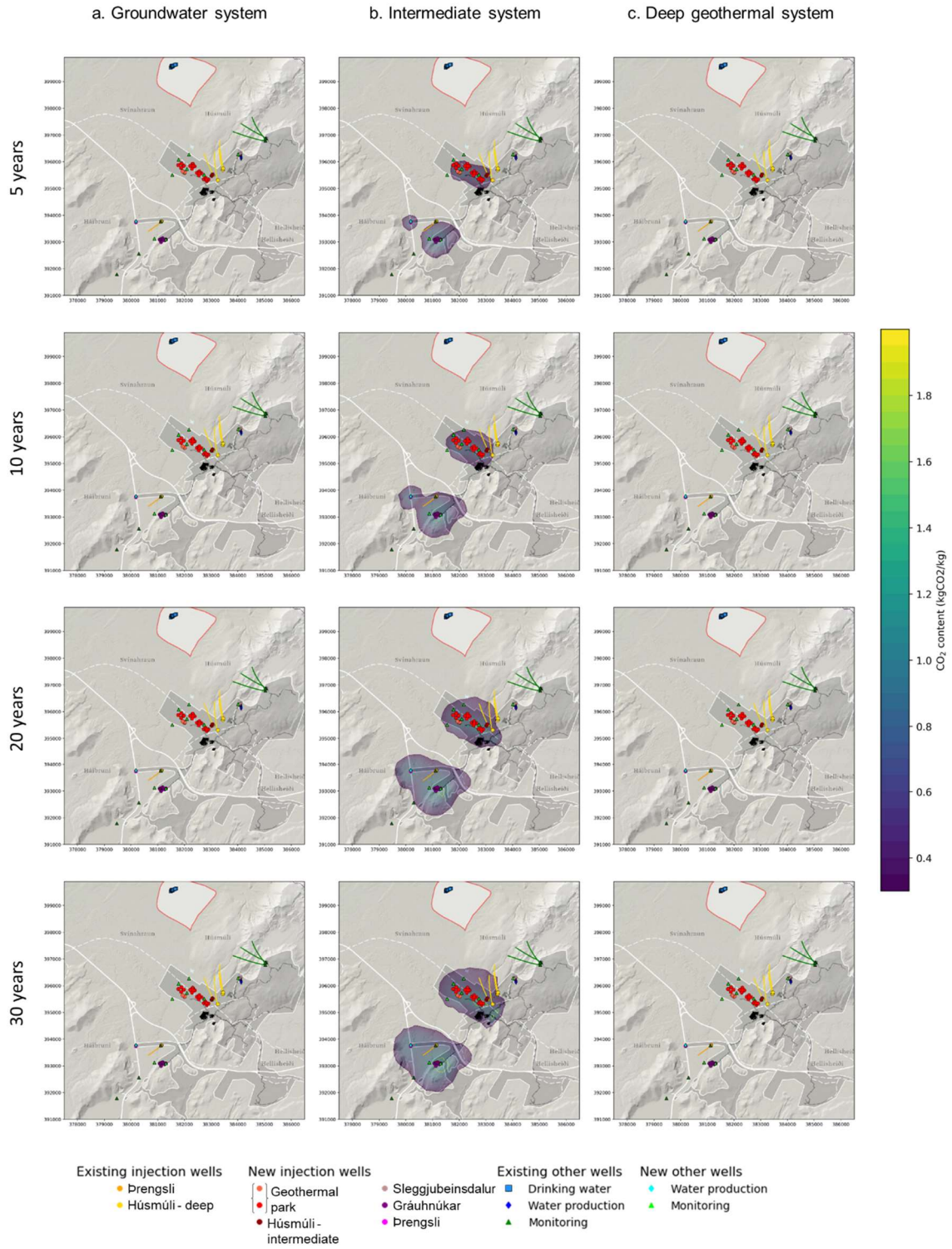

Figure 30: Scenario 1: Areal view of the modelled solubility trapping in the storage reservoir after 5, 10, 20, and 30 years in the groundwater, intermediate, and geothermal systems.

- *Pressure and temperature impact on the Intermediate system*

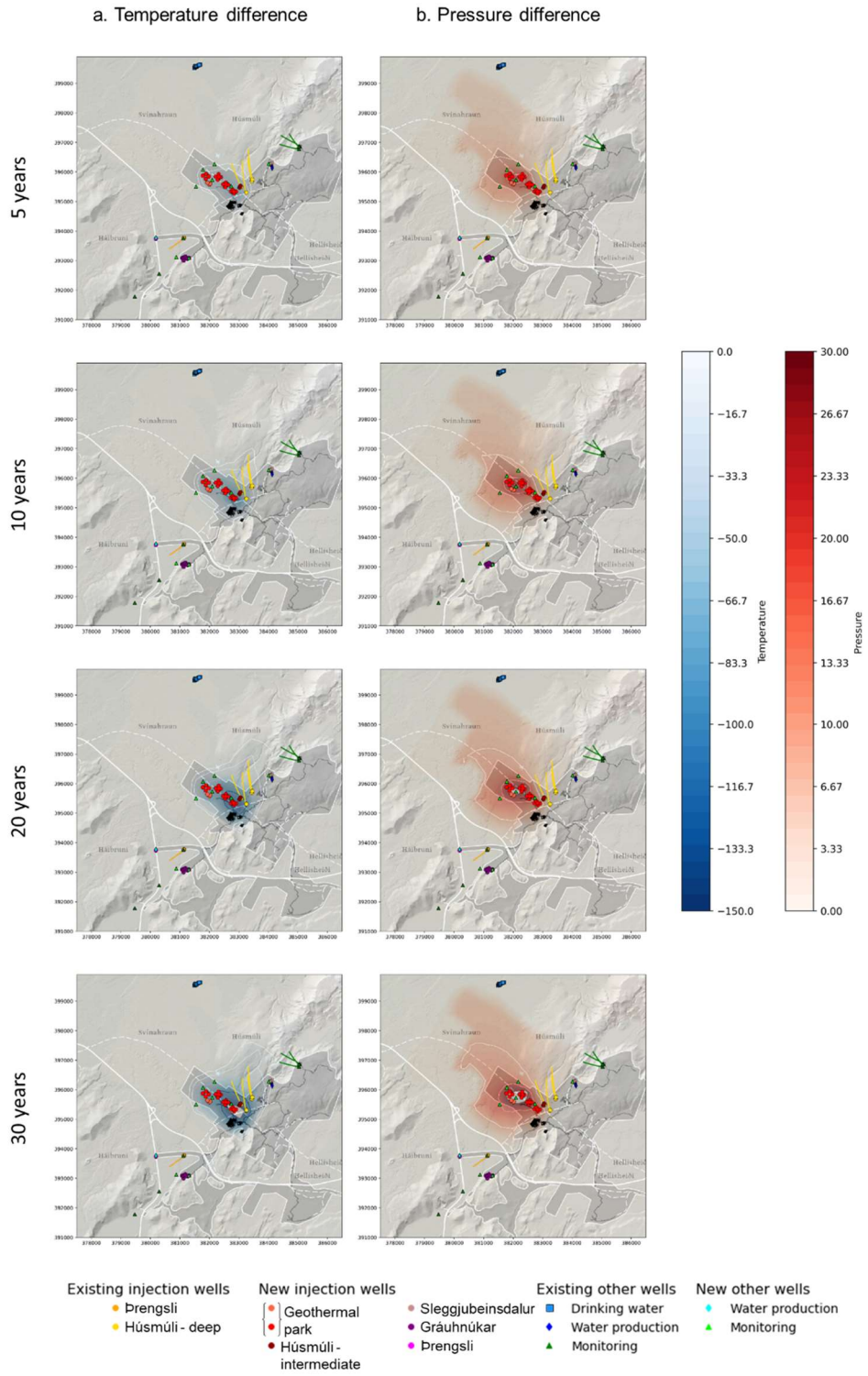

Figure 31: Scenario 1: Areal view of the modelled temperature (ºC) and pressure (bar) difference in the storage reservoir after 5, 10, 20, and 30 years in the intermediate system.

10.2 Scenario 1b

– *CO_2 content – maximum extent of the storage reservoir*

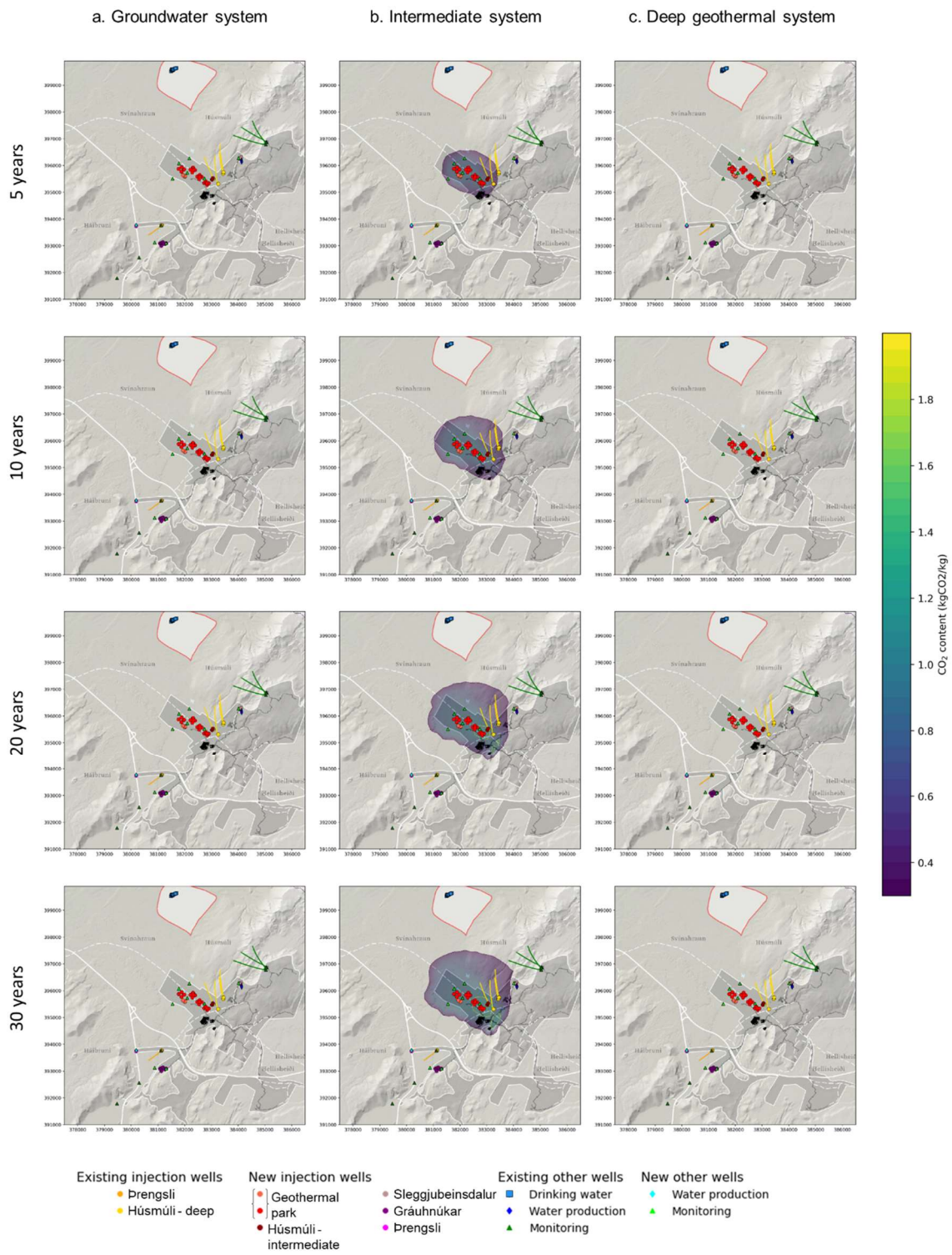

Figure 32: Scenario 1b: Areal view of the modelled CO_2 content in the storage reservoir after 5, 10, 20, and 30 years in the groundwater, intermediate, and geothermal systems.

– *Solubility trapping condition – Storage security*

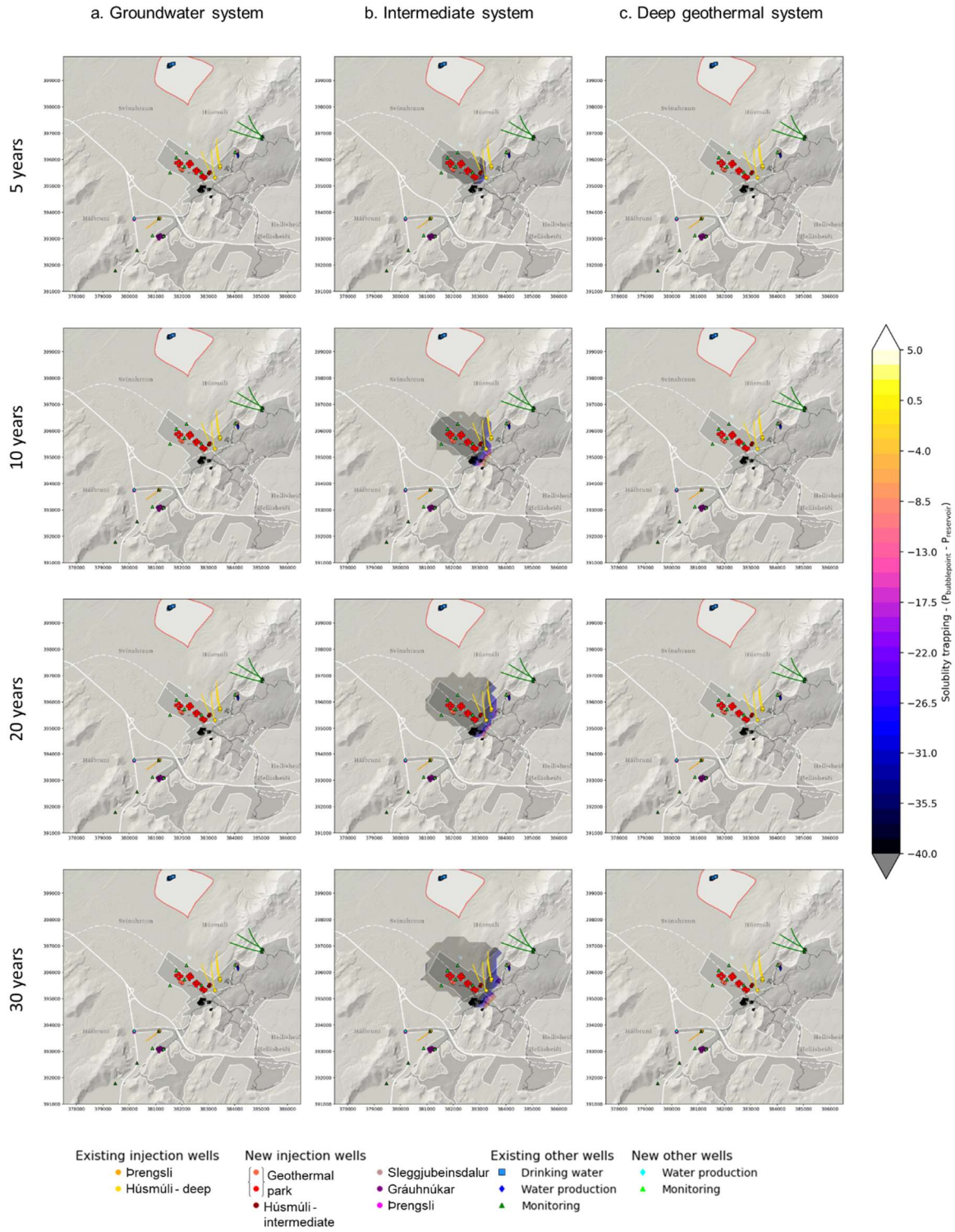

Figure 33: Scenario 1b: Areal view of the modelled solubility trapping in the storage reservoir after 5, 10, 20, and 30 years in the groundwater, intermediate, and geothermal systems.

- *Pressure and temperature impact on the Intermediate system*

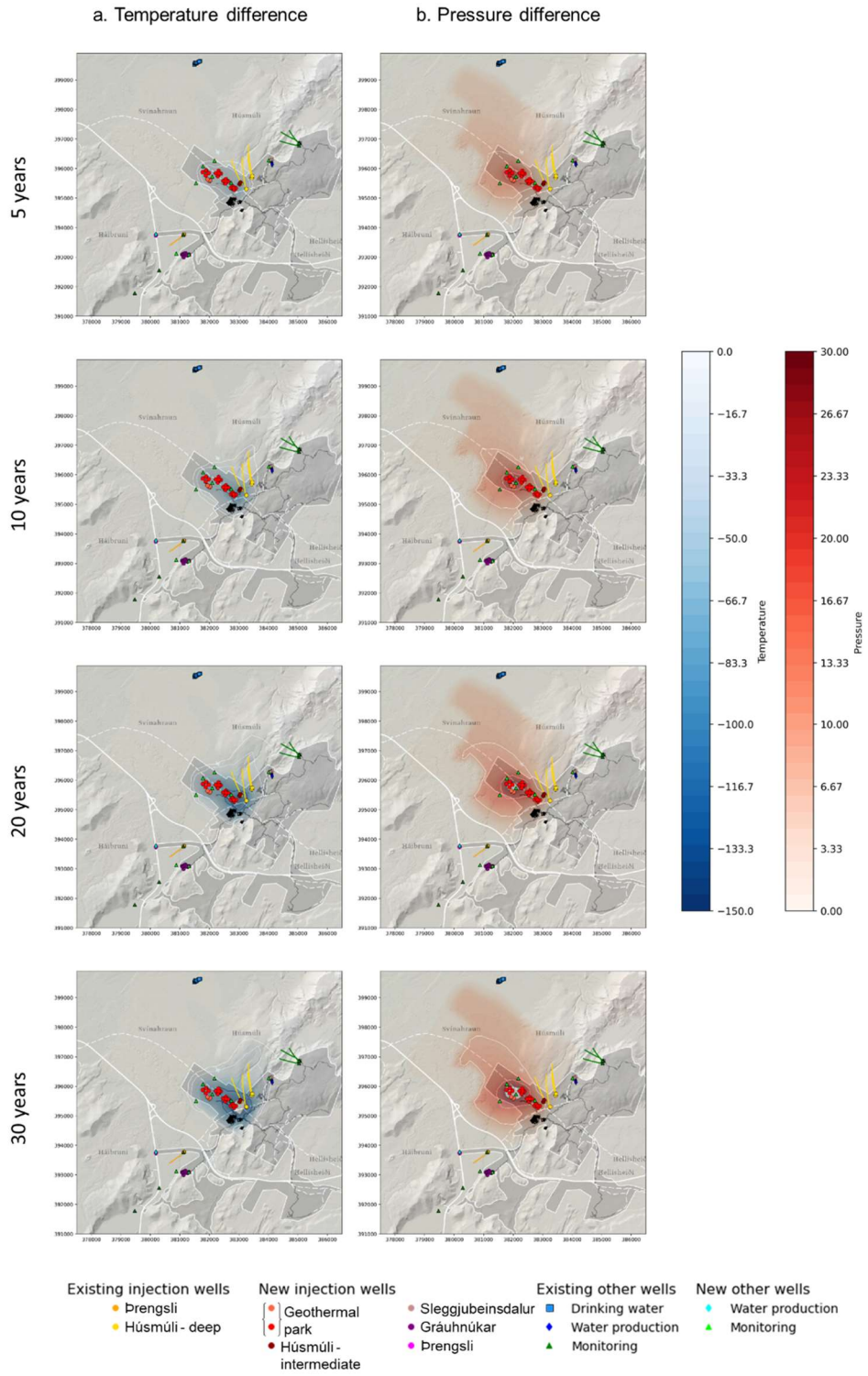

Figure 34: Scenario 1b: Areal view of the modelled temperature (ºC) and pressure (bar) difference in the storage reservoir after 5, 10, 20, and 30 years in the intermediate system.

10.3 Scenario 1c

– *CO_2 content – maximum extent of the storage reservoir*

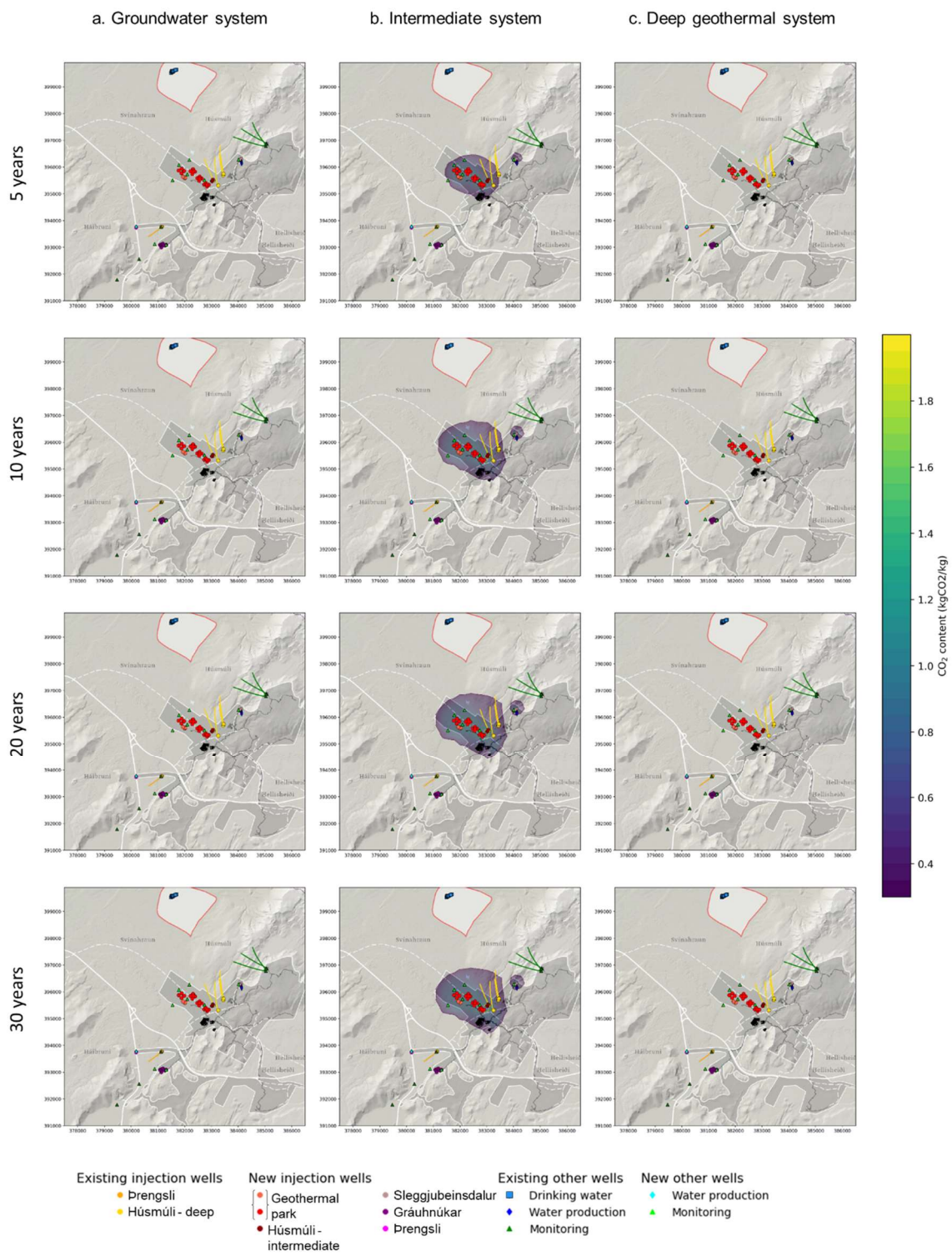

Figure 35: Scenario 1c: Areal view of the modelled CO_2 content in the storage reservoir after 5, 10, 20, and 30 years in the groundwater, intermediate, and geothermal systems.

– *Solubility trapping condition – Storage security*

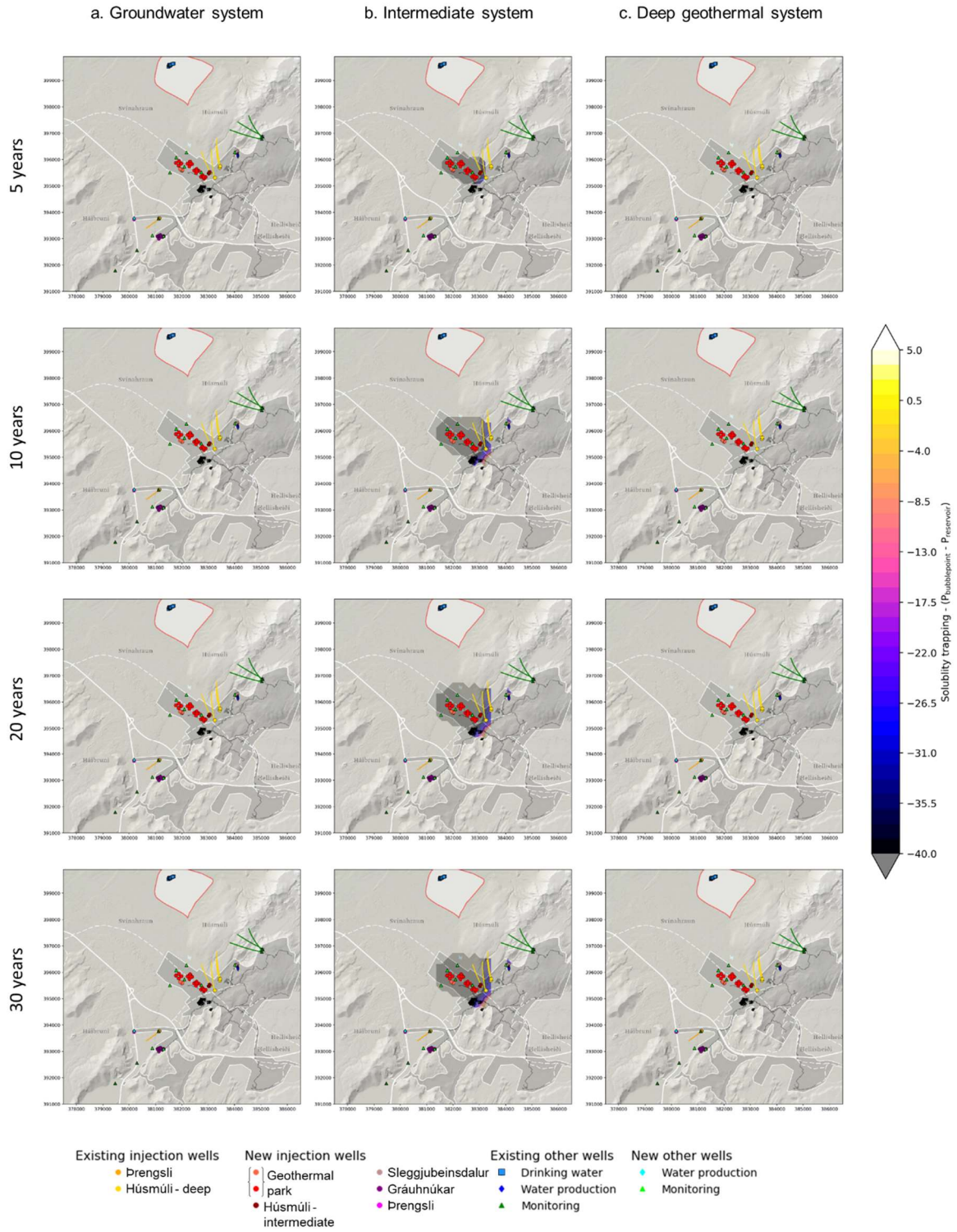

Figure 36: Scenario 1c: Areal view of the modelled solubility trapping in the storage reservoir after 5, 10, 20, and 30 years in the groundwater, intermediate, and geothermal systems.

- *Pressure and temperature impact on the Intermediate system*

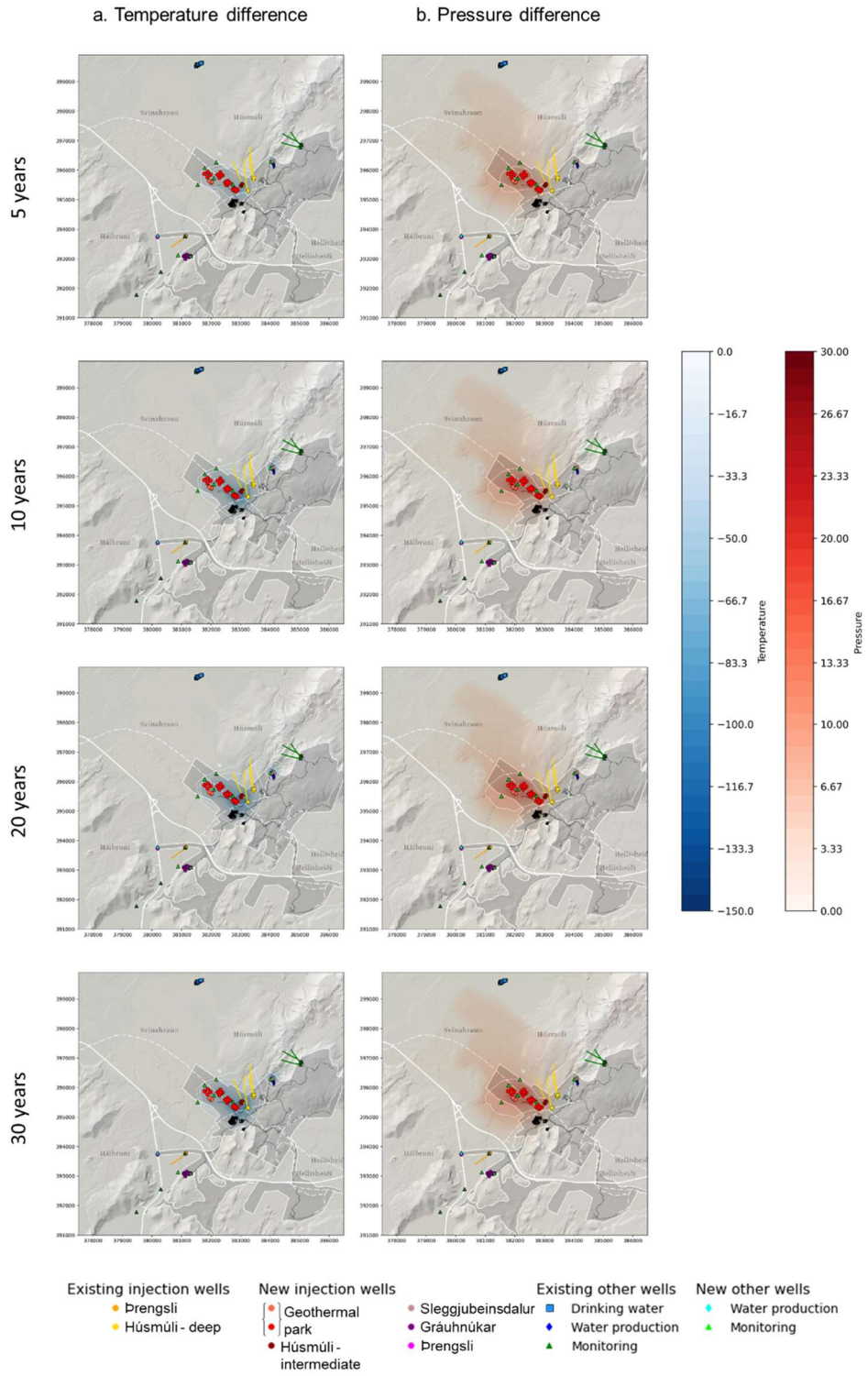

Figure 37: Scenario 1c: Areal view of the modelled temperature (ºC) and pressure (bar) difference in the storage reservoir after 5, 10, 20, and 30 years in the intermediate system.

10.4 Scenario 2

– *CO_2 content – maximum extent of the storage reservoir*

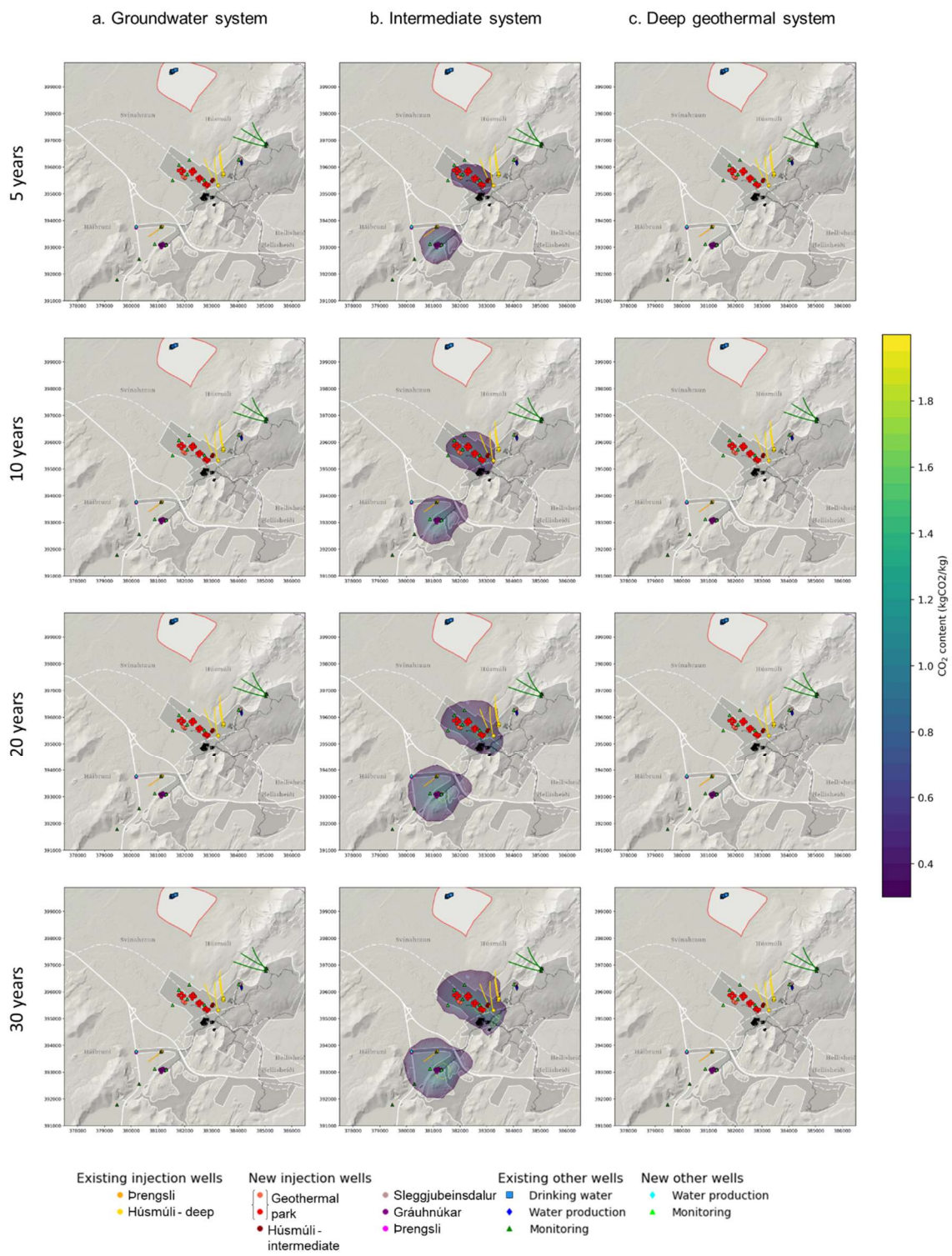

Figure 38: Scenario 2: Areal view of the modelled CO_2 content in the storage reservoir after 5, 10, 20, and 30 years in the groundwater, intermediate, and geothermal systems.

– *Solubility trapping condition – Storage security*

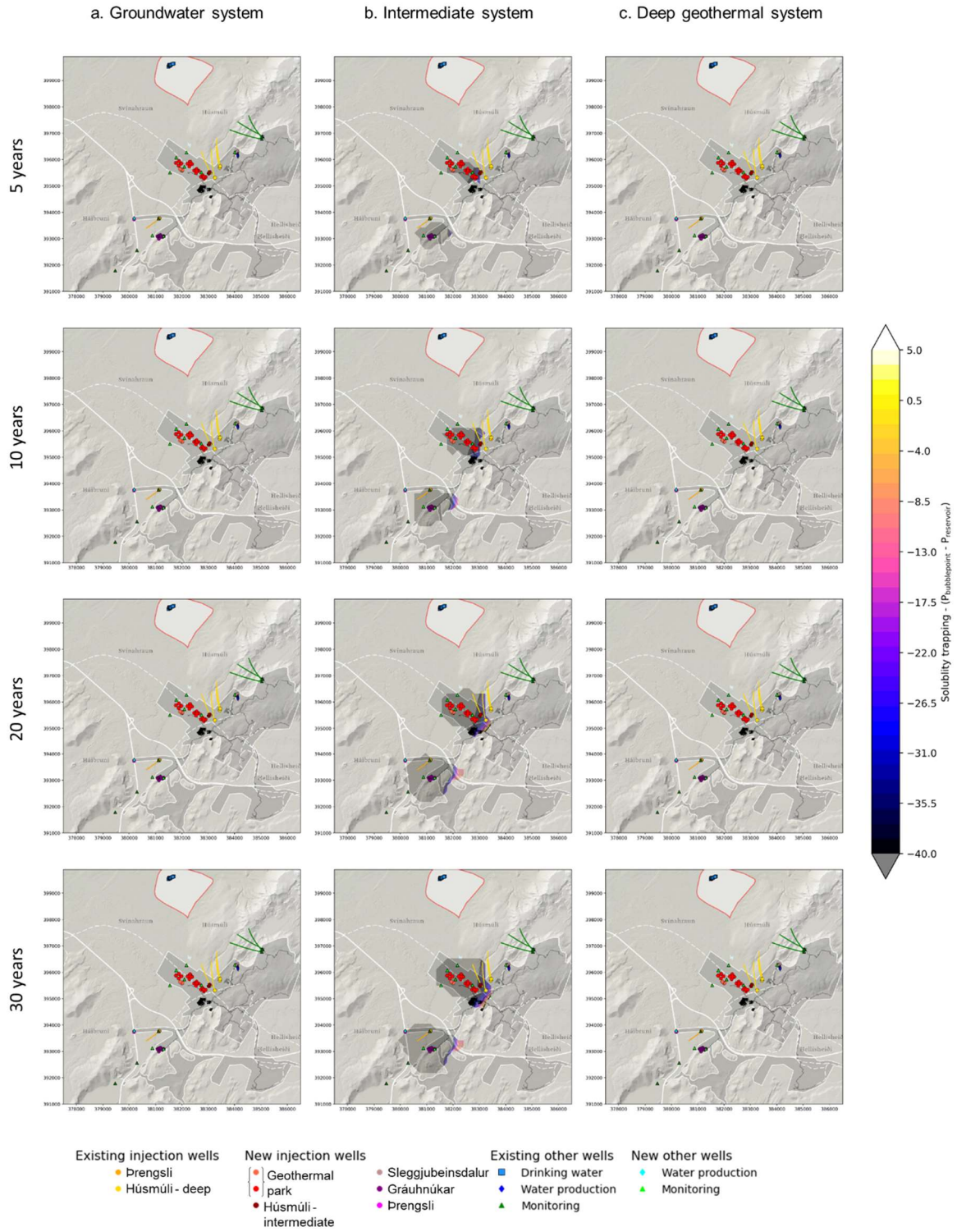

Figure 39: Scenario 2: Areal view of the modelled solubility trapping in the storage reservoir after 5, 10, 20, and 30 years in the groundwater, intermediate, and geothermal systems.

- *Pressure and temperature impact on the Intermediate system*

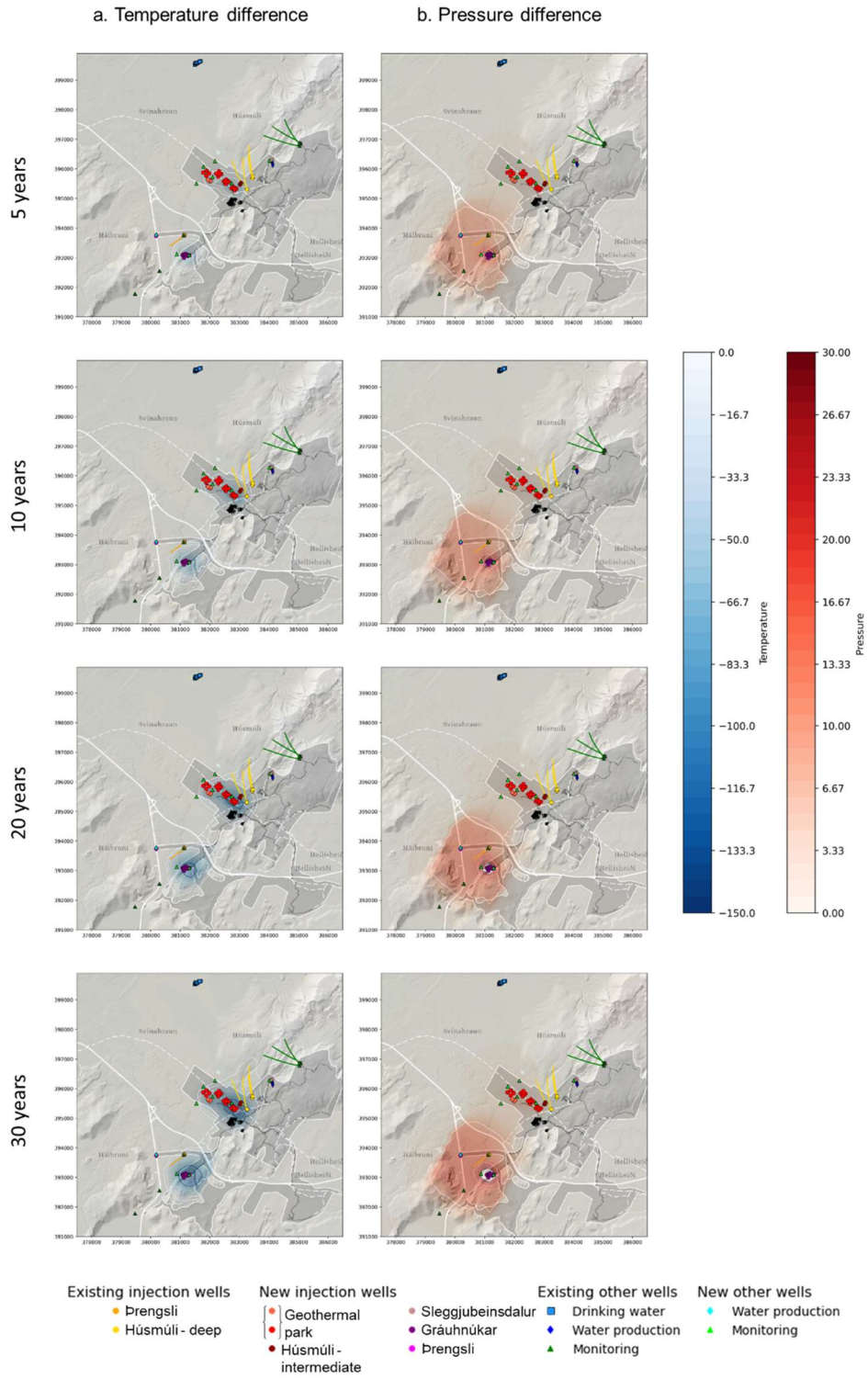

Figure 40: Scenario 2: Areal view of the modelled temperature (ºC) and pressure (bar) difference in the storage reservoir after 5, 10, 20, and 30 years in the intermediate system.

10.5 Scenario 3

– *CO_2 content – maximum extent of the storage reservoir*

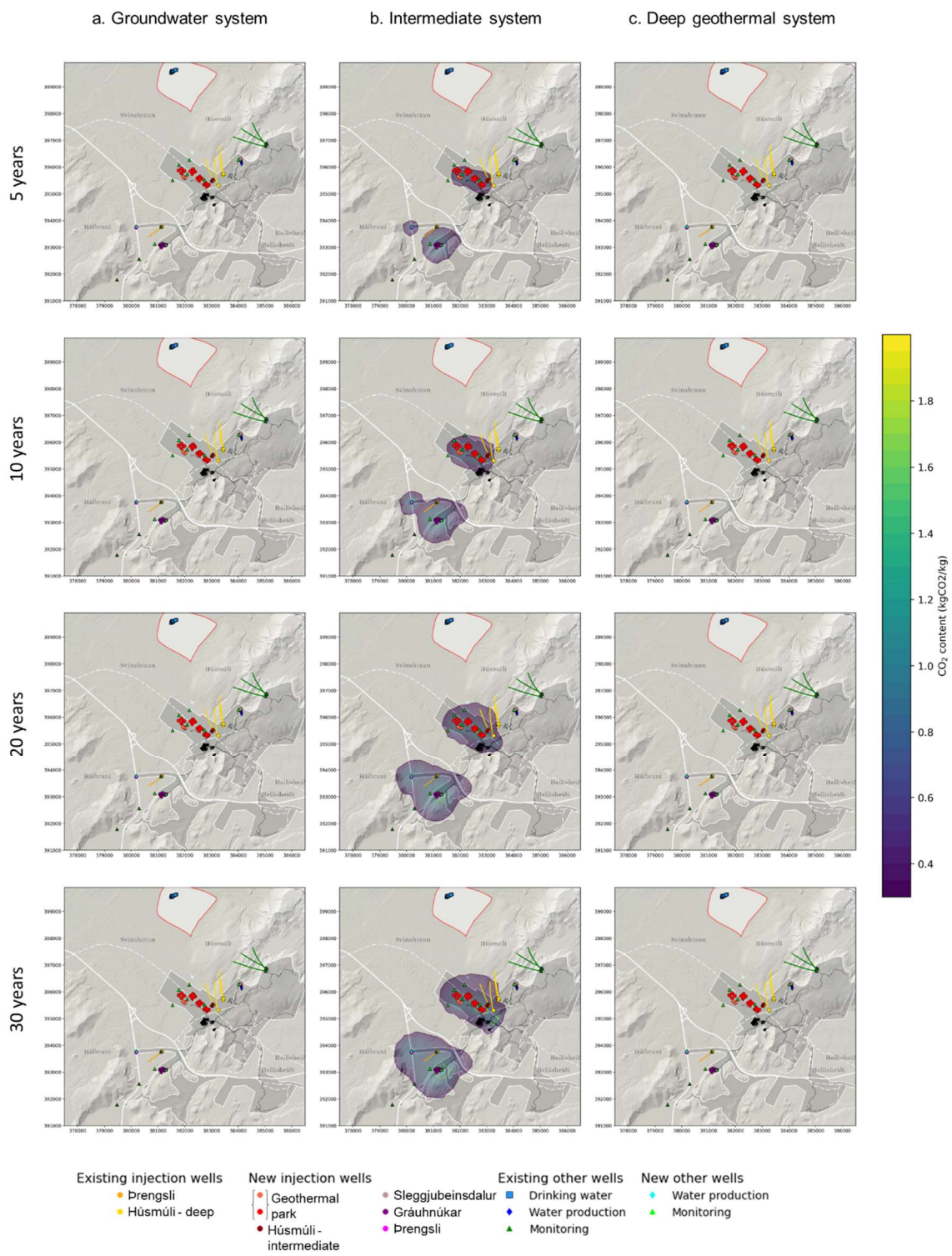

Figure 41: Scenario 3: Areal view of the modelled CO_2 content in the storage reservoir after 5, 10, 20, and 30 years in the groundwater, intermediate, and geothermal systems.

– *Solubility trapping condition – Storage security*

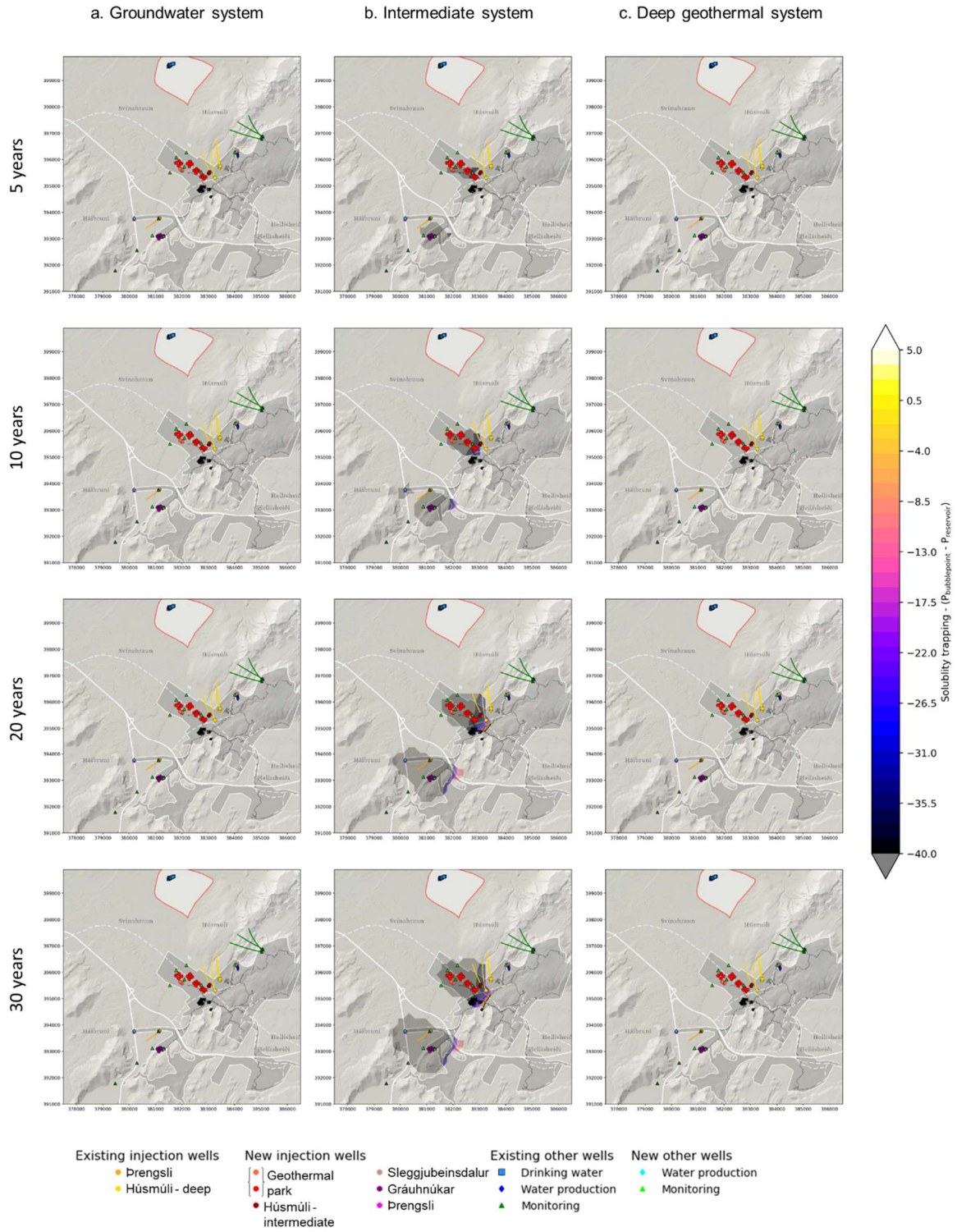

Figure 42: Scenario 3: Areal view of the modelled solubility trapping in the storage reservoir after 5, 10, 20, and 30 years in the groundwater, intermediate, and geothermal systems.

- *Pressure and temperature impact on the Intermediate system*

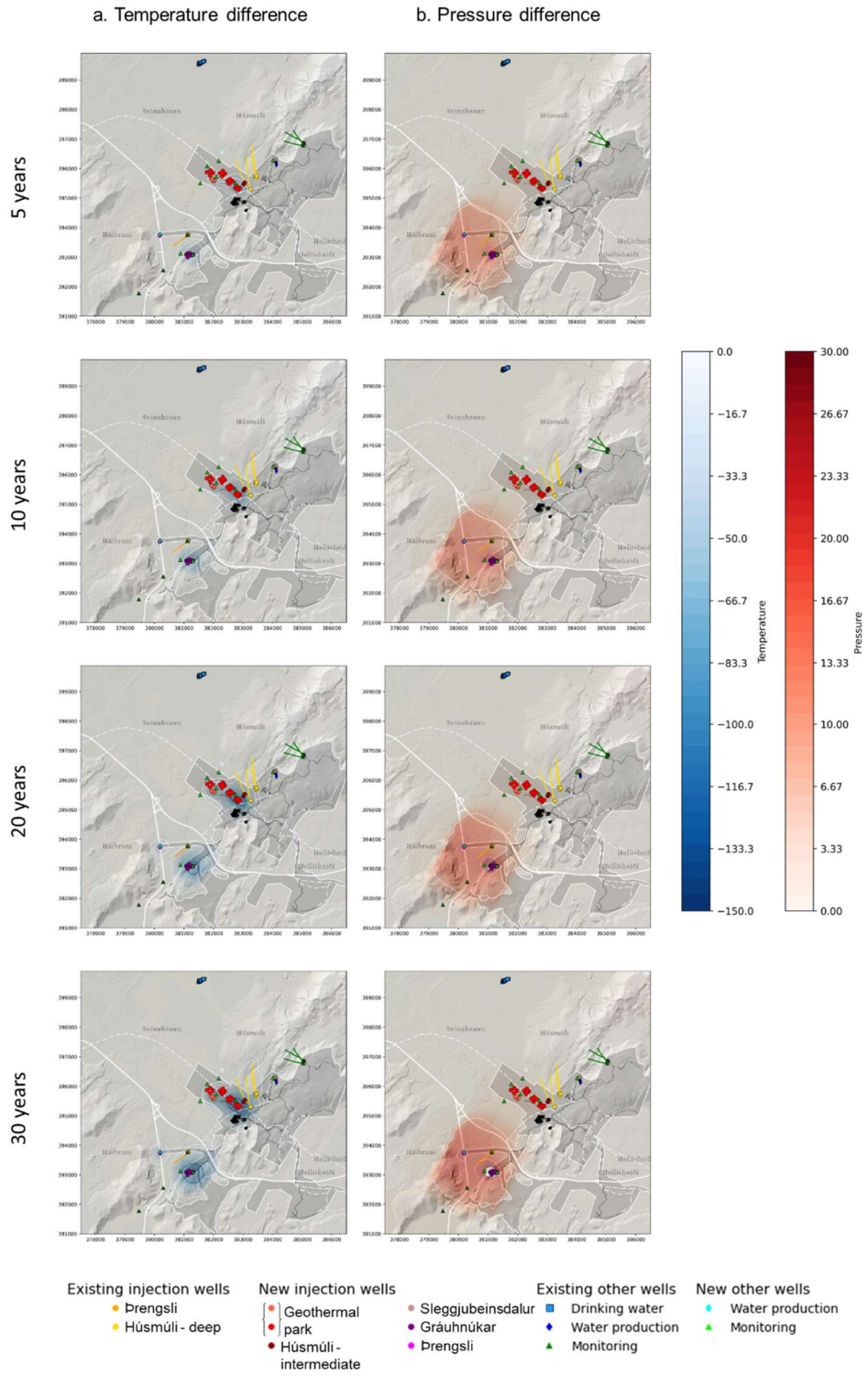

Figure 43: Scenario 3: Areal view of the modelled temperature (ºC) and pressure (bar) difference in the storage reservoir after 5, 10, 20, and 30 years in the intermediate system.

11 Annex 2 – Modelling results – Deep geothermal system

11.1 Scenario 1

– *CO_2 content – maximum extent of the storage reservoir*

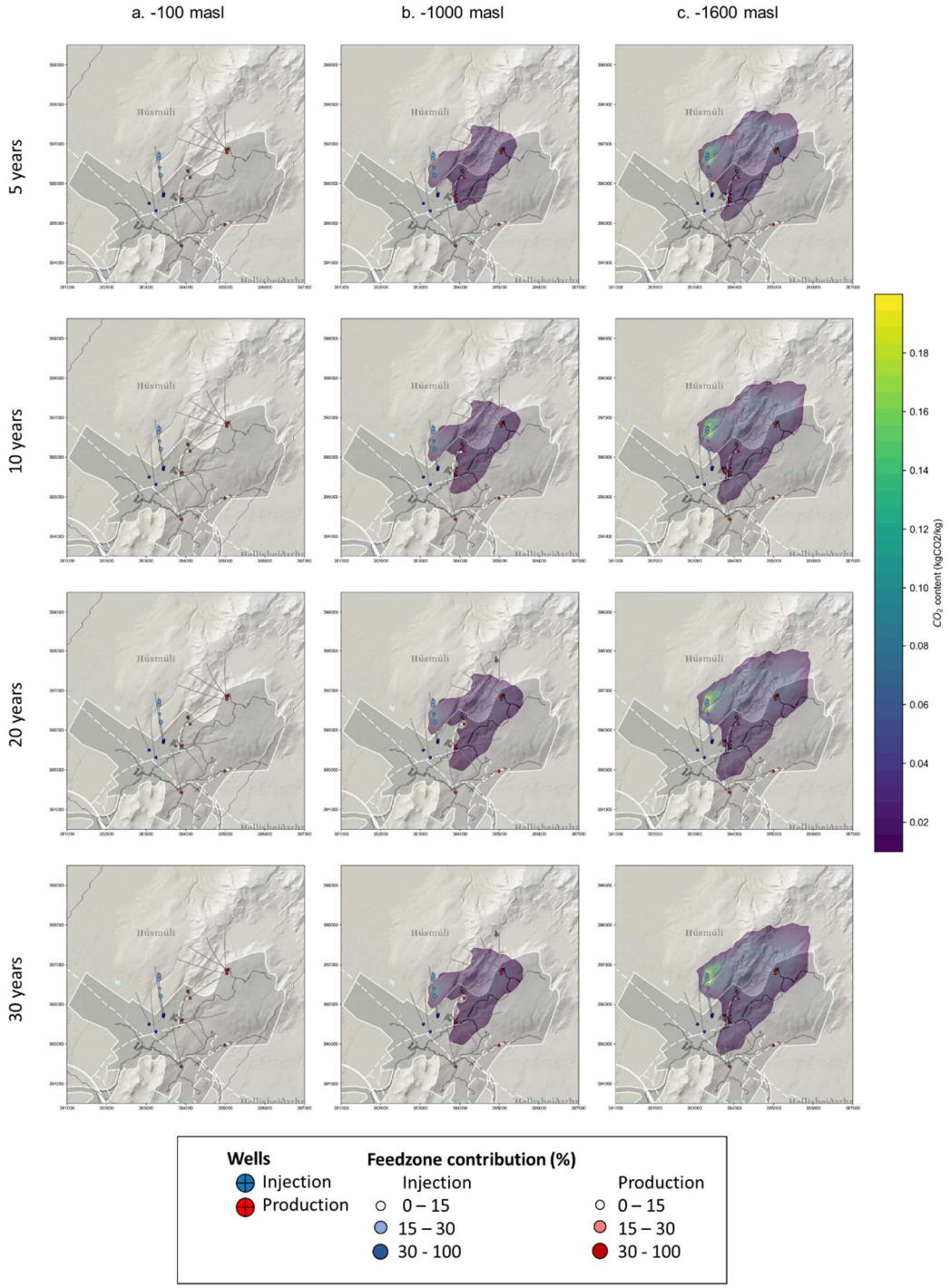

Figure 44: Scenario 1: Areal view of the modelled CO_2 content in the storage reservoir after 5, 10, 20, and 30 years at -100, -1000, and -1600 masl within geothermal systems.

– *Solubility trapping condition – Storage security*

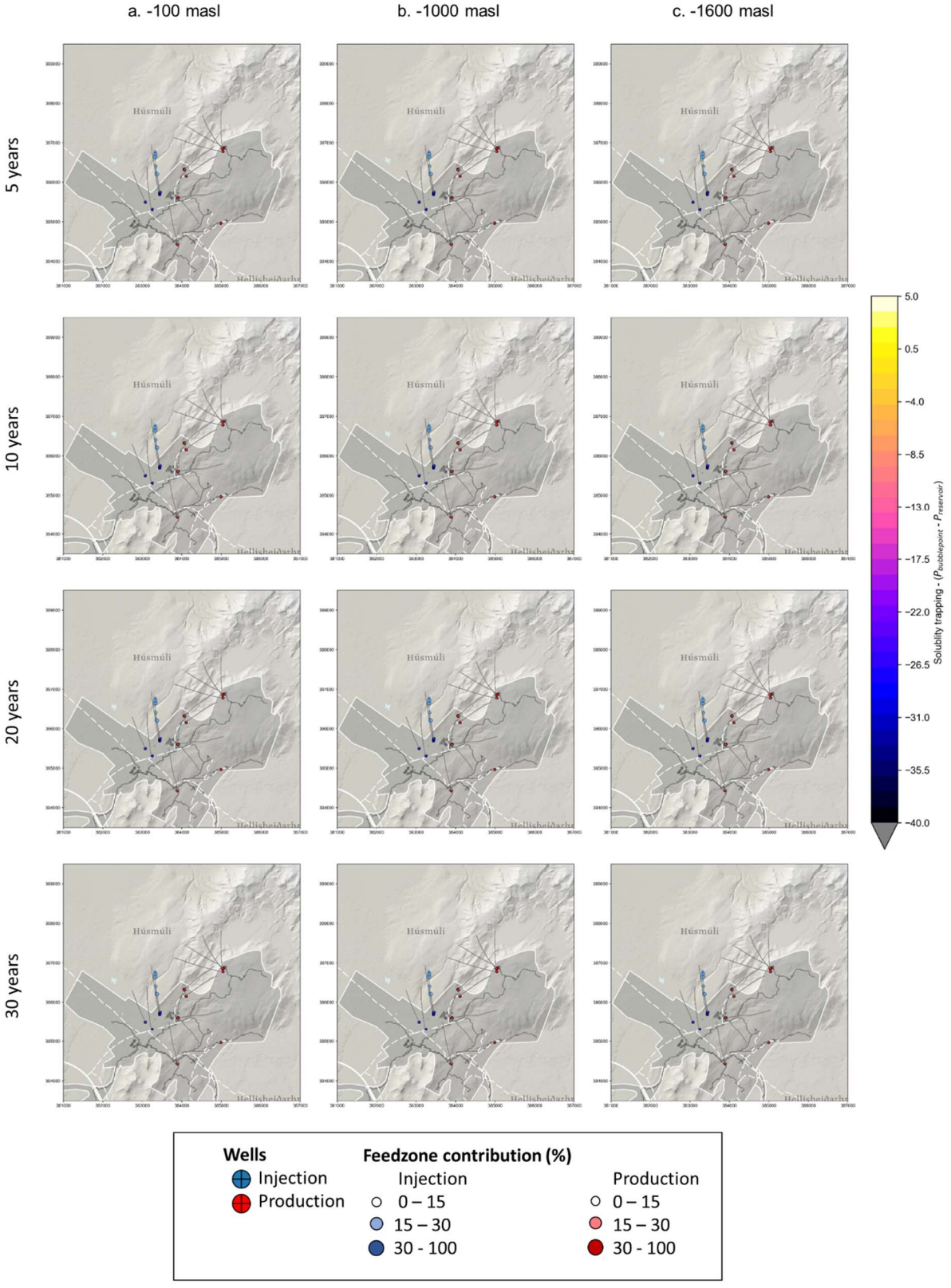

Figure 45: Scenario 1: Areal view of the modelled solubility trapping in the storage reservoir after 5, 10, 20, and 30 years at -100, -1000, and -1600 masl within geothermal systems.

- *Pressure and temperature impact on the deep geothermal system*

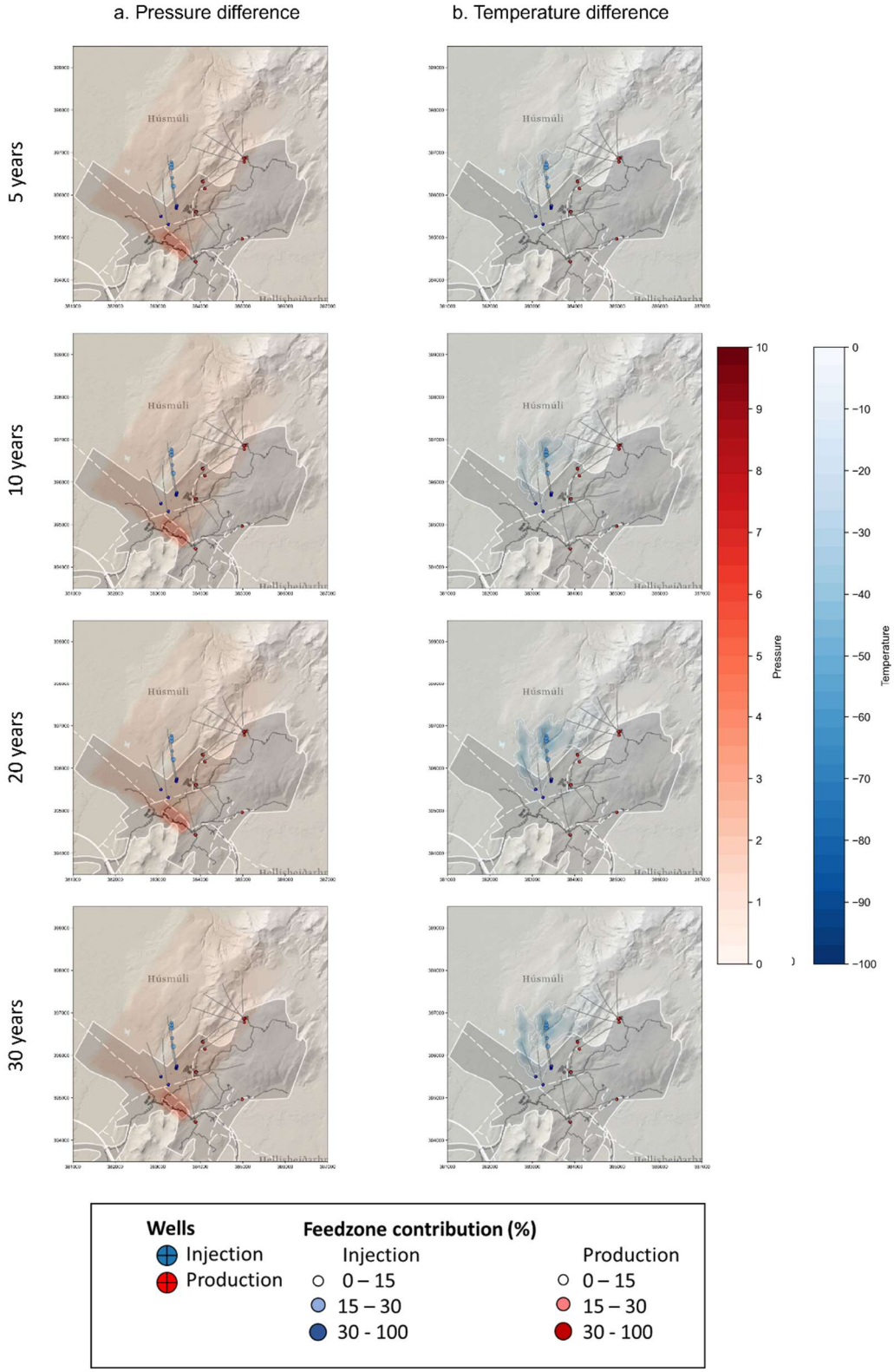

Figure 46: Scenario 1: Areal view of the modelled pressure (bar) and temperature (°C) differences in the storage reservoir after 5, 10, 20, and 30 years at -1600 masl within the geothermal system.

11.2 Scenario 2

– *CO_2 content – maximum extent of the storage reservoir*

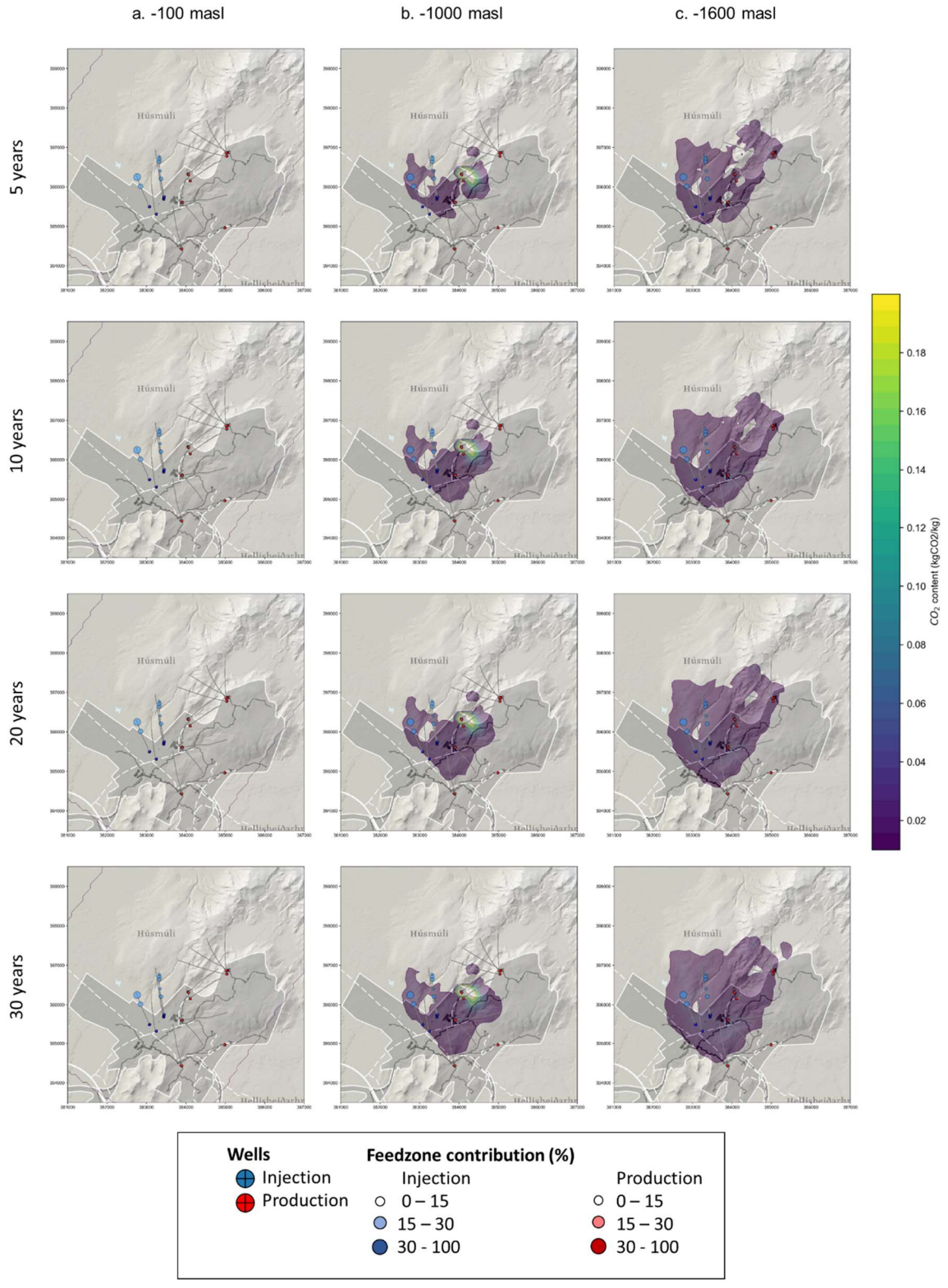

Figure 47: Scenario 2: Areal view of the modelled CO_2 content in the storage reservoir after 5, 10, 20, and 30 years at -100, -1000, and -1600 masl within geothermal systems.

– *Solubility trapping condition – Storage security*

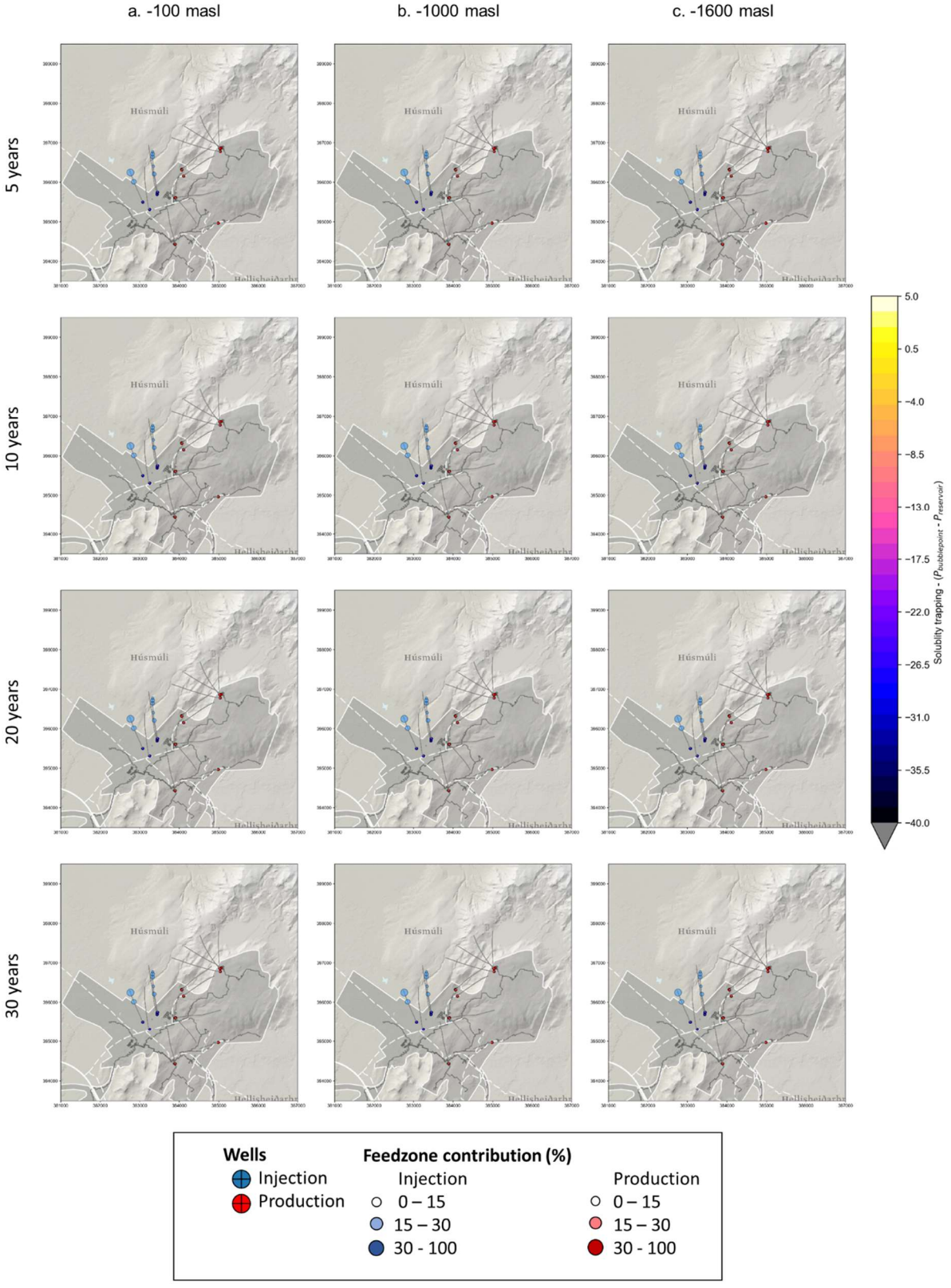

Figure 48: Scenario 2: Areal view of the modelled solubility trapping in the storage reservoir after 5, 10, 20, and 30 years at -100, -1000, and -1600 masl within geothermal systems.

- *Pressure and temperature impact on the deep geothermal system*

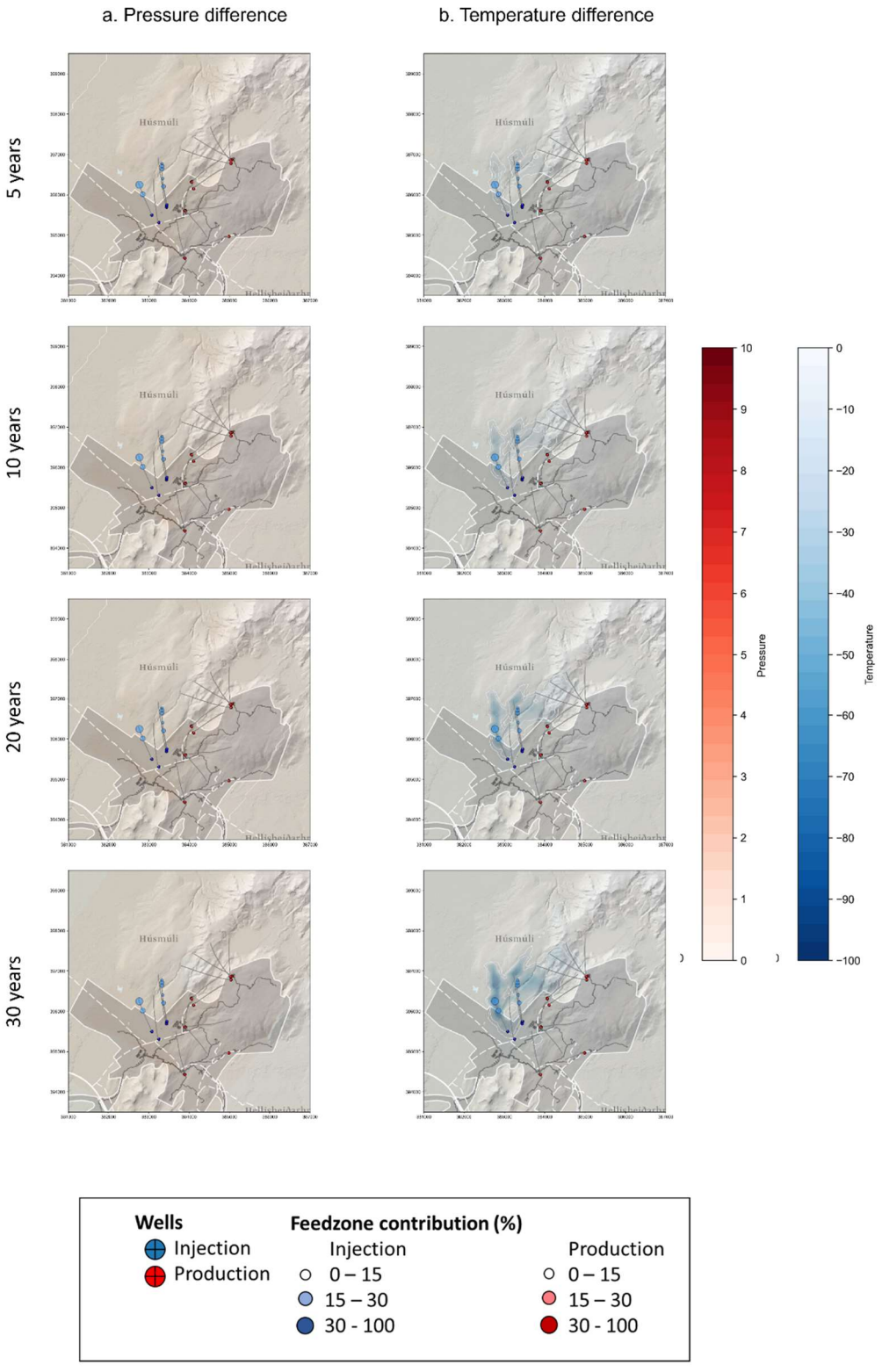

Figure 49: Scenario 2: Areal view of the modelled pressure (bar) and temperature (°C) differences in the storage reservoir after 5, 10, 20, and 30 years at -1600 masl within the geothermal system.

11.3 Scenario 3

– *CO_2 content – maximum extent of the storage reservoir*

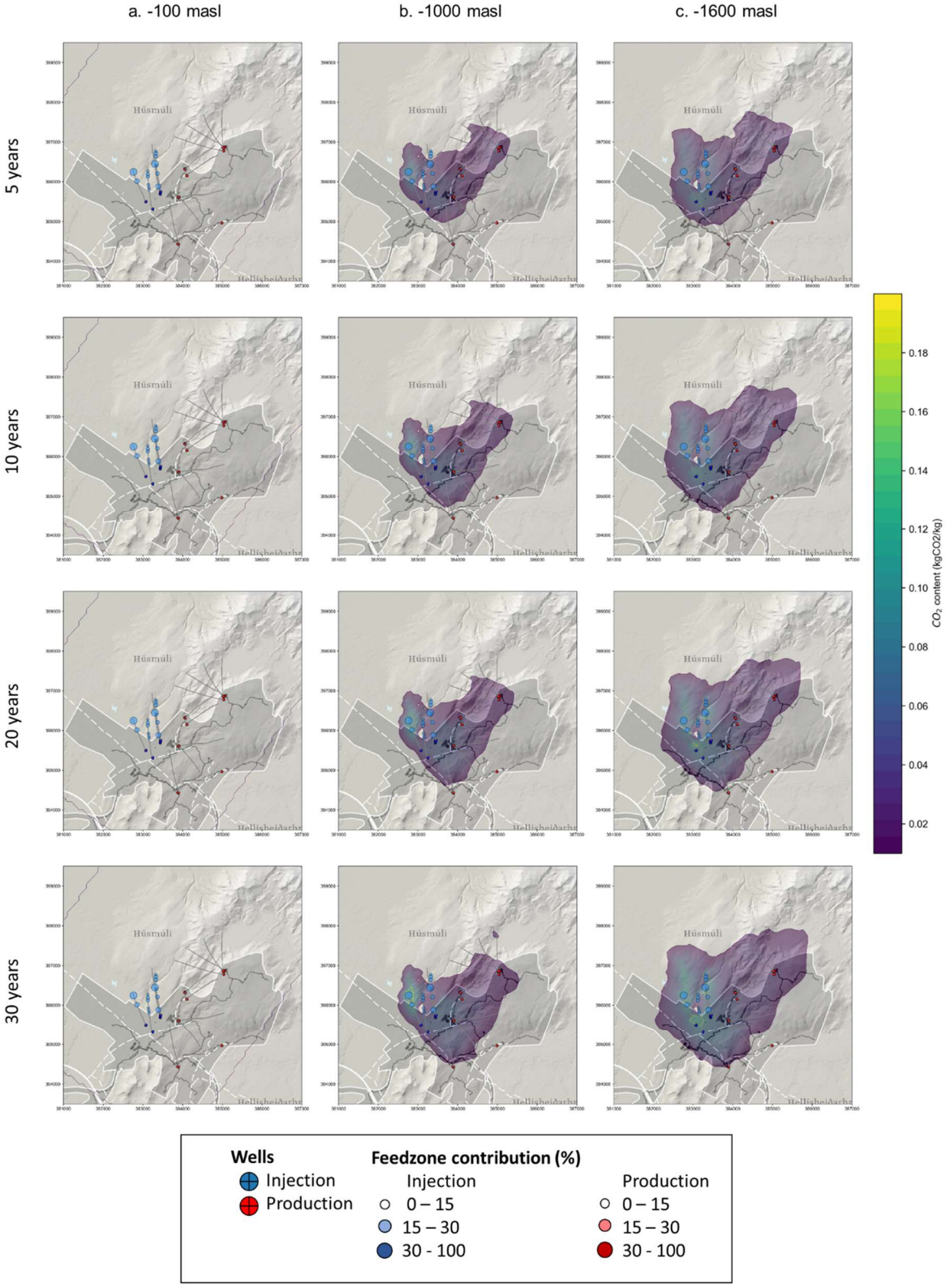

Figure 50: Scenario 3: Areal view of the modelled CO_2 content in the storage reservoir after 5, 10, 20, and 30 years at -100, -1000, and -1600 masl within geothermal systems.

– *Solubility trapping condition – Storage security*

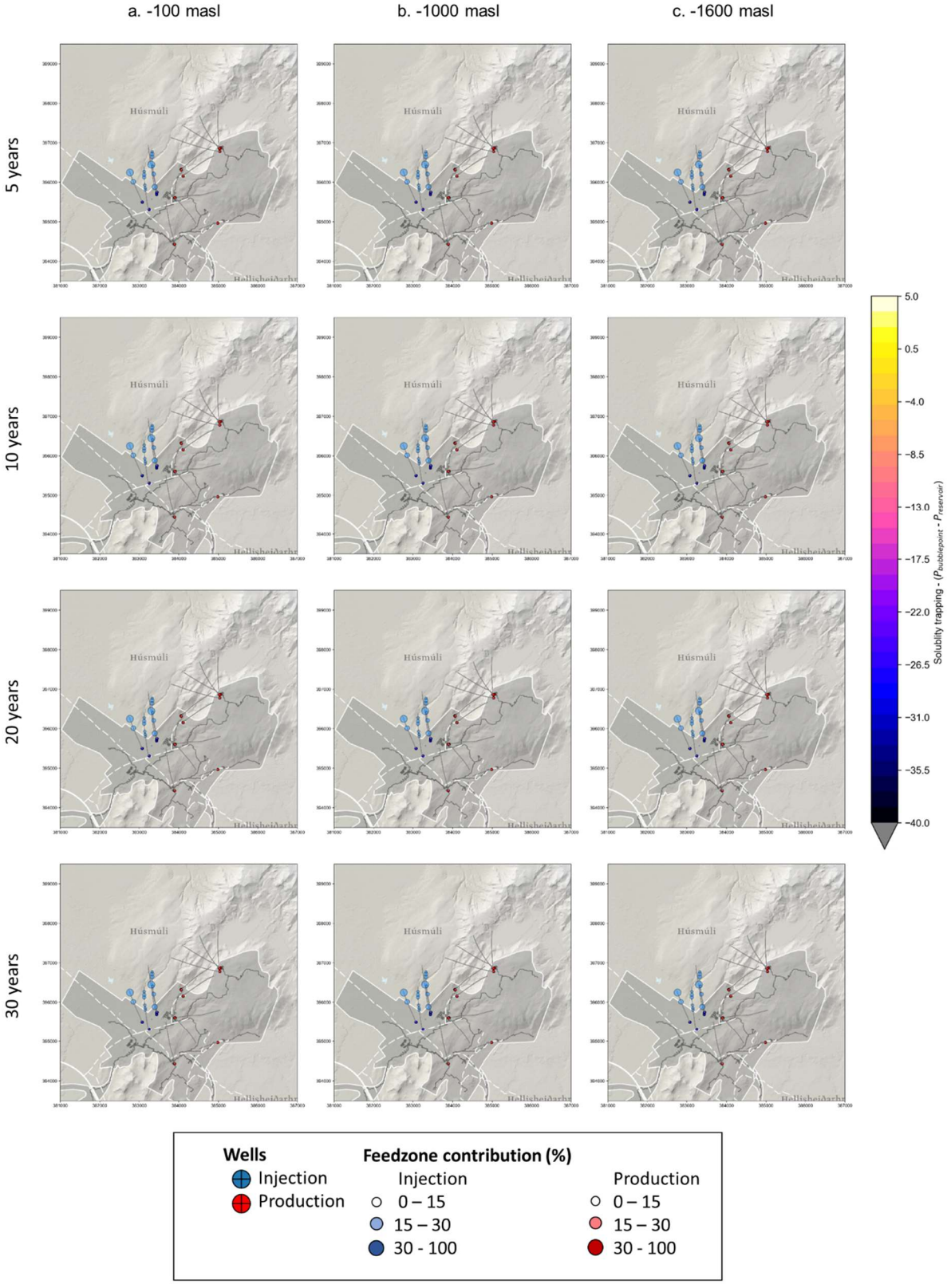

Figure 51: Scenario 3: Areal view of the modelled solubility trapping in the storage reservoir after 5, 10, 20, and 30 years at -100, -1000, and -1600 masl within geothermal systems.

- *Pressure and temperature impact on the deep geothermal system*

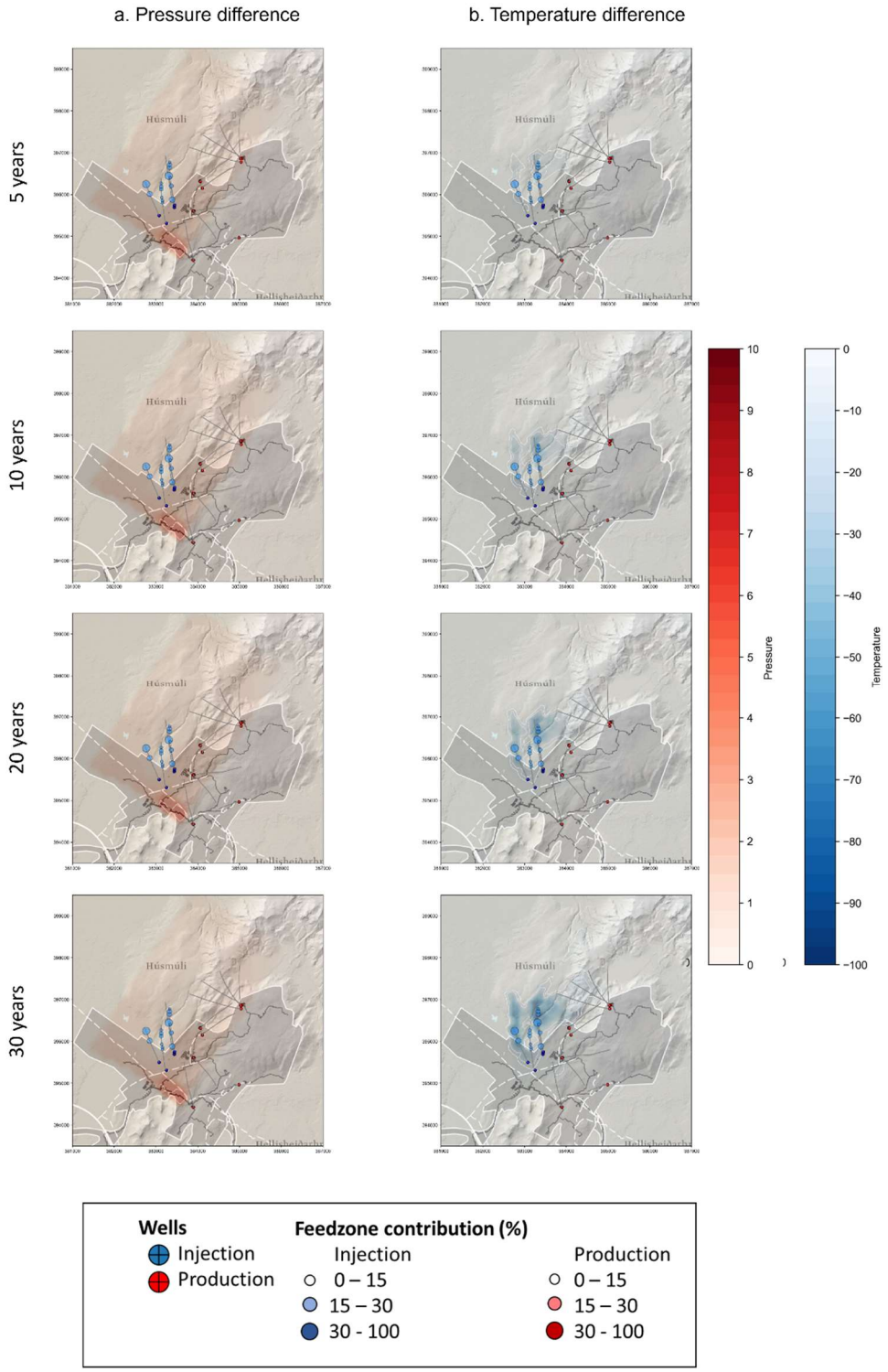

Figure 52: Scenario 3: Areal view of the modelled pressure (bar) and temperature (°C) differences in the storage reservoir after 5, 10, 20, and 30 years at -1600 masl within the geothermal system.